Department of Chemical Engineering
Fuels and Energy Technology Institute

Transformation of Char Structure and Alkali and Alkali Earth Metallic Species during Pyrolysis and Gasification

Lei Zhang

This thesis is presented for the Degree of

Doctor of Philosophy

Of

Curtin University

March 2015

Declaration

To the best of my knowledge and belief this thesis contains no material previously published by any other person except where due acknowledgement has been made.

This thesis contains no material which has been accepted for the award of any other degree or diploma in any university.

Signature:……

Date: ……

Contents

Abstract

Gasification is one of the most efficient and versatile technology that can embrace a wide range of fuels. Low-grade fuels such as biomass, brown coal and sub-bituminous, which are not suitable for traditional combustion technology, are very suitable for gasification based technology due to their high gasification reactivity. When the fuels are fed into the gasifier, they will undergo fast pyrolysis and generate primary volatiles and nascent chars. The nascent char that still keeps the high gasification reactivity determines the overall char gasification rate.

AAEM species and char structure are two major factors influencing char reactivity. However, the quantitative analysis of char structure is much more difficult than that of AAEM species or char reactivity. Recently, with the development of the methodology to characterise char structure, Raman spectroscopy has been proved as a powerful technique to gain information about char structural features quantitatively.

The purpose of this study was to investigate the transformation of nascent char structure and alkali and alkali earth metallic species (AAEM) during pyrolysis in He or gasification in CO_2/O_2. The nascent char was produced using a wire-mesh reactor that can control the holding time and heating rate accurately. More importantly, the wire-mesh reactor can minimise the effects of volatile-char interaction on the properties of nascent chars. The nascent char was characterised by Fourier-transform Raman/infrared spectroscopy. The AAEM species and nascent char reactivity were determined by inductively coupled plasma optical emission spectroscopy (ICP-OES) and thermogravimetric analysis (TGA), respectively.

The results showed that the transformation of char structure was significantly determined by temperature during pyrolysis. At relatively high temperature (e.g. 1000 °C), the changes in char structure took place rapidly within 1 s during pyrolysis. The structural changes in nascent char during gasification in CO_2 was also largely affected by temperature, while the reaction pathways of nascent char gasification

changed little during heating from 1000 to 1200 °C in CO_2. Furthermore, significant structural changes in nascent char during gasification in O_2 indicated that the initial char structure is as important as AAEM species affecting the gasification rate. Finally, the effect of AAEM species concentration and nascent char structure on nascent char reactivity was investigated. It is indicated that the catalytic effect of AAEM species on the char-O_2 reaction was significantly inhibited by the increasingly stabilised char structure.

Acknowledgements

I wish to express my sincere thanks to my supervisor, Prof. Chun-Zhu Li, for his patient guidance, support and encouragement throughout my candidature. I would also wish to thank all the students and stuffs at the Fuels and Energy Technology Institute. Specially, I wish to thank Prof. Penghua Qiu who gave me many invaluable suggestions for my research work, Dr Xun Gong who taught me how to operate wire-mesh reactor, Tingting Li who instructed me in Raman spectrometer. I would like to thank Dr Dimple Quyn for her helps on my paper revising. I am grateful to Caroline Lievens who showed me the procedure for inorganic species detection and Pertrina Thompson who trained me to use inductively coupled plasma optical emission spectrometry (ICP-OES) and gave me some suggestion about how to improve the detection limit.

I am grateful to acknowledge the financial support of this study from the Australian Research Council (DP110105514), the Commonwealth of Australia under the Australia-China Science and Research Fund and WA Department of Mines and Petroleum. I also wish to thank Muja power plant for providing Collie raw coal. This research used samples of mallee biomass supplied without cost by David Pass and Wendy Hobley, from their property in the West Brookton district. I would like to thank Dr Dimple Quyn again for the preparation of Loy Yang coal samples.

Finally, I wish to appreciate my parents, my parents-in-law, my wife and my dear son for their unconditional love and support.

List of Tables

List of Figures

Chapter 1

Introduction

1.1 Utilisation of low rank coal and biomass

1.1.1 Importance of low-rank coal and biomass in energy supply

The fast growth in population and the improvement of living standards are the major driving force for the increasing demand of energy all over the world. Energy Outlook 2035 [1], which was reported by BP, predicted that the population would continuously increase from ~7.2 billion to ~8.7 billion from 2014 to 2035. This means that there will be additional ~1.5 billion people requiring energy.

The sharing of energy demand between different fuels is illustrated in Fig. 1-1 [2]. The total demand of energy will gradually increase in next two decades. Among these fuels, the utilisation of coal will experience large reductions from 2015 to 2040. Nevertheless, it will still be one of the primary energy resources in the long term (accounting for ~28% in 2015 and ~17% in 2040). This dominant position of coal in the global energy supply is mainly due to its large reserves and wide distribution all over the world. A report [3] issued by World Energy Council in 2013 estimated that there were 869 billion tonnes of proved coal reserves that can be used for 115 years according to the current production rate, lasting longer than oil and gas.

Of the proved reserves of coal, ~55% are low rank coals (sub-bituminous coal and brown coal) and ~45% are high rank coals (anthracite and bituminous coal) [4]. The utilisation of low rank coals is more difficult than high rank coals due to their high moisture contents, high ash yields and low calorific values. However, the low cost and large reserve have attracted the scientists and the technologists to develop technologies for a cheap and efficient way of using them. The gasification technology is one of the suitable options for the utilisation of low rank coals [5], which will be discussed further in following sections.

As is shown in Fig. 1-1, the demand of bioenergy accounts for ~10% of total energy consumption currently. It will grow quickly over the following 25 years and be close to the usage of coal in 2040. The increasing demand of bioenergy derives from the

anxiety of diminishing reserves of fossil fuels and the great potential for the development of bioenergy. Biomass, which stores energy in carbonaceous structures (similar to fossil fuels), is found all over the world. Similar to low-rank coal, biomass has low energy density, which is not suitable for the traditional combustion technology. However, they are quite suitable for the gasification technology.

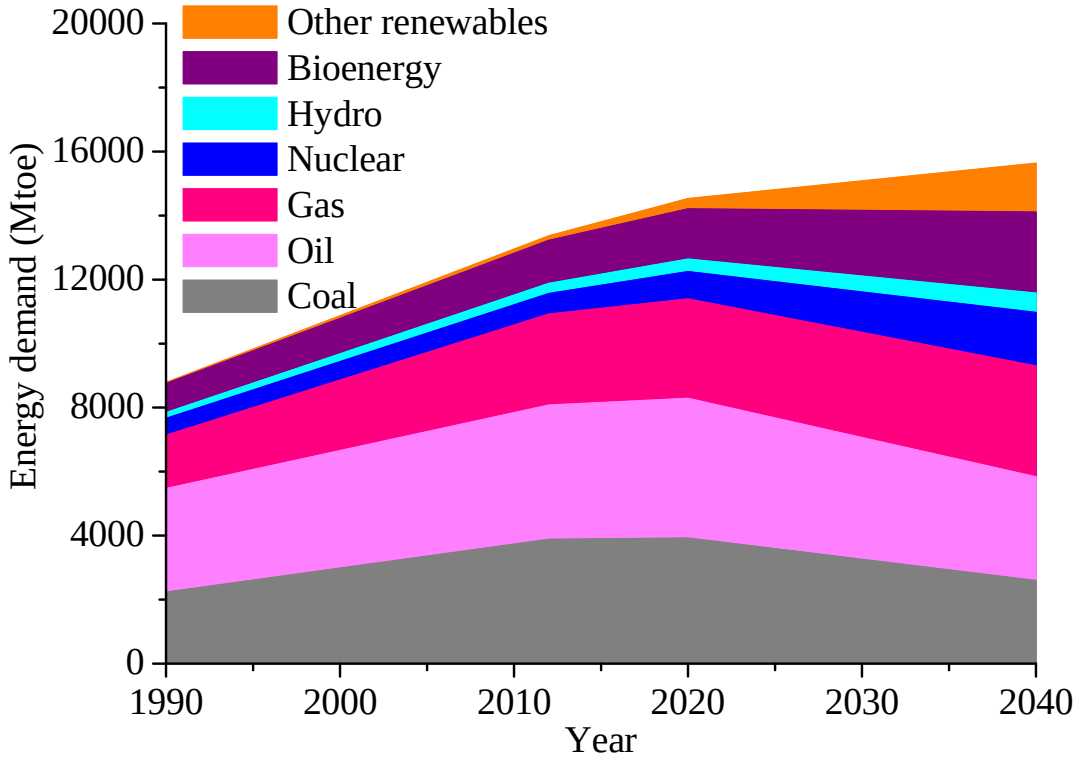

Figure 1-1 The energy demand of different fuels. Bioenergy includes traditional and modern uses of biomass (based on the data in [2]).

1.1.2 Importance of gasification technology for the utilisation of low-rank coal and biomass

As was mentioned above, gasification is one of the promising technologies for the utilisation of a wide range of fuels. The low-grade fuels such as brown coal, lignite, peat, biomass and solid wastes, which are not suitable for traditional combustion technology, are appropriate for gasification due to their high conversion efficiency during gasification [5]. In combination with fuel cells and/or efficient gas turbine

technology, the gasification of low-rank coals, biomass or a mixture of them can achieve much higher efficiency than pulverised fuel combustion technology to generate electricity [6]. The highly efficient use of low-grade fuels indicates that we can consume less fuel to meet our demand of energy, which means less emissions of CO_2 as well.

Gasification technology can convert low-rank coal and biomass to syngas, which mainly consists of CO and H_2. The syngas can be used to synthesise liquid fuels (indirect liquefaction). The conversion of low-grade fuels to high-quality liquid fuels offers many benefits for the utilisation of low-rank coals and biomass. Firstly, low rank coal and biomass, which normally have high contents of moisture and high yields of ash, are not economical for long-distance transportation. Liquid fuels can be easily transported following indirect liquefaction, thereby reducing the limitation of the use of low-grade fuels. Secondly, the gasification-based power plant can generate electricity and produce liquid fuels simultaneously on the basis of demand. More electricity is needed during daytime, while the liquid fuels production can be performed in the night times when the electricity demand is relatively lower than in daytime. The capture and storage of CO_2 is easier to be implemented with the application of such poly-generation plant [7].

In general, for the reasons of economy and environment, the interests in gasification of low-rank coal and biomass will continuously increase in the long term.

1.2 Effects of chemical structure and properties on gasification rate

The basic chemical reactions in the gasification of fuels can be summarised in Table 1-1 [8]. Among these reactions, reactions 1-4 (between char and H_2O) and 1-5 (between char and CO_2) are relatively slow, which are the rate-limiting steps and control the overall gasification reactivity. Therefore, many efforts [9-10] have been made to study the factors influencing the gasification reactivity of chars in H_2O and CO_2. The central topics, about the main reasons affecting the gasification rate, focus on the behaviour of AAEM species and char structures for low-rank coal and

biomass. There are three aspects of AAEM species to be considered: the chemical form of AAEM species in char, the concentration of AAEM species in char and their dispersion as catalysts on char (pore) surface. Regarding char structure, many reports indicate its importance on reactivity. However, it is difficult to quantitatively establish char structures and to understand its direct effects on reactivity due to the unsuitability method of many common analytical techniques for char characterisation. Recently, the FT-Raman spectroscopy has been applied to the quantitative study of char structural features, as will be further discussed below.

Table 1-1 Basic chemical reactions occurs in the coal/biomass gasification [8]

Type of reaction	Reaction	No.
Combustion	$C + O_2 = CO_2$	(1-1)
Partial oxidation	$C + ½ O_2 = CO$	(1-2)
Steam gasification	$C + H_2O = CO + H_2$	(1-3)
Reverse Boudouard reaction	$C + CO_2 = 2CO$	(1-4)
Hydrogasification	$C + 2H_2 = CH_4$	(1-5)
Water-gas shift reaction	$CO + H_2O = CO_2 + H_2$	(1-6)
Methanation	$CO + 3H_2 = CH_4 + H_2O$	(1-7)

1.2.1 Characterisation of char structure

Many techniques have been applied to characterise the structural features of the chars produced from different feedstocks (e.g. biomass and different ranked coals). Firstly, HRTEM (high resolution transmission electron microscopy) is a useful technique to investigate the morphology of different carbonaceous materials such as coal/coal char [11-17] and biomass char [18-20]. It provides important insights into the progressive change in crystalline structure during heat treatment. Sharma and co-workers [13, 14] successfully used HRTEM as a new image analysis technique to

quantify the graphene layer size, the interlayer space, the number of layers per stack and their distribution. However, this technique mainly focuses on the surface morphology of carbon materials, which has limited capacity to quantify the chemical structures (especially amorphous carbon structures) in the whole matrix of carbonaceous material. Secondly, elemental analysis is commonly used to in trace the loss of aliphatics, the reaction of dehydrogenation and the oxidation of carbon by calculating H/C, C/O etc., which shows very limited information about the char structural features. Thirdly, X-ray diffraction (XRD) has also been employed to examine the structural changes in the chars produced from coals of different ranks [21-23], biomass [24] or petroleum coke [25] during gasification. These studies investigated the evolution of crystalline structures and correlated the structural change with the char reactivity. However, low-rank coals and biomass contain abundant amorphous (disordered) structures that can be hardly detected by XRD [26, 27]. Moreover, some other techniques, such as XPS, NEXAFS and EELS, which can be used to analyse the surface composition and functional groups of carbonaceous material but cannot provide the structural information of char matrix.

Raman spectroscopy, which has long been used to investigate the bulk properties of carbonaceous structures, can provide more comprehensive information about both amorphous and crystalline structures than the above techniques. Potgieter-Vermaak and co-workers [28] reviewed the advances in this technique in the characterisation of coal/char structures over four decades from 1970 to 2010. In the initial three decades, studies were mainly focused on the assignment of the G band and the D band in different carbon materials such as macerals in coal, graphite, cokes and coals of different ranks to investigate the coalification or graphitisation behaviour of carbon materials. From the year of 2000 to 2009, the application of Raman spectroscopy entered a new era of char structure determination. Li and co-workers [27, 29] employed Raman spectroscopy to quantify the structure features in the chars produced from Victorian brown coal during pyrolysis and gasification. Much progress in the methodology to acquire the high quality Raman spectra of the brown coal chars has been described in the review given by Li and co-workers [30]. Briefly, the laser source was changed to a near-infrared laser at 1064 nm in Raman

spectroscopy so as to minimise the interference from fluorescence. Char samples were mixed and ground with KBr at very low weight percentage (~0.25%) so as to prevent the heating up of the char samples by the absorption of laser power. After the improvements of analytical methods, a high quality (high ratio of signal to noise) Raman spectrum was acquired. Additionally, only a small amount of sample is required for achieving repeatable analysis. Briefly, ~0.13 g of sample/KBr mixture was essential to fill in the sample holder. As the concentration of the sample in the mixture is ~0.25 wt%, the minimum amount of sample that required for analysis is only ~0.33 mg. Therefore, this technique is well applicable for small-scale reactors, such as wire-mesh reactors or Curie-point reactors. In practice, to ensure representation of the sample analysed, more than 0.33 mg char was mixed with KBr in the required proportion. The char-KBr mixture was then ground very finely for about 20 min, which reduce the heating up of the char by laser and ensures the complete mixing of char with KBr at a microscopic level. The Raman spectrum was deconvoluted into 10 bands (see Table 1-2). The characterisation of nascent char structure is mainly focused on six bands (G, Gr, Vl, Vr, D and S) that occupy a large percentage of Raman area from 800 to 1800 cm^{-1}. The three bands (Gr, Vl and Vr) are combined and considered as one group representing the amorphous structures, especially the relatively small aromatic rings (3~5 fused rings). In the rest four bands (Gl, Sl, Sr and R), R band (representing alkane structures, cyclic alkane structures or C-H on aromatic rings) is significantly intensive in this study comparing with that in previous work and will be described in the following chapters.

1.2.2 Evolution of char structure during pyrolysis and gasification and its effect on char reactivity

After the establishment of the methodology of char structure characterisation, Li and co-workers [27, 29] initially studied the effects of temperature, coal rank and catalyst on char structure during pyrolysis. It was shown that FT-Raman spectroscopy is a very powerful technique to investigate many aspects of structural features such as the aromatic ring systems, O-containing functional groups, cross-links. During the slow pyrolysis in a TGA [29] and the fast pyrolysis in a fluidised bed [27], different coals

Table 1-2 Summary of Raman band assignment [27]. Copyright (2006), with permission from Elsevier.

Band name	Band position, cm^{-1}	Description	Bond type
Gl	1700	Carbonyl group C=O	sp^2
G	1590	Graphite $E^2{}_{2g}$; aromatic ring quadrant breathing; alkene C=C	sp^2
Gr	1540	Aromatics with 3~5 rings; amorphous carbon structures	sp^2
Vl	1465	Methylene or methyl; semi-circle breathing of aromatic rings; amorphous carbon structures	sp^2, sp^3
Vr	1380	Methyl group; semi-circle breathing of aromatic rings; amorphous carbon structures	sp^2, sp^3
D	1300	D band on highly ordered carbonaceous materials; C-C between aromatic rings and aromatics with not less than 6 rings	sp^2
Sl	1230	Aryl-alkyl ether; para-aromatics	sp^2, sp^3
S	1185	$C_{aromatic}$-C_{alkyl}; aromatic (aliphatic) ethers; C-C on hydroaromatic rings; hexagonal diamond carbon sp^3; C-H on aromatic rings	sp^2, sp^3
Sr	1060	C-H on aromatic rings; benzene (ortho-di-substituted) ring	sp^2
R	960~800	C-C on alkanes and cyclic alkanes; C-H on aromatic rings	sp^2, sp^3

showed large differences in char structure at low temperatures. This difference gradually diminished with increasing temperature. These studies also indicated that the formation of char structures would be influenced by the presence of catalysts (Na and Ca) during pyrolysis. After that, Li and co-workers also studied the changes in char structure during the catalytic gasification in air [31] and steam [32]. The gasification reaction could take place preferentially at the catalyst sites. However, the gasification reactivity was largely affected by the changes in char structure, which influenced the dispersion of catalysts and subsequently determined the catalyst concentration on the char surface. These studies provided direct and quantified experimental evidence about the significant structural changes during gasification and revealed the importance of such changes to gasification reactivity.

Besides the use of Victorian brown coal to study the structural changes, an Australian cane trash was also used to investigate the reactions taking place in the changes in char structure during the gasification in air [33] and steam [34]. The results indicated there were different reaction pathways dominating between the gasification of cane trash in O_2 and in steam. The major distinction was the role of intermediate H radicals, which were produced from the char-steam reactions, deeply penetrating into the char matrix and bringing about the enhancement of ring condensation. Another type of biomass (Australian mallee wood) was also used to investigate the evolution of the char structure from the pyrolysis of feedstock of different particle sizes [35]. The results indicated that the effects of particle size on structural changes were more significant in fast pyrolysis than in slow pyrolysis. Subsequently, the structural changes in fast pyrolysis on the gasification reactivity [36] were further studied. Some fluctuating reactivity was observed for the chars made from the pyrolysis at 800 °C and 900 °C with the increase in char conversion. It was thought to be mainly due to the migration of AAEM species to the surface by the condensation of ring systems. The results suggested that, similar to the brown coal, biomass also showed a significant role of char structure in determining the char reactivity, which changed the distribution of catalysts and subsequently influenced the gasification reactivity. Shu and co-workers [37] continued the work on the effect of the biomass particle size on the structural changes in mallee wood during gasification in steam. For large particle size, they found a significant change in the

distribution of aromatic ring systems during the initial gasification (~30 s) of the fast pyrolysed mallee wood char. It revealed a significant role of free radicals such as H^- and OH^-, which absorbed on the metastable structure in char and caused their rapid breakages. Besides the free radicals produced from the gasification agents, volatiles would also carry a large amount of radicals and interact with char during gasification. Taking advantage of the high extent of volatile-char interactions in a novel fluidised-bed/fix-bed quartz reactor, Shu and co-workers [38] studied the effects of volatile-char interactions on the changes in char structure during the gasification of Loy Yang brown coal in steam. The study indicated that the H radicals originating from volatiles would attach and activate the aromatic ring systems to intensify the aromatic ring condensation.

Recently, the change in the Raman band ratio of $I_{(Gr+Vl+Vr)}$ to I_D, which mainly represents the ratio of small to large aromatic rings (distribution of aromatic ring systems), have been used to judge the reaction pathway during gasification. Guo and co-workers [39] and Tay and co-workers [40, 41] applied this method to evaluate the reaction pathways of char-H_2O, char-O_2 and char-CO_2 reactions. It was concluded that the reaction pathways in the three atmospheres are different under their experimental conditions (holding at 800 °C in the novel fluidised-bed/fixed-bed quartz reactor). Li and co-workers [42] studied the mechanism of char-CO_2 and char-H_2O reactions more deeply. They found that CO_2 and H_2O competed for active sites and the competition most likely happened on the char surface.

In summary, with the application of Raman spectroscopy, extensive work has been done to build new understanding of solid char structure. Much useful information was obtained about the evolution of nascent char structure and its effects on gasification reactivity.

1.3 Justification of this study

Firstly, many experiments carried out in fluidised-bed reactors have shown that the changes in char structure already rapidly occur during the initial feeding process [38,

40, 42]. These studies have suggested the significant changes in the nature of char structure during the initial formation and transformation of nascent char structure. A Wire-mesh reactor, which is well-known for being capable of providing accurate heating rate and residence time, is very suitable to produce "nascent" char during the initial evolution of char properties. Many previous studies used this reactor to investigate the primary pyrolysis over a wide range of temperature, heating rate and pressure. However, these studies mainly focused on the evolution of volatiles. There is still a lack of knowledge about the initial evolution of char structure/properties during pyrolysis and gasification. As mentioned above, Raman spectroscopy is a very powerful technique to quantify the chemical structural features of char. In this study, a wire-mesh reactor was jointly applied with Raman spectroscopy to gain quantitative information of nascent char structure during the initial pyrolysis/gasification steps. After establishing a better understanding of structural changes of nascent char, the effect of nascent char structure and AAEM species on the nascent char reactivity will be finally studied in this thesis.

Secondly, it has been proved that the volatile-char interactions can significantly affect many aspects of char gasification reactions such as the volatilisation of AAEM and the changes in char structure. It is necessary to have a fundamental study about the mechanism of the pyrolysis/gasification of feedstock with the minimisation of volatile-char interactions. The wire-mesh reactor can achieve this due to its unique structure. Briefly, as is shown in Fig. 1-2, a large stream of carrier gas passes through the sample particles vertically at the flow rate of 0.1 m s^{-1} when the sample is heating up. The cooling gas immediately chills the volatiles and take them away from the solid residues (nascent char), preventing the nascent char from interacting with volatiles. Therefore, this study employed a wire-mesh reactor, in order to analyse the changes in char structural properties due to thermal decomposition without interference from volatile-char interactions.

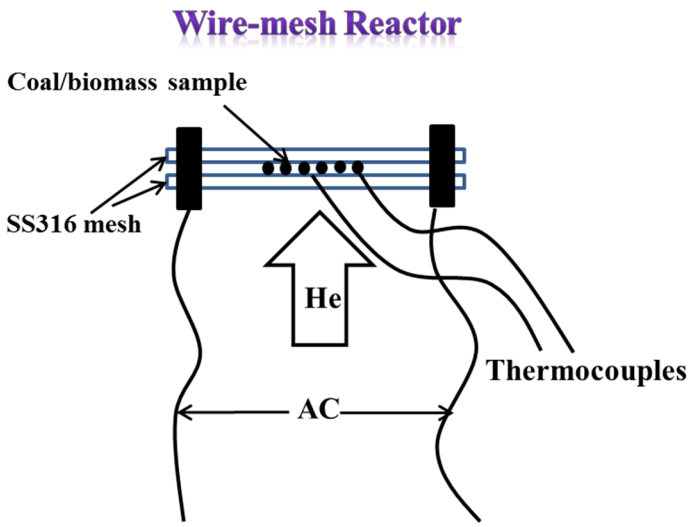

Figure 1-2 Simplified structure of wire-mesh reactor.

Finally, low-rank coals and biomass have high potential to be cleanly and efficiently used by gasification technologies. This study used two low-rank coals and a biomass to study their similarities and differences in the structural changes during the formation and transformation of nascent char.

1.4 Scope of this study

This study examines the formation and transformation of nascent char structure during the pyrolysis and gasification of three fuels. The volatilisation of AAEM species during the pyrolysis of two low rank coals is also investigated. Finally, the effects of char structure and AAEM species on the nascent char reactivity are discussed. There are 7 chapters in this thesis. The structures of the following 6 chapters are given below.

Chapters 2 to 6 describe the experimental results and discussion. Each of the chapters has a section of introduction to introduce the background of that chapter and a section of experimental to describe the related experimental procedure and analysis method.

Chapters 2 and 3 study the formation and transformation of nascent char structure during the fast pyrolysis of three fuels (sub-bituminous coal, brown coal and biomass). Chapter 2 focuses on the initial evolution of structural changes from the raw fuels to nascent char (chars prepared at 600 °C), when the primary volatiles (especially tar) are explosively released. Chapter 3 focuses on the changes in nascent char structure during the further thermal cracking of char particles from 600 to 1200 °C.

Chapter 4 describes the structural changes in nascent char structure during the gasification of sub-bituminous coal and brown coal in CO_2. The rapid changes in char structure during the initial gasification have been discussed at relatively high temperatures of 1000 and 1200 °C. Some chars that were produced from a drop tube furnace (shown in Fig. 1-3) were used for comparison purposes.

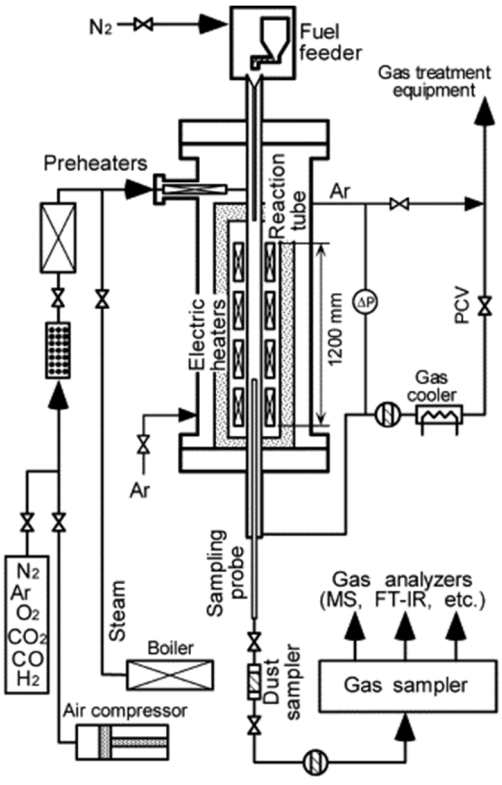

Figure 1-3 Simplified structure of drop tube reactor [43]. Copyright (2006), with permission from Elsevier.

Chapter 5 discusses the behaviour of very reactive structures in nascent char, which was produced from the two coals at 600 °C with 0 s holding, during the further thermal treatment at low temperatures (from 270 to 600 °C). In addition, the changes in the char structure of theses reheated chars during the gasification in O_2 are also investigated to probe the role of nascent char during gasification in O_2.

Chapter 6 studies the combined effects of AAEM species and char structure on the nascent char reactivity. The volatilisation of AAEM species during the fast pyrolysis of the two coals is also investigated.

Chapter 7 presents the conclusions of this study and the recommendations for future work.

1.5 References

[1] BP global. BP energy outlook 2035 booklet. BP 2015.

[2] IEA, World Energy Outlook 2014. Information Energy Agency 2014.

[3] WEC. World energy resources: 2013 survey. World Energy Council 2013.

[4] BP Global. BP statistical review of world energy. BP 2014.

[5] Li C-Z. Special issue-gasification: a route to clean energy. Process Safety and Environmental Protection 2006;84:407-8.

[6] Li C-Z. Importance of volatile-char interactions during the pyrolysis and gasification of low-rank fuels-A review. Fuel 2013;112:609-23.

[7] Bhattacharya S, Tsutsumi A. An overview of advanced power generation technologies using brown coal. In: Li C-Z, editor. Advances in the science of Victorian brown ocal. Oxford: Elsevier; 2004. P. 223-85 [chapter 7].

[8] Tomita A, Ohtsuka Y. Gasification and combustion of brown coal . In: Li C-Z, editor. Advances in the science of Victorian brown ocal. Oxford: Elsevier; 2004. P. 223-85 [chapter 5].

[9] Miura K, Hashimoto K, Silveston PL. Factors affecting the reactivity of coal chars during gasification, and indices representing reactivity. Fuel 1989;68:1461-75.

[10] Mulcahy MFR, Morley WJ, Smith IW. In: Durie RA, editor. The science of Victorian brown coal. Oxford, UK: Butterworth; 1991[chapter 8].

[11] Davis KA, Hurt RH, Yang NYC, Headley TJ. Evolution of char chemistry, crystallinity, and ultrafine structure during pulverizes-coal combustion. Combustion and Flame 1995; 100:31-40.

[12] Russell NV, Gibbins JR, Williamson J. Structural ordering in high temperature coal chars and the effect on reactivity. Fuel 1999; 78:803-7.

[13] Sharma A, Kyotani T, Tomita A. A new quantitative approach for microstructural analysis of coal char using HRTEM images. Fuel 1999; 78:1203-12.

[14] Sharma A, Kyotani T, Tomita A. Direst observation of raw coals in lattice fringe mode using high-resolution transformation electron microscopy. Energy & fuels 2000;14:1219-25.

[15] Feng B, Bhatia SK, Barry JC. Structural ordering of coal char during heat treatment and its impact on reactivity. Carbon 2002;40:481-96.

[16] Lu L, Kong C, Sahajwalla V, Harries D. Char structural ordering during pyrolysis and combustion and its influence on char reactivity. Fuel 2002;81:1215-25.

[17] Roberts MJ, Everson RC, Neomagus HWJP, Niekerk DV, Mathews JP, Branken DJ. Influence of maceral composition on the structure, properties and behaviour of chars derived from South African coals. Fuel 2015;142:9-20.

[18] Wornat MJ, Hurt RH, Yang NYC, Headley TJ. Structural and compositional transformations of biomass chars during combustion. Combustion and Flame 1995;100:131-43.

[19] Miser DE, Baliga VL, Sharma RK, Hajaligol MR. Microstructure of tobacco chars and the origin of associated graphite as determined by high-resolution transmission electron microscopy (HRTEM). Journal of Analytical and Applied Pyrolysis 2003;68-9:425-42.

[20] Wiinikka H, Weiland F, Pettersson E, Ohrman O and Carlsson P etc. Characterisation of submicron particles produced during oxygen blown entrained flow gasification of biomass. Combustion and Flame 2014; 161:1923-34.

[21] Wu S, Gu J, Zhang X, Wu Y, Gao J. Variation of carbon crystalline structure and CO_2 gasification reactivity of Shenfu coal chars at elevated temperatures. Energy and Fuels 2008;22:199-206.

[22] Jing X, Wang Z, Zhang Q, Yu Z, Li C, Huang J, Fang Y. Evaluation of CO_2 gasification reactivity of different coal rank chars by physicochemical properties. Energy and Fuels 2013;27:7287-93.

[23] Jing X, Wang Z, Yu Z, Zhang Q, Li C, Fang Y. Experimental and kinetic investigations of CO_2 gasification of fine chars separated from a pilot-scale fluidized-bed gasifier. Energy and Fuels 2013;27:2422-30.

[24] Min F, Zhang M, Zhang Y, Cao Y, Pan W-P. An experimental investigation into the gasification reactivity and structure of agricultural waste chars. Journal of Analytical and Applied Pyrolysis 2011;92:250-7.

[25] Li Y, Yang H, Hu J, Wang X, Chen H. Effect of catalysts on the reactivity and structure evolution of char in petroleum coke steam gasification. Fuel 2014;117:1174-80.

[26] Bayarsaikhan B, Hayashi J-I, Shimada T, Sathe C, Li C-Z, Tsutsumi A, et al. Kinetics of steam gasification of nascent char from rapid pyrolysis of a Victorian brown coal. Fuel 2005;84:1612-21.

[27] Li X, Hayashi J-I, Li C-Z. FT-Raman spectroscopic study of the evolution of char structure during the pyrolysis of a Victorian brown coal. Fuel 2006;85:1700-7.

[28] Potgieter-Vermaak S, Maledi N, Wagner N, Van Heerden JHP, Grieken RV, Potgieter JH. Raman spectroscopy for the analysis of coal: a review. Journal of Raman Spectroscopy 2010;42:123-9.

[29] Li X, Li C-Z. FT-Raman spectroscopic characterisation of chars from the pyrolysis of coals of varying rank. Journal of Fuel Chemistry and Technology 2005;4:385-90.

[30] Li C-Z. Some recent advances in the understanding of the pyrolysis and gasification behaviour of Victorian brown coal. Fuel 2007;86:1664-83.

[31] Li X, Hayashi J-I, Li C-Z. Volatilisation and catalytic effects of alkali and alkaline earth metallic species during the pyrolysis and gasification of Victorian brown coal. Part VII. Raman spectroscopic study on the changes in char structure during the catalytic gasification in air. Fuel 2006;85:1509-17.

[32] Li X, Li C-Z. Volatilisation and catalytic effects of alkali and alkaline earth metallic species during the pyrolysis and gasification of Victorian brown coal. Part VIII. Catalysis and changes in char structure during gasification in steam. Fuel 2006;85:1518-25.

[33] Keown DM, Li X, Hayashi J-I, Li C-Z. Evolution of biomass char structure during oxidation in O_2 as revealed with FT-Raman spectroscopy. Fuel Processing Technology 2008;89:1429-35.

[34] Keown DM, Hayashi J-I, Li C-Z. Drastic changes in biomass char structure and reactivity upon contact with steam. Fuel 2008;87:1127-32.

[35] Asadullah M, Zhang S, Li C-Z. Evaluation of structural features of chars from pyrolysis of biomass of different particle sizes. Fuel Processing Technology 2010; 91:877-81.

[36] Asadullah M, Zhang S, Min Z, Yimsiri P, Li C-Z. Effects of biomass char structure on its gasification reactivity. Bioresource Technology 2010;101:7935-43.

[37] Zhang S, Min Z, Tay H-L, Wang Y, Dong L, Li C-Z. Changes in char structure during the gasification of mallee wood: effects of particle size and steam supply. Energy & Fuels 2012;26:193-8.

[38] Zhang S, Min Z, Tay H-L, Asadullah M, Li C-Z. Effects of volatile-char interactions on the evolution of char structure during the gasification of Victorian brown coal in steam. Fuel 2011;90:1529-35.

[39] Guo X, Tay H-L, Zhang S, Li C-Z. Changes in char structure during the gasification of a Victorian brown coal in steam and oxygen at 800 °C. Energy & Fuels 2008;22:4034-8.

[40] Tay H-L, Li C-Z. Changes in char reactivity and structure during the gasification of a Victorian brown coal: Comparison between gasification in O_2 and CO_2. Fuel Processing Technology 2010;91:800-4.

[41] Tay H-L, Kajitani S, Zhang S, Li C-Z. Effects of gasifying agent on the evolution of char structure during the gasification of Victorian brown coal. Fuel 2013;103:22-8.

[42] Li T, Zhang L, Dong L, Li C-Z. Effects of gasification atmosphere and temperature on char structural evolution during the gasification of Collie sub-bituminous coal. Fuel 2014;117:1190-5.

[43] Kajitani S, Suzuki N, Ashizawa M, Hara S. CO_2 gasification rate analysis of coal char in entrained flow coal gasifier. Fuel 2006;85:163-9.

Chapter 2

Formation of nascent char structure during the fast pyrolysis of mallee wood and low-rank coals

2.1 Introduction

Gasification converts solid fuels into clean syngas and is the core of many low-emission energy technologies [1]. As the char gasification rate controls the overall gasification rate [2], effort has been made to evaluate the possible factors influencing the char reactivity [2-4]. Among many important factors, the structural evolution of char has been shown [4-17] to be a significant aspect that affects the changes in coal [4-7] or biomass [8-11] char reactivity and the behaviour of catalysts [13-15].

The formation of char is complicated. Several structural changes could take place in the initial transition from coal to char with the concurrent release of volatiles. For example, while large aromatic and heteroaromatic ring systems (e.g. with more than 4 or 5 fused benzene rings) dominate in the char structure, they exist in low-rank coals at relatively low concentrations [18, 19]. The long-chain aliphatics in a low-rank coal are almost absent in its chars formed at 600 °C and higher [20]. Many O-containing functional groups (e.g. carboxylic acids) in abundance in a low-rank coal will also be decomposed and released as gases [20] during the initial process to form a char. Some recent studies in our group focused on the changes in relatively "old" char structure during pyrolysis/gasification in fluidised bed for biomass [8-11] and low-rank coal [12-14, 16-17]. However, there is a lack of experimental data on the detailed structural features of the newly formed (nascent) char. The time scale for the conversion of coal to char is very short: the evolution of tar is completed as soon as the coal particles are heated up to 600 °C at 1000 K s^{-1} [21, 22]. Very few reactors are capable of providing a well-controlled heating rate and a high resolution of holding time. A wire-mesh reactor [21-23] is one reactor that can control linear heating rate over a wide range from 0.1-5000 K s^{-1} and to provide holding time in increments of 10 ms.

Volatile-char interactions can drastically change the pathway of char structural evolution [3]. A wire-mesh reactor has the special advantage in that volatiles, once released from the parent pyrolysing coal/char particles, are swept away and will have minimal inter-particle interactions with the char particles. Therefore, the wire-mesh

reactor provides a means to investigate the structural formation of nascent char in the absence of the influence of volatile-char interactions.

A quantitative method to describe the char chemical structural features is a necessity to trace the development of char structure during pyrolysis. Our recent studies have shown that FT-Raman spectroscopy combined with spectral deconvolution is a powerful technique to semi-quantify the structural features of chars produced from the pyrolysis/gasification of biomass [8-11] and coal [12-14, 16-17]. The FT-Raman spectra of coal/char over the range between 800 and 1800 cm^{-1} were deconvoluted into 10 bands [12]. The overall changes in the aromatic structures, oxygen-containing functional groups and cross-links can be investigated.

The purpose of this study is to characterise the chemical structural features of nascent chars during the pyrolysis of Loy Yang brown coal, Collie sub-bituminous coal and Western Australian mallee wood. By using FT-Raman spectroscopy for the analysis of the chars prepared in a wire-mesh reactor, our results reveal some details about the structural evolution of the nascent char, especially the changes in char structure during the initial release of tar at < 600 °C with 1000 K s^{-1} heating rate and the changes after further holding at 600 °C with the holding time up to 50 s. All experiments were carried out at atmospheric pressure.

2.2 Experimental

2.2.1 Samples preparation

Collie sub-bituminous coal from Western Australia, Loy Yang brown coal from Victoria and mallee wood from Western Australia were used. The preparation procedure of Collie coal was the same as that for Loy Yang coal [24]. Briefly, “as mined” coal with particle sizes mainly around 10-20 cm was obtained and dried at ambient temperature. The air-dried raw coal was pulverised and screened to the particle size range of 106-150 μm. The preparation of mallee wood was described

elsewhere [25]. The wood with particle size range of 180-400 μm was chosen. As the mallee wood particles were long and thin, the particles were cut into circular-like pieces by knife to obtain a better particle distribution on the sample holder. The proximate and ultimate analyses of the three fuels are shown in Table 2-1.

Table 2-1 Properties of three fuels [10,16,26]

	Proximate analyses (wt%)		Ultimate analyses (wt%)				
	Ash[a]	Volatile matter[b]	C[b]	H[b]	N[b]	S[b]	O[b.c]
Mallee wood	0.9	81.6	48.2	6.1	0.2	0.0	45.5
Loy Yang coal	1.1	52.2	70.4	5.4	0.6	0.3	23.3
Collie coal	5.7	38.8	75.7	4.5	1.4	0.5	17.9

(a, dry basis; b, dry and ash-free basis; c, by difference)

2.2.2 Pyrolysis

The pyrolysis of the three fuels was carried out using a wire-mesh reactor at a fast heating rate of 1000 K s^{-1}. The details of the wire-mesh reactor and the operation procedure can be found elsewhere [23, 24]. Briefly, a small amount of coal or biomass (typically less than 10 mg) was sandwiched between two layers of mesh made from grade 316 stainless steel with an aperture of 45 μm. The mesh was stretched between two electrodes for heating samples with an alternating current. During the heating of the particles, a stream of ultra-high purity helium passed through the mesh vertically at the flow rate of 0.1 m s^{-1} (measured under ambient conditions). With the contribution of the cooling carrier gas (helium), volatiles were quenched and removed out of char immediately after evolution from the samples to minimise the volatile-char interactions.

The temperature of sample was detected by two pairs of chromel/alumel alloy wires. One pair was inserted at the centre of the area containing the coal particles and the other was inserted at around 1 mm from the edge. The average of these two temperatures was used as a feedback for controlling the mesh temperature with a

PID control system. The holding time can be pre-set and controlled at 10 ms increments. The empty stainless steel sample holder was preheated to the target temperatures to prevent further weight loss in pyrolysis experiments. A balance with precision of 0.01 mg was used for all weight measurement. Char yield was determined by the difference in the weight of the loaded sample holder before and after an experiment. In addition, all the char in a single experiment was collected and directly mixed with KBr for Raman analysis.

2.2.3 Raman spectroscopy for char characterisation

The FT-Raman spectra of fuels and chars were acquired by using a Perkin-Elmer Spectrum GX FT-Raman spectrometer. The fuel/char sample was mixed, diluted and ground with spectroscopic grade potassium bromide (KBr) that was used as a heat dissipating agent [12]. The selection of coal/char concentration in KBr will be discussed in Section 2.3.3.1. The Raman spectra in the range between 800 and 1800 cm^{-1} were deconvoluted into 10 Gaussian bands. The assignment of 10 bands was summarised in our previous study [12]. An example of Raman spectrum with 10 bands deconvolution is shown in Fig. 2-1. The total Raman area and Raman band ratios were used to characterise the fuel/char structural features in this study.

2.3 Results and discussion

2.3.1 Char yields of three fuels during initial pyrolysis

Figure 2-2 shows the changes in char yield as a function of holding time during the pyrolysis of Loy Yang brown coal, Collie sub-bituminous coal and Western Australia mallee wood at 600 °C with a heating rate of 1000 K s^{-1}. All the char yields were on dry basis. As shown in Fig. 2-2, the char yields of all three fuels had fast declines within 1 s and then only slight changes in weight loss were observed during further holding. The differences in char yields between three fuels were quite large at 600 °C; these differences were firstly observed with 0 s holding at 600 °C. The 0 s

holding means the char only underwent the heating from room temperature to 600 °C at 1000 K s^{-1} and then naturally cooled down to the room temperature without any residence at peak temperature.

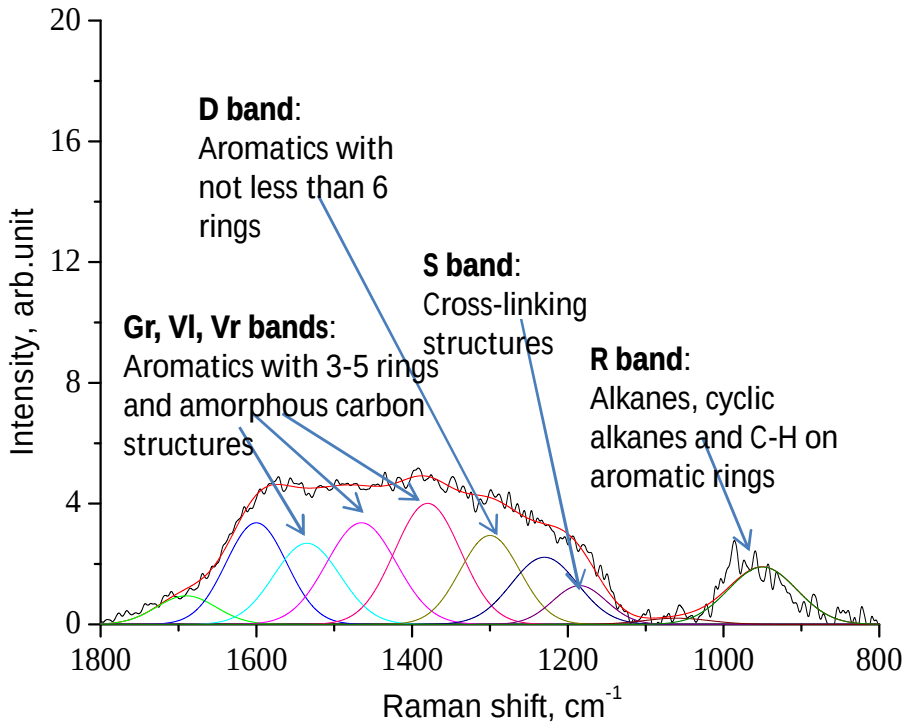

Figure 2-1 Deconvolution of a Raman spectrum of Loy Yang char pyrolysed at 600 °C with 0 s holding. Redrawn using new data based on that in [12], Copyright (2006), with permission from Elsevier.

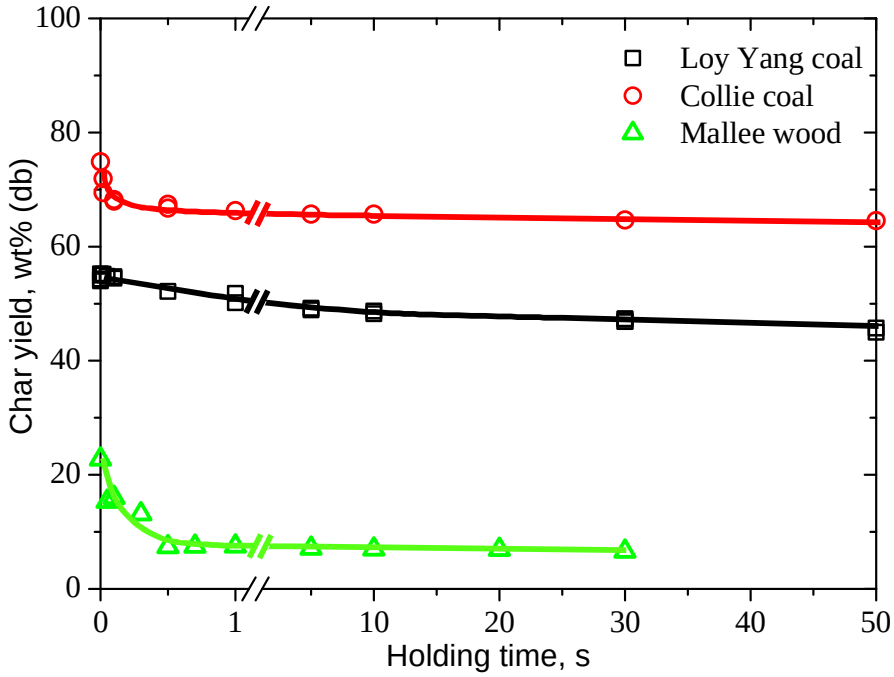

Figure 2-2 Char yields of three fuels as a function of holding time at 600 °C.

2.3.2 Raman spectra of raw fuels and nascent chars

Figure 2-3 shows the Raman spectra of three fuels and their nascent chars with 0 s and 10 s holding. Mallee wood had a distinctively different spectrum from other two fuels/chars. It is indicated that the structure of mallee wood that is different from the coals/chars could not be deconvoluted by the same method. However, after fast heating to 600 °C, the Raman spectrum of mallee wood char showed a similar shape to those of coal chars.

The changes in the Raman spectra of three fuels mainly occurred in three areas. Firstly, the Raman intensity decreased at wavenumbers between 1300 cm^{-1} (D band) and 1590 cm^{-1} (G band). The overlap between D band and G band is normally divided into 3 bands (Gr, Vl and Vr) which represent the highly disordered amorphous carbon structure and small aromatic rings with 3-5 rings. Secondly, the D band at 1300 cm^{-1}, which represents large aromatic rings with $\geq$ 6 rings, showed a gradual growth during pyrolysis. Thirdly, the band at ~960 cm^{-1}, which is called the R band, decreased significantly during the initial pyrolysis of all three fuels. It

mainly represents the alkane structures, cyclic alkane structures or C-H on aromatic rings. In order to analyse the changes in char structural features during fast pyrolysis, the Raman spectra were deconvoluted into 10 bands, which are shown in Fig. 1. The changes in total Raman area, (Gr+Vl+Vr)/D, S band and R band will be discussed in the following sections.

2.3.3 Changes in char structure during the initial pyrolysis

2.3.3.1 Total Raman area as a function of coal/char concentration in coal/char-KBr mixture

Figure 2-4 shows the total Raman areas between 800 and 1800 cm^{-1} as a function of coal/char concentration in the coal/char-KBr mixture of three fuels. It is clear that, for all char samples, with the increase in coal/char concentration in the mixture, the Raman intensity has an initial rapid increase and gradually reaches a plateau. Our previous work indicated that the char that had higher light absorptivity would cause the total Raman area to reach the plateau much quicker and at a much lower concentration [12]. As discussed in Section 2.3.2, the Raman spectrum of raw mallee wood was different from that of coals and chars that cannot be deconvoluted by the 10 bands method. Therefore, the total Raman area of the two raw coals and the nascent chars of the three fuels were studied in this section. As shown in Fig. 2-4 (a), the total Raman area of Loy Yang coal had not reached a plateau at a concentration of 5%. It is indicated that Loy Yang coal is not rich in structures with high light absorptivity such as large aromatic ring systems. Additionally, the higher total Raman area of Loy Yang coal than that of Collie coal indicated greater amounts of O-containing functional groups in the Loy Yang coal. Although the total Raman area of Loy Yang coal was much higher than that of Collie coal, the total Raman area of the chars produced at 600 °C with 0 s holding [Fig. 2-4 (b)] were close for the two coals. The reason for this rapid decrease in total Raman area of Loy Yang coal will be discussed in following sections. For the mallee wood char produced at 600 °C with 0 s holding [Fig. 2-4 (b)], it reached a plateau at ~0.8%. However, for the mallee wood chars produced at 600 °C with 0.1 s holding, the total Raman area

reached a plateau at concentrations < 0.25%. Fig. 2-4 (b) also shows that a concentration of 0.25% was high enough for the total Raman area of the chars from the two coals to reach a plateau.

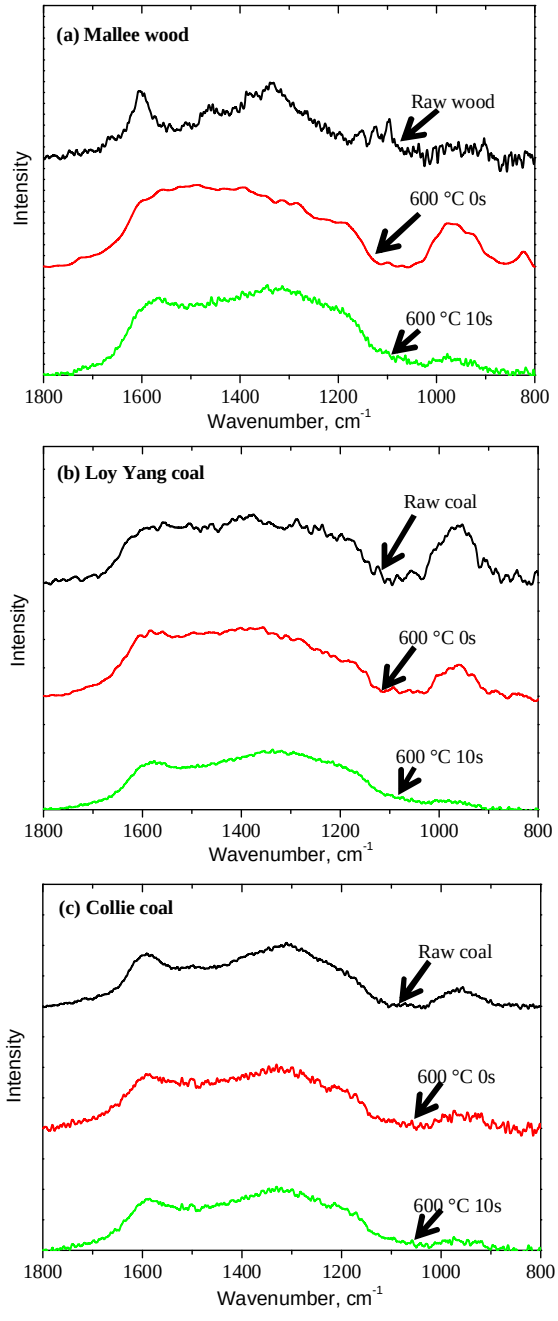

Figure 2-3 Raman spectra of three fuels and their nascent chars.

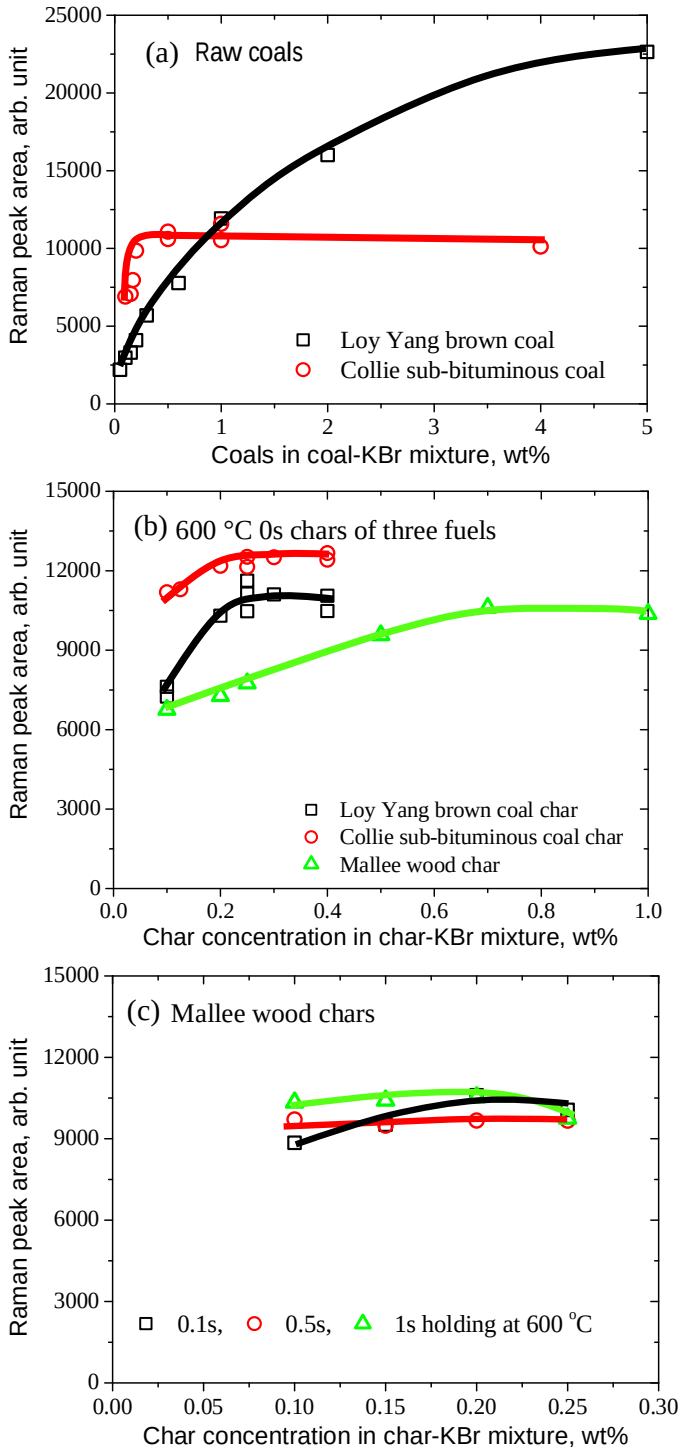

Figure 2-4 Total Raman areas of coal/char as a function of the concentration of coal or char in coal/char-KBr mixture.

2.3.3.2 Changes in total Raman area during initial pyrolysis

The total Raman areas between 800 and 1800 cm^{-1} as a function of holding time and temperature are shown in Fig. 2-5. The data at 100% char yield represent the total Raman areas of two raw coals, while all the other points refer to the total Raman areas of the chars produced from the pyrolysis of three fuels at 600 °C. The starting point of mallee wood char in Fig. 2-5 was the char produced at 600 °C with 0 s holding time. The sample concentrations in the sample-KBr mixtures for Loy Yang raw coal and Collie raw coal were chosen as 5% and 1%. As was mentioned above, the total Raman area of Loy Yang raw coal had not reached the plateau value when the concentration was 5%. Therefore, the actual plateau total Raman area of Loy Yang coal would be expected to be higher than the value shown in Fig. 2-5. The concentration of all other samples was selected where the total Raman area of nascent chars already reached a plateau (Fig. 2-4).

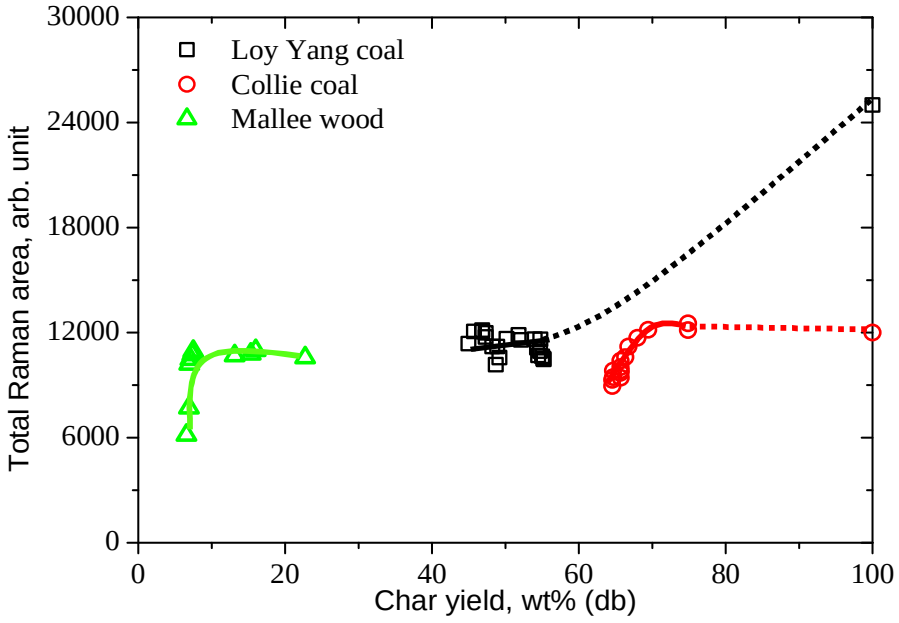

Figure 2-5 Total Raman areas of raw fuels and their chars produced by pyrolysis at 600 °C, as a function of char yield. The residence time of mallee wood was 0-30 s and two coals was 0-50 s at 600 °C.

Total Raman area is mainly affected by the oxygen containing functional groups and the aromatic ring systems. The former would have a resonance effect with the aromatic ring to which it connects and increase the Raman scattering intensity, while the latter would enhance the light absorptivity and weaken the Raman intensity. As shown in Fig. 2-5, the total Raman area of Loy Yang coal decreased significantly during initial heating from raw coal at the char yield of 100% to nascent char (600 °C with 0 s holding) at the char yield of 55%, while the total Raman area changed little during holding at 600 °C. As for Collie coal, negligible changes in total Raman area occurred during heating from raw coal to nascent char (600 °C with 0 s holding), while a rapid decrease took place in the total Raman area of Collie coal when the nascent char was holding at 600 °C. Similarly, mallee wood also showed a rapid decline in total Raman area during holding at 600 °C. For all of the decreases in the total Raman area of the three fuels, it might be attributed to the loss of O-containing functional groups and/or the condensation of aromatics, which will be discussed further below.

2.3.3.3 Changes in ring systems during initial pyrolysis

Figure 2-6 shows the changes in the ratio of $I_{(Gr+Vl+Vr)}$ to I_D that refers to the ratio of small (3 to 5 rings) to large aromatic rings (≥ 6 rings) during the initial pyrolysis of the two coals from room temperature to 600 °C and the further pyrolysis of the three fuels during holding at 600 °C.

For Loy Yang coal, char yield decreased from 100 to ~55% during the heating from room temperature to 600 °C (with 0 s holding), while negligible change was observed in the ratio between small and large rings. During the initial pyrolysis of Collie coal, the char yield dropped from 100 to ~75% with only very slight increase in the ratio of small to large rings when heating from room temperature to 600 °C. It is indicated that little changes happen in aromatic ring systems during the initial pyrolysis for two coals. Additionally, as was shown in Fig. 2-2, volatiles from two coals were rapidly released during initial heating from room temperature to 600 °C.

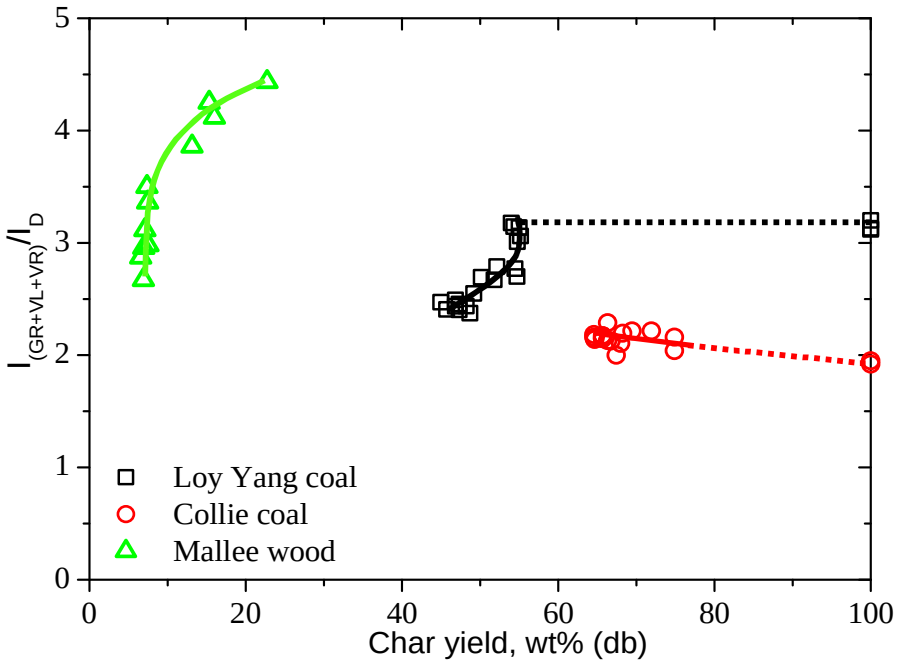

Figure 2-6 $I_{(GR+VL+VR)}/I_D$ of raw fuels and their chars produced by pyrolysis at 600 °C, as a function of char yield. The residence time of mallee wood was 0-30 s and two coals was 0-50 s at 600 °C.

During this explosive release of volatiles, most tar molecules that were rich in aromatic rings were also released [21, 22]. The source of these aromatic rings in tar might be from the direct detachment of original aromatic rings from the parent fuels, or from the newly formed aromatics via reactions such as dehydrogenation of hydroaromatics. Therefore, the negligible changes in Collie coal and Loy Yang coal on heating up suggested that the formation and growth (if any) of aromatic rings during the release of tar would have very limited effects on aromatic ring systems in the two coals. In other words, the tar precursor might be mainly formed through the breakage of aliphatic structures and released with little effect on the original ring systems in the residual chars.

Besides the tar evolution, there are other factors that may affect the formation of ring systems in char. Firstly, the aromatic rings in volatiles may recombine on the char matrix to form more condensed aromatic rings. Secondly, the loss of substituent groups during the initial pyrolysis may create free sites on aromatic rings, which

combine to form larger ring systems or cross-links. However, as discussed above, insignificant changes in ring systems were observed for the two coals. It may be due to two reasons. Firstly, during fast pyrolysis, the volatile precursors largely build up the pressure within the pyrolysing coal particles and release explosively [22]. Thus, the volatiles only have a very short residence time to react with char. Secondly, the presence of long chain aliphatic or other bulky substitution groups in low-rank coals may create steric hindrance for the recombination of free sites on char [27], causing the free sites to be well detached and preventing the formation of larger rings and cross-links. In any case, the structures in coal were not reactive enough to form additional aromatic structures during the very short period of heating up.

During holding at 600 °C, the three fuels showed different extents of changes in ring systems. With the decrease in char yield from ~75 to ~65%, Collie coal showed insignificant changes in ring systems during holding up to 50 s. With the decrease in char yield from ~55 to ~45%, Loy Yang coal showed significant decreases in the ratio of $I_{(Gr+Vl+Vr)}/I_D$ within the holding time of 50 s. This could be attributed to the selective loss of small aromatic ring systems or the condensation of ring systems. However, the changes in the total Raman area as a function of char yield shown in Fig. 2-5 revealed that there was no significant change during holding at 600 °C for Loy Yang coal. As ring condensation would greatly increase the light absorptivity of char and decrease the total Raman area, the decrease in $I_{(Gr+Vl+Vr)}/I_D$ with little change in total Raman area should be mainly due to the selective release of small ring systems, although some ring growth cannot be ruled out. Mallee wood also showed a decrease in ratio between small and large rings during holding at 600 °C up to 30 s. However, it decreased gradually before the char yield reached 9% and then decreased significantly after the char yield reduced to < 9%. At the char yield > 9%, with the decrease in $I_{(Gr+Vl+Vr)}/I_D$, the total Raman area changed little with decrease in char yield (Fig. 2-5), indicating it was mainly due to the selective release of small ring systems. By contrast, after further holding at 600 °C, the char yield changed very little while the ratio decreased sharply. This indicates that the changes is mainly due to ring condensation that results in the conversion of small to large ring systems with the release of very light gases: particularly H_2. The decline in the

total Raman area of mallee wood, shown in Fig. 2-5, might be mainly due to the ring condensation and the loss of O-containing functional groups.

Comparing the differences in the formation of ring systems in three fuels during holding at 600 °C in Fig. 2-6, it is clear that the three fuels have different ratios of small to large rings at the beginning of holding ($I_{(Gr+Vl+Vr)}/I_D$ of mallee wood at ~23% > Loy yang coal at ~55% > Collie coal at ~75%). Subsequently, it is easier to have thermal decomposition or condensation of ring systems taken place for the brown coal and wood than that for the sub-bituminous coal. It is suspected that the smaller ring systems in char have fewer cross-links than the bigger ones [28]. Therefore, the thermal breakdown would be easier in the brown coal and wood that are richer in smaller rings than in sub-bituminous coal at the same temperature. This view is supported by the greater release of volatiles for brown coal and wood than sub-bituminous coal shown in Fig. 2-2.

As was discussed in Section 2.3.3.2, the decrease in the total Raman area of the three fuels shown in Fig. 2-5 might be attributed to two reasons: the loss of O-containing functional groups and/or the condensation of aromatics. On the basis of the discussion about the ring systems above, for the two coals, with the total Raman area decreasing (Fig 2-5), insignificant changes in ring systems were observed (Fig. 2-6). This reveals that the reduction in Raman intensity is mainly due to the loss of O-containing functional groups. Correlating the changes in the total Raman area (Fig. 2-5) with the changes in the ratio of small to large rings (Fig. 2-6), the two coals showed different reaction pathway from mallee wood. As for the two coals, the total Raman area significantly decreased when the ratio of small to large rings changed little (Loy Yang coal at char yield from 100 to ~55%; Collie coal at char yield from ~75 to ~65%). However, for mallee wood, the total Raman area decreased when the aromatic ring systems correspondingly changed (mallee wood at char yield < 9%). This suggests that the reactions for the release of O-containing functional groups and those for the changes in ring size distribution happens independently for the two coals but simultaneously for mallee wood.

2.3.3.4 Changes in cross-links during initial pyrolysis

The ratios of S band area to the total Raman area as a function of holding time and temperature are shown in Fig. 2-7. It represents cross-links in the carbonaceous structure. Although there were large amounts of volatiles released, Loy Yang coal and mallee wood showed little increase in the relative intensity of S band during the initial stage of pyrolysis. The reason for this might be the same as the reason for the insignificant changes in ring systems during initial pyrolysis shown in Section 2.3.3.3. Briefly, the residence time of volatile precursors in the nascent char particle was too short for significant secondary reaction involving volatile precursors to take place. Furthermore, the possible free radical sites generated in char from the breakage of the bulky substitution groups in biomass or Loy Yang coal caused the free sites must have been well separated for them to recombine. Both reasons enhanced the chance for the free sites to be stabilised rather than to form cross-links. Collie coal showed slightly higher cross-links than the other fuels during initial heating. It might be attributed to the lower amount of volatiles released during the initial pyrolysis and the more cracking of structures in char for enhanced formation of cross-links and more cross-links were original existing in Collie coal. During holding at 600 °C, a rapid increase in cross-links was observed for all three fuels. It implies that the significant formation of cross-links follows the thermal decomposition of bulky substitutions.

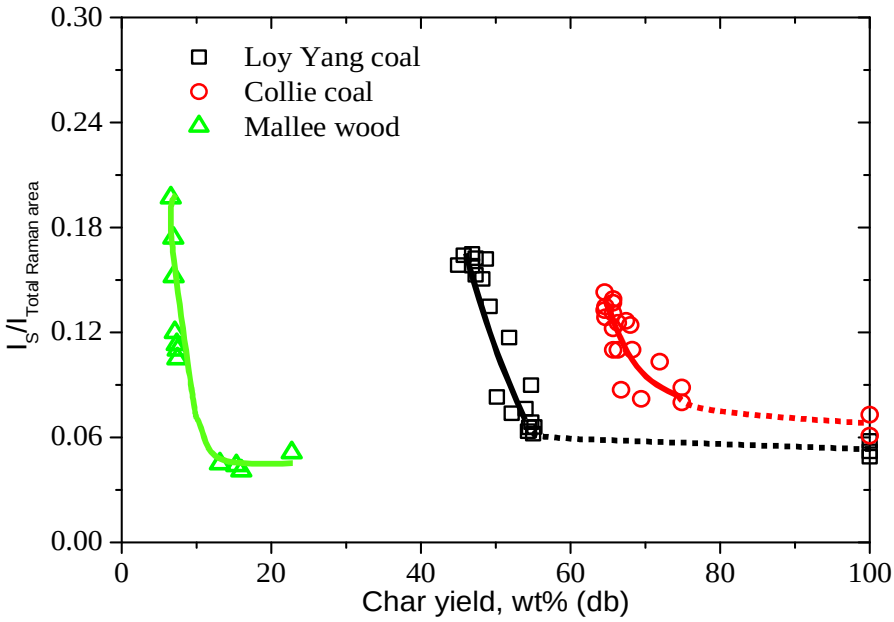

Figure 2-7 $I_S/I_{Total\ Raman\ area}$ of raw fuels and their chars produced by pyrolysis at 600 °C, as a function of char yield. The residence time of mallee wood was 0-30 s and two coals was 0-50 s at 600 °C.

2.3.3.5 Changes in R band during initial pyrolysis

The ratios of the R band area to the total Raman area as a function of char yield are shown in Fig. 2-8. The R band represents the presence of alkane structures, cyclic alkane structures (e.g. hydro-aromatics) or the C-H bond on aromatic rings. Given the highly reactive nature of these aliphatic and cyclic aliphatic structures, the changes in the relative R band intensity provide another dimension of the structural transformation from fuel to nascent char.

Again, three fuels show very different behaviours. For the Collie sub-bituminous coal, the initial heating up to 600 °C caused little changes in the relative intensity of the R band, indicating that the release of volatiles was quick and that the volatiles had very similar structures (in terms of R band) to the remaining nascent char. On holding at 600 °C, the hydroaromatics would dehydrogenate and some aliphatic long chain structures would be broken off.

The data in Fig. 2-8 indicate that significant changes in the R band intensity took place during the initial heating/devolatilisation of the Loy Yang brown coal. Clearly, the volatiles released had different structures from the remaining char. Certainly, much of the long-chain aliphatics would be released during the initial release of volatiles due to the high heating rate. On holding, the relative R band intensity decreased rapidly, most probably due to the combined effects of dealkylation and dehydrogenation of hydroaromatics structures.

The nascent char from wood also underwent drastic changes in the relative intensity of the R band. In addition to dealkylation and dehydrogenation reactions mentioned above for the brown coal and sub-bituminous coal, dehydration reactions (e.g. the dehydration of sugar-type structures) followed by the growth of aromatic rings would have also contributed to the changes in the R band intensity.

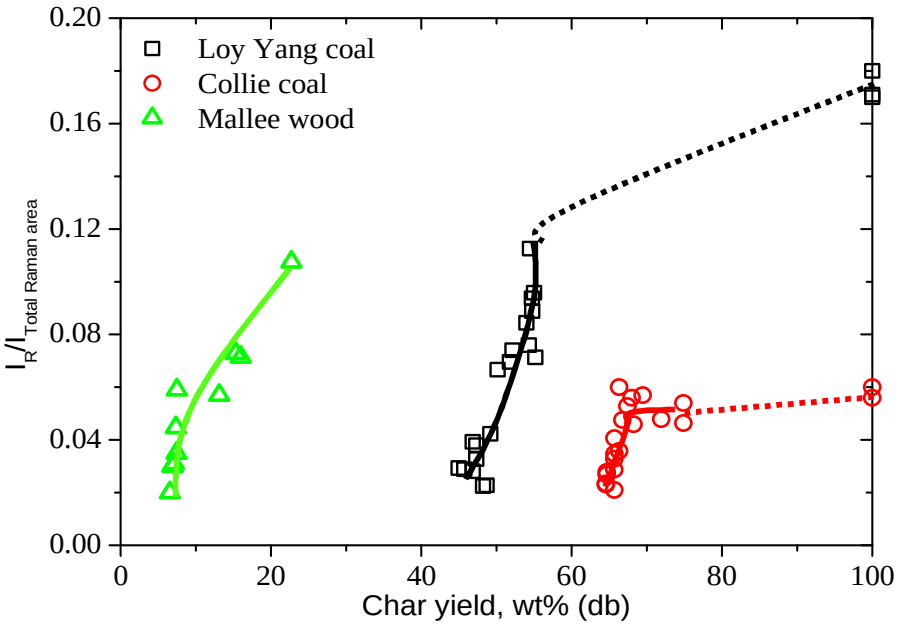

Figure 2-8 $I_R/I_{\text{Total Raman area}}$ of raw fuels and their chars produced by pyrolysis at 600 °C, as a function of char yield. The residence time of mallee wood was 0-30 s and two coals was 0-50 s at 600 °C.

2.4 Conclusions

This study was an investigation of the reactions taking place during the transition from coal/biomass to char, in particular the formation of structural features of nascent char.

1. Mallee wood has different reaction pathway from two coals during the formation of nascent char structure. Mallee wood shows a significantly different carbon structure to that of coals (Raman spectroscopy). However, it changed significantly during initial pyrolysis and approached the carbon structure of coal chars.

2. The release of O-containing functional groups (in terms of total Raman area) occurred independently with the changes in ring size distribution for the two coals but simultaneously for mallee wood.

3. All three fuels showed selective release of small aromatic ring systems during holding at 600 °C. However, only mallee wood showed ring condensation during holding at 600 °C (char yield < 9%).

4. Loy Yang brown coal and Collie sub-bituminous coal show only slight changes in ring systems and cross-linking structures during the initial heating process when there were large amounts of volatiles released. Since tar molecules are primarily released during the initial heating process, the insignificant changes in ring systems of two coals indicated that the formation and release of ring systems in tar mainly occurred through the breakage of aliphatic structures and released with little effect on the original ring systems in the two coals.

5. During holding at 600 °C, when the release of volatiles was low, different changes in ring systems occurred for the three fuels. The lower-rank fuels that were rich in small aromatic rings more readily underwent decomposition and/or condensation of ring systems than the higher-rank fuel.

6. The R band represents alkane structures, cyclic alkane structures or C-H on aromatic rings, which are very reactive; the R band of three fuels decreased very fast during holding at 600 ℃ up to 50 s.

2.5 References

[1] Li C-Z. Special issue-gasification: a route to clean energy. Process Safety and Environmental Protection 2006;84:407-8.

[2] Miura K, Hashimoto K, Silveston PL. Factors affecting the reactivity of coal chars during gasification, and indices representing reactivity. Fuel 1989;68:1461-75.

[3] Li C-Z. Some recent advances in the understanding of pyrolysis and gasification behaviour of Victorian brown coal. Fuel 2007;86:1664-83.

[4] Van Heek KH, Mühlen HJ. Aspects of coal properties and constitution important for gasification. Fuel 1985;64:1405-14.

[5] Davis KA, Hurt RH, Yang NYC, Headley TJ. Evolution of char chemistry, crystallinity, and ultrafine structure during pulverized-coal combustion. Combustion and Flame 1995;100:31-40.

[6] Senneca O, Salatino P, Masi S. Microstructural changes and loss of gasification reactivity of chars upon heat treatment. Fuel 1998;77:1483-93.

[7] Chan M-L, Jones JM, Pourkashanian M, Williams A. The oxidative reactivity of coal chars in relation to their structure. Fuel 1999;78:1539-52.

[8] Keown DM, Hayashi J-I, Li C-Z. Drastic changes in biomass char structure and reactivity upon contact with steam. Fuel 2008;87:1127-32.

[9] Keown DM, Li X, Hayashi J-I, Li C-Z. Characterization of the structural features of char from the pyrolysis of cane trash using fourier transform-Raman spectroscopy. Energy & Fuels 2007;21:1816-21.

[10] Asadullah M, Zhang S, Min Z, Yimsiri P, Li C-Z. Effects of biomass char structure on its gasification reactivity. Bioresource Technology 2010;101:7935-43.

[11] Zhang S, Min Z, Tay H-L, Wang Y, Dong L, Li C-Z. Changes in char structure during the gasification of mallee wood: effects of particle size and steam supply. Energy & Fuels 2012;26:193-8.

[12] Li X, Hayashi J-I, Li C-Z. FT-Raman spectroscopic study of the evolution of char structure during the pyrolysis of a Victorian brown coal. Fuel 2006;85:1700-7.

[13] Li X, Li C-Z. Volatilisation and catalytic effects of alkali and alkaline earth metallic species during the pyrolysis and gasification of Victorian brown coal. Part VIII. Catalysis and changes in char structure during gasification in steam. Fuel 2006;85:1518-25.

[14] Li X, Hayashi J-I, Li C-Z. Volatilisation and catalytic effects of alkali and alkaline earth metallic species during the pyrolysis and gasification of Victorian brown coal. Part VII. Raman spectroscopic study on the changes in char structure during the catalytic gasification in air. Fuel 2006;85:1509-17.

[15] Wu H, Hayashi J-I, Chiba T, Takarada T, Li C-Z. Volatilisation and catalytic effects of alkali and alkaline earth metallic species during the pyrolysis and gasification of Victorian brown coal. Part V. Combined effects of Na concentration and char structure on char reactivity. Fuel 2004;83:23-30.

[16] Tay H-L, Li C-Z. Changes in char reactivity and structure during the gasification of a Victorian brown coal: Comparison between gasification in O_2 and CO_2. Fuel Processing Technology 2010;91:800-4.

[17] Guo X, Tay H-L, Zhang S, Li C-Z. Changes in char structure during the gasification of a Victorian brown coal in steam and oxygen at 800 °C. Energy & Fuels 2008;22:4034-8.

[18] Kashimura N, Hayashi J-I, Li C-Z, Sathe C, Chiba T. Evidence of poly-condensed aromatic rings in a Victorian brown coal. Fuel 2004;83:97-107.

[19] Hayashi J-I, Li C-Z. Structure and properties of Victorian brown coal. In: Li C-Z, editor. Advances in the science of Victoria brown coal. Oxford: Elsevier; 2004. P. 11-77 (Chapter 2).

[20] Hayashi J-I, Miura K. Pyrolysis of Victorian brown coal. In: Li C-Z, editor. Advanced in the science of Victorian brown coal. Oxford: Elsevier; 2004. P. 134-217(Chapter 4).

[21] Sathe C, Hayashi J-I, Li C-Z. Release of volatiles from the pyrolysis of a Victorian lignite at elevated pressures. Fuel 2002;81:1171-8.

[22] Jamil K, Hayashi J-I, Li C-Z. Pyrolysis of a Victorian brown coal and gasification of nascent char in CO_2 atmosphere in a wire-mesh reactor. Fuel 2004;83:833-43.

[23] Gibbins J.R., King R.A.V., Wood R.J., Kandiyoti R.. Variable-heating-rate wire-mesh pyrolysis apparatus. Review of Scientific Instruments 1989;60:1129-39.

[24] Sathe C, Pang Y, Li C-Z. Effect of heating rate and ion-exchangeable cations on the pyrolysis yields from a Victorian brown coal. Energy & Fuels 1999;13:748-55.

[25] Asadullah M, Zhang S, Li C-Z. Evaluation of structural features of chars from pyrolysis of biomass of different particle sizes. Fuel Processing Technology 2010; 91:877-81.

[26] Li T, Zhang L, Dong L, Li C-Z. Effects of gasification atmosphere and temperature on char structural evolution during the gasification of Collie sub-bituminous coal. Fuel 2014;117:1190-5.

[27] Sathe C. Fates and roles of alkali and alkaline earth metallic species during the pyrolysis of low-rank coals. PhD Thesis, Monash University, 2001:189-98.

[28] Li C-Z, Madrali E.S, Wu F, Xu B, Cai H-Y, Güell AJ et al. Comparison of thermal breakdown in coal pyrolysis and liquefaction. Fuel 1994;73:851-65.

Chapter 3

Structural transformation of nascent char during the fast pyrolysis of mallee wood and low-rank coals

3.1 Introduction

Gasification is a well-known technology that efficiently converts solid fuels into clean syngas. Low-rank fuels (e.g. brown coal and biomass) have been considered as suitable feedstocks for gasification due to their high gasification reactivities [1]. Conceptually, low-rank fuels undergo two consecutive steps during gasification: the initial fast pyrolysis to produce tar, light gases and nascent char and the subsequent gasification of these products with gasifying agents such as steam, oxygen and carbon dioxide. During the initial gasification, the reactivity of nascent char reduces rapidly when exposed to high temperatures in a gasifier. Further conversion of the char is the rate-controlling step that is relatively slow and determines the overall gasification reactivity [2]. Many factors have been found to correlate with the reduction of char gasification reactivity [2-5].

The structural evolution of char is one of the key factors that results in char deactivation [3-10]. Many techniques have been applied to characterise structural features of char, such as X-ray diffraction (XRD), high-resolution transmission electron microscopy (HRTEM), FT-IR spectroscopy and Raman spectroscopy. FT-Raman spectroscopy is a technique that can detect changes in both crystalline and amorphous carbonaceous structures. In recent studies, it has been used to characterise the chemical structure of chars produced from low-rank fuels during pyrolysis and gasification [6, 9-19].

Previous work in our group showed that there were drastic changes in the structural features of char during the initial stage of gasification when the nascent char only contacted with steam for 20 s (or even possibly shorter) at 700 to 900 °C [10]. For the gasification of Victorian brown coal in steam at 800 °C in a fluidised bed, significant increases in ring condensation occurred during the initial coal feeding. It was mainly due to thermal annealing and volatile-char interactions [18]. However, little information was obtained about the initial conversion of nascent char structure during pyrolysis or gasification over a wide temperature range.

The transformation of char structure in the early stages of pyrolysis and gasification would also vary with the "rank" of the substrate. Little direct information is currently available in this aspect. For example, it is not clear how differently a nascent char from biomass would behave from a nascent char even from a sub-bituminous coal.

In this study, the changes in the chemical structural features, especially the distribution of aromatic ring systems of nascent chars, were characterised by using FT-Raman/IR spectroscopy. With a wire-mesh reactor, volatile-char interactions were minimised and accurate control of time-temperature history was possible. The aim of this study was to examine (a) the growth of large aromatic rings over a broad range of temperatures (600-1200 °C), (b) the changes in cross-linking structures during fast pyrolysis, and (c) the difference in structural features among three fuels of different rank: biomass, brown coal and sub-bituminous coal.

3.2 Experimental

3.2.1 Sample preparation

Three fuels of different rank (Western Australian mallee wood, Victorian Loy Yang brown coal and Western Australian Collie sub-bituminous coal) were used in this study. The detailed sample preparation steps can be found elsewhere [9, 20]. The particle size of Loy Yang coal and Collie coal samples was 106-150 microns, while the particle size of mallee wood sample was 180-400 microns in this study. The properties of these three fuels can be found in Chapter 2.

3.2.2 Pyrolysis

A wire-mesh reactor [20-23] was used to carry out the fast pyrolysis experiments. The heating rate was chosen to be 1000 K s^{-1}. Fuel particles were rapidly heated to pre-set temperatures ranging from 600 ° to 1200 °C (accurately measured) followed by a pre-set period of holding up to 50 s. The details of the pyrolysis experiments

have been described elsewhere [20, 23]. Briefly, a 325-mesh stainless steel 316 mesh was used as the sample holder. It was preheated to target reaction conditions and proved to have no further weight loss during experiments. Approximately 10 mg of sample was tightly sandwiched between two mesh layers that were then stretched between two electrodes. Two pairs of thermocouple wires were inserted through the meshes at the edge and in the middle of the area where the fuel particles were held. When the sample was heated by an alternating current, the temperature was detected every 0.01 s and provided feedback to the control system. While the sample was being heated, a stream of helium (purity > 99.999 vol%) passed through the sample-laden meshes vertically at a flow rate of 0.1 m s^{-1} (measured at 25 °C and 0.1 MPa). This flow of helium also allowed the char to be cooled down rapidly to room temperature, reaching a cooling rate of ~500 K s^{-1} in the range between peak temperature and ~50 °C. After pyrolysis, the weight of char-loaded mesh was weighed and the char was collected.

As the char particles may have fragmented during pyrolysis, especially at high temperatures, some fine particles may have been blown away from the mesh by the high flow rate of helium and thus caused a reduction in the char yield. One test was carried out using each of the three fuels under the most extreme experimental conditions (the longest holding time at the highest temperature) used in this study. Prior to heating the sample, the inlet valve of helium was turned off and the experiment was then started immediately. Comparing the char yield with no flow passing through to the char yield with high helium flow rate, the char yields showed only < 1% difference, i.e. within experimental errors. This indicates that the loss of fine particles from mesh during pyrolysis was negligible in this study.

3.2.3 FT-Raman/IR spectroscopy for char characterisation

A Perkin-Elmer GX FT-Raman/IR spectrometer was used for the characterisation of char structure. The char sample was firstly diluted and ground with spectroscopic grade potassium bromide (KBr). The concentration was chosen so that a plateau value had been reached for the total Raman area, as discussed in [11, 22]. The

Raman spectra in the range between 800 and 1800 cm^{-1} were deconvoluted into 10 Gaussian bands by the GRAMS/32 AI software (version 6.0). The assignment of 10 bands has been described in our previous study [11]. The total Raman area, the (G_r+V_l+V_r) band, D band and S band were used to characterise the structural features of nascent char. The strong peak of the FT-IR spectrum at ~1600 cm^{-1} was used in this study to gain some further information about the rapid changes in the aromatic ring systems at high temperatures.

3.3 Results and discussion

3.3.1 Char yields of three fuels during fast pyrolysis

Figure 3-1 shows the char yields of three fuels as a function of holding time at different temperatures. As there were rapid changes in the char yields of three fuels observed during the initial 1 s holding at different temperatures, the x-axis was drawn at a different (expanded) scale, at the holding time between 0 and 1 s, from the rest of the range.

In Fig. 3-1 (a), mallee wood only had a rapid change in char yield during the initial holding at 600 °C within 0.5 s. Further holding at 600 °C or heating to ≥ 800 °C showed negligible changes in the char yield of mallee wood.

For the char yields of Loy Yang coal shown in Fig. 3-1 (b), a significant decrease in the char yield had occurred before the temperature reached 600 °C and 700 °C with 0 s holding time. At 600 °C and 700 °C, the char yield decreased gradually within 50 s holding at 600 °C and 30 s holding at 700 °C. When the Loy Yang coal was heated to 800 °C, a rapid decrease in the char yield was observed during the initial holding at 800 °C at < 0.5 s. However, there is an insignificant change in the weight loss of Loy Yang char after further holding at 800 °C or further heating to higher temperatures.

For the char yields from Collie coal in Fig. 3-1 (c), obvious changes in the char yield happened during the initial holding at the temperatures lower than 800 °C. With the temperature increasing to ≥ 800 °C, lesser changes in char yield were observed than the changes at the temperature < 800 °C.

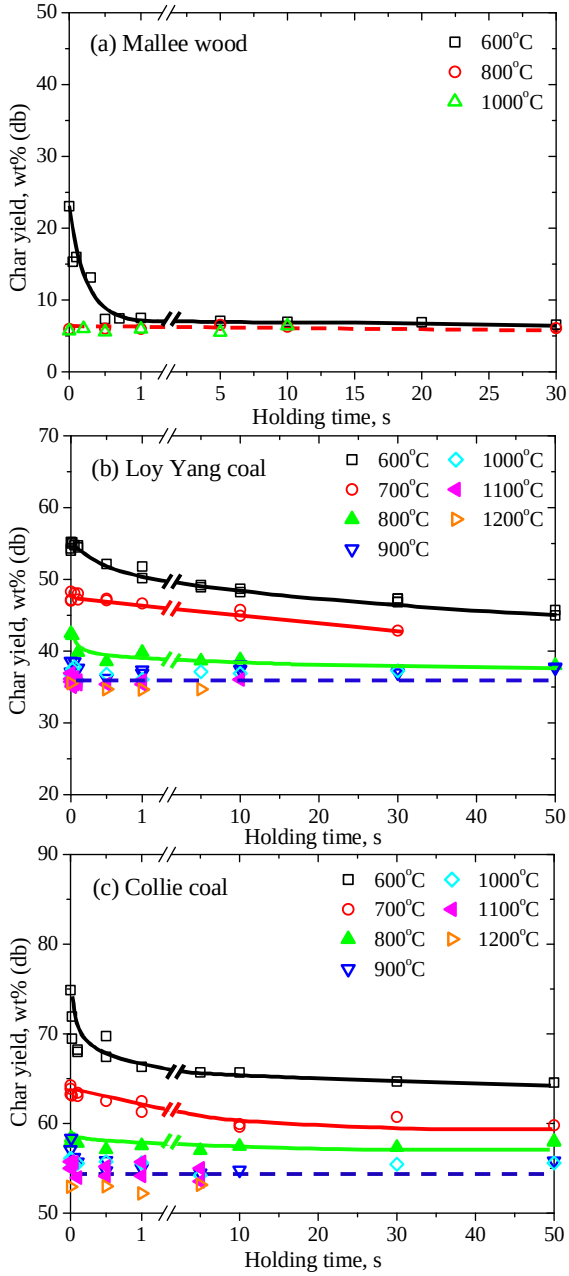

Figure 3-1 Char yields of three fuels as a function of holding time and temperature.

The data in Fig. 3-1 show that while the char from the mallee wood reached a plateau char yield at 800°C, the chars from the brown coal and sub-bituminous coals required much higher temperatures to reach a plateau char yield. These differences are related to the differences in their structure, which will be discussed below. However, it will be noted that the changes in char yield are not always accompanied by the changes in char structure.

3.3.2 Growth of large ring systems during the fast pyrolysis of three fuels

3.3.2.1 Changes in the ratio of $I_{(Gr+Vl+Vr)}$ to I_D with char yield

Figure 3-2 shows the changes in the ratio of $I_{(Gr+Vl+Vr)}$ to I_D as a function of char yield during the fast pyrolysis of the three fuels at the temperatures from 600 °C to 1200 °C. As the (Gr+Vl+Vr) bands broadly represent "small" aromatics with < 6 fused benzene rings and the D band represents "big" aromatics with ≥6 rings, the ratio between the band areas of (Gr+Vl+Vr) and D bands reflects the ratio between small and large aromatic ring systems in the nascent char [11]. The decrease in the ratio of (Gr+Vl+Vr) to D in Fig. 3-2 might be due to two possibilities: the selective release of small aromatic rings and/or the condensation of small aromatic rings.

In Fig. 3-2, the changes in $I_{(Gr+Vl+Vr)}/I_D$ had two different stages (slow and rapid) with the changes in char yield. It was manually distinguished by a dotted line and divided into regions A and B in Fig. 3-2. It is clear that the changes in $I_{(Gr+Vl+Vr)}/I_D$ were much more related to char yield in region A than in region B, reflecting different main reactions taking place in each region.

In region A, the mallee wood and the Loy Yang brown coal showed significant decreases in $I_{(Gr+Vl+Vr)}/I_D$ with the reduction in char yield from ~23 to ~9% and ~55 to ~45%, respectively. These significant changes in ring systems that occurred at 600 °C, as discussed in Ref. 20, were more likely attributed to the selective release of small aromatic rings, although ring growth cannot be ruled out. As the changes in

ring systems in region A were a strong function of the char yield and the changes in char yield mainly occurred within 1 s of holding at 600 °C (Fig. 3-1), this indicates that the significant changes in ring systems in region A for the mallee wood and the Loy Yang brown coal mainly occurred during the initial holding at 600 °C. The Collie sub-bituminous coal showed much less changes in ring systems in region A with decreasing char yield from ~75 to ~62% at 600 °C than the other two fuels. It indicates the higher stability of Collie coal char structure compared to the nascent chars from other two lower-ranked feedstocks.

During further weight loss of the Loy Yang coal from ~45 to ~40%, the changes in the ratio of small to large rings became relatively slow. This indicates the char structure became relatively stable at 700-800 °C after the selective decomposition of the active small ring systems in char. For the Collie coal, after the temperature increased to 700 and 800 °C, the ratio of small to large rings gradually decreased while the char yield decreased from ~62 to ~58%, which indicates that some small rings might be activated and then released/condensed with the increase in temperature. As shown in Fig. 3-1 (c), most changes in char yield of Collie coal occurred < 1 s holding at 700 and 800 °C. This is inferred that the changes in ring systems of Collie coal due to weight loss mainly happened within < 1 s at 700 °C and 800 °C.

In contrast to the different behaviours for the three fuels in region A, all three fuels showed a rapid decrease in $I_{(Gr+Vl+Vr)}/I_D$ in region B with insignificant changes in char yield. In particular, with the decreases in the char yield of mallee wood from ~9 to ~6% in region B, there were very drastic decreases in the ratio of small to large rings from ~3.5 to ~1.5. These significant changes in the ratio were most likely due to ring condensation that might cause massive conversion from small to large rings with the release of very light gases such as H_2. For the Loy Yang brown coal, when the char yield dropped to lower than ~40% in region B, there were also significant decreases in the ratio between small and large rings. With the slight change in char yield from ~40 to ~35%, the ratio of small to large rings decreased significantly from ~2.3 to ~1.3. Similar to the discussion above about mallee wood, the fast reduction

in $I_{(Gr+Vl+Vr)}/I_D$ seemed mainly to be due to ring condensation. Similarly, for the Collie sub-bituminous coal, the ratio largely dropped from ~1.8 to ~1.2 while the char yield decreased from 56 to 52% in region B. This also appears to be mainly due to ring condensation.

As was stated above, the changes in the ring systems of the three fuels in region A were stronger functions of char yield than those in region B. However, with the decrease in $I_{(Gr+Vl+Vr)}/I_D$ in region B, the drastic growth of large aromatic rings due to ring condensation in the three fuels seemed more related to the peak temperature and holding time rather than char yield. The exact reasons will be further discussed in next section. It is important to note here that the temperatures in region B where significant extents of ring condensation began were different among the three fuels. There was drastic ring condensation at 600 °C for mallee wood, 800 °C for Loy Yang brown coal and 900 °C for Collie sub-bituminous coal. In other words, significant ring condensation during fast pyrolysis happened at relatively higher temperature for higher ranked fuels in this study. This may be attributed to the increasing stability of char structure with the increase in fuel rank.

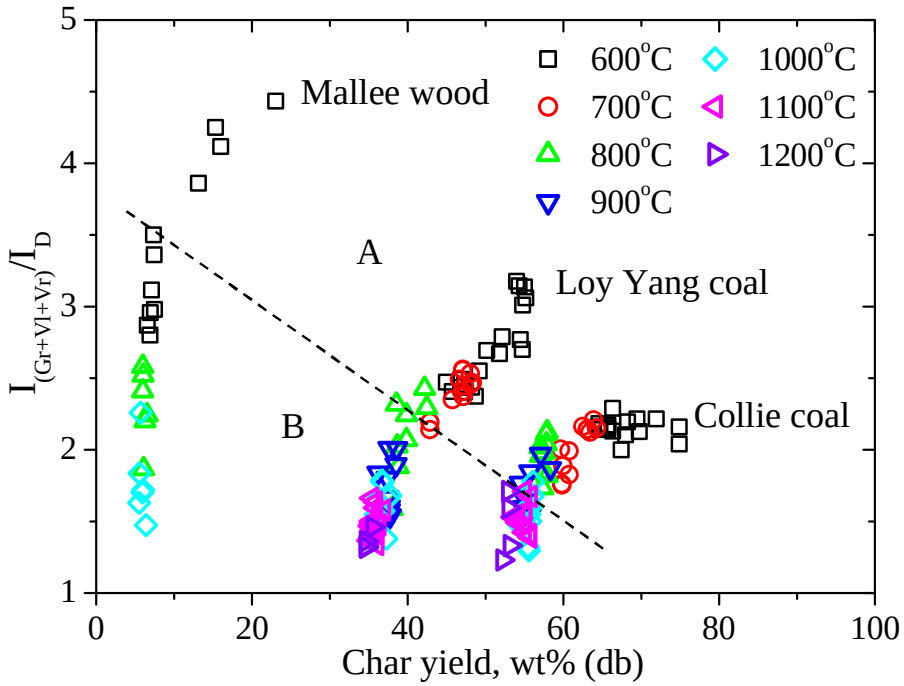

Figure 3-2 Changes in the ratio of $I_{(Gr+Vl+Vr)}$ to I_D as a function of char yield.

3.3.2.2 Growth of large aromatic rings by ring condensation

The previous section showed that significant ring condensation occurred during the fast pyrolysis of three fuels at different temperatures. In this section, the changes in $I_{(Gr+Vl+Vr)}/I_D$ ratio as a function of holding time at different temperatures will be discussed, to gain insight into the mechanism of the reaction of ring condensation.

Figure 3-3 shows the changes in $I_{(Gr+Vl+Vr)}/I_D$ for the three fuels. As discussed in the previous section, the reaction of ring condensation mainly occurred in region B (Figure 3-2), which corresponded to the region below the dashed lines in Figs. 3-3 (a), (b) and (c). For mallee wood shown in Fig. 3-3 (a), ring condensation gradually took place during holding from 0.5 s to 30 s at 600 °C. With increasing temperature to 800 and 1000 °C, a significant decrease of $I_{(Gr+Vl+Vr)}/I_D$ was observed with 0 s holding at 800 °C and < 0.5 s holding at 1000 °C. Although there were gradual increases in ring condensation during further holding at 800 and 1000 °C, the differences in $I_{(Gr+Vl+Vr)}/I_D$ at different temperatures were firstly observed during the initial holding (< 0.5 s) at peak temperatures.

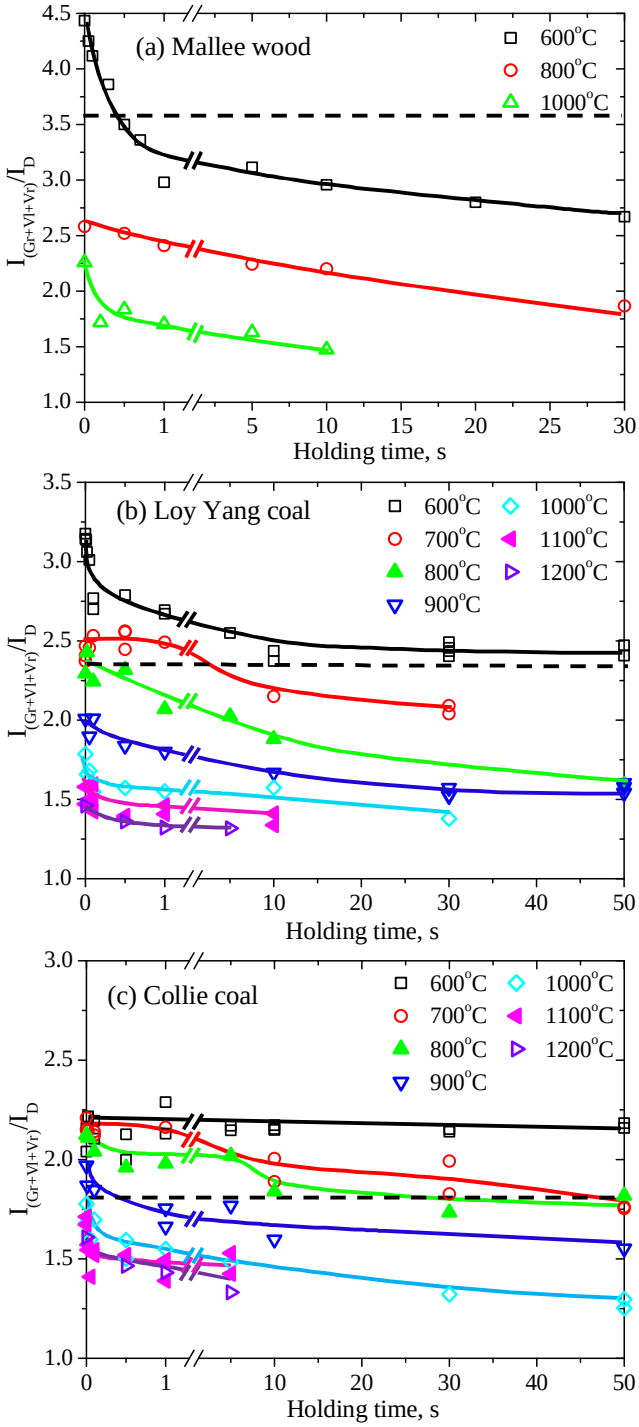

Figure 3-3 Ratios between small and large rings of three fuels as a function of holding time and temperature. The data above/below the dash line were replotted from the data in region A/B shown in Fig 3-2.

The change in $I_{(Gr+Vl+Vr)}/I_D$ for the two coals were similar. The ring condensation rate was slow at relatively low temperatures (Loy Yang coal at 800 °C and Collie coal at 900 °C). However, with the rise of temperature, the reaction rates of ring condensation seemed to become increasingly fast. At high temperatures such as 1000 °C, most changes in the conversion of small to large rings in three fuels are completed within < 0.5 s holding time. Furthermore, although the distribution of the ring systems in the three fuels was very different during the initial pyrolysis at 600 °C, $I_{(Gr+Vl+Vr)}/I_D$ of three fuels approached to each other at the temperature ≥ 1000 °C.

3.3.3 Changes in the total Raman area during fast pyrolysis

Figure 3-4 shows the changes in the total Raman area as a function of holding time at the temperature from 600 to 1200 °C. There may be two key factors causing the total Raman area to decrease during the pyrolysis of low-rank fuels [11]. The loss of O-containing functional groups would largely decrease the resonance effects to reduce the observed Raman intensity. Further, the condensation of aromatic ring systems would greatly increase the light absorptivity, which in turn would decrease the total Raman intensity.

In Fig. 3-4 (a), the total Raman area of the mallee wood char gradually decreased during holding at 600 °C and rapidly reduced during the initial holding at 800 °C and 1000 °C; this shows some correlation with the increase in ring condensation shown in Fig. 3-3 (a). It also indicates that the loss of O-containing functional groups occurred simultaneously with ring condensation for mallee wood. As for the Loy Yang coal shown in Fig. 3-4 (b), when the temperature increased to ≥ 700 °C, similar to the mallee wood, the decrease in total Raman area was largely related to ring condensation shown in Fig. 3-3 (b). For the Collie coal shown in Fig. 3-4 (c), the total Raman area changed rapidly at temperatures < 900 °C, while there were insignificant changes in ring systems during holding at this temperature range. Therefore, the rapid change in the total Raman area of Collie coal char was mainly due to the loss of O-containing functional groups and it happened before the

significant growth of large aromatic rings. Comparing the three fuels, it can be inferred that deoxygenation proceeded together with ring condensation for the lower-ranked fuels (e.g. mallee wood and Loy Yang coal) and occurred before ring condensation for the relatively higher-ranked fuel (e.g. Collie coal).

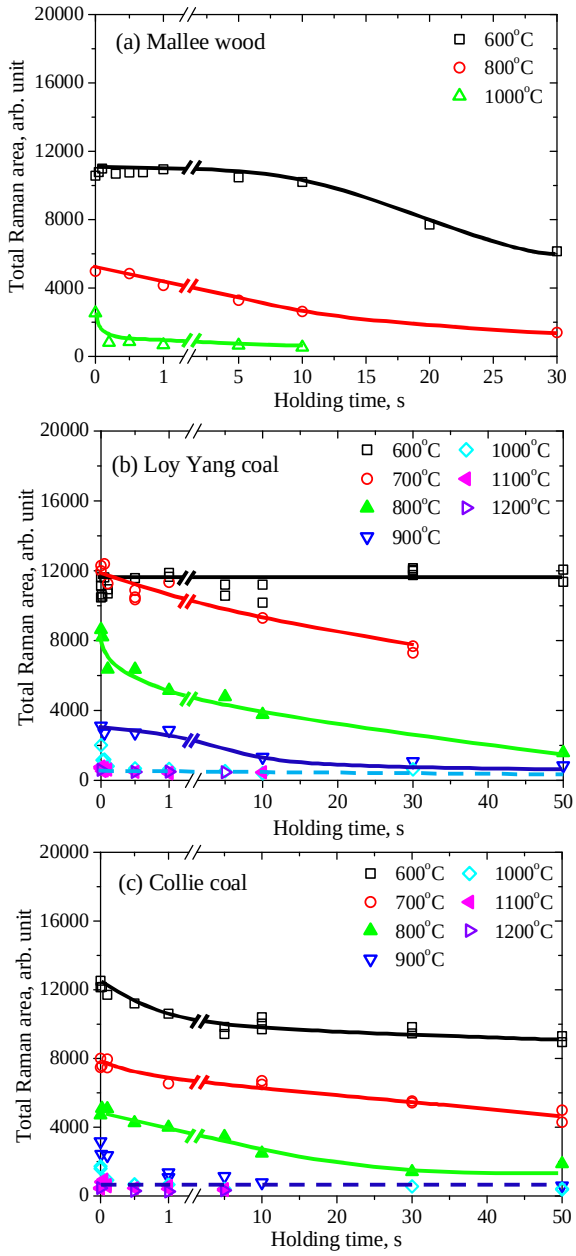

Figure 3-4 Total Raman areas between 800 and 1800 cm^{-1} as a function of holding time and temperatures.

3.3.4 Confirmation of fast growth of large aromatic rings

The IR spectrum near 1600 cm^{-1} is usually the strongest band in coal char. It is assigned mainly as aromatic C=C stretching [24-25]. Our previous study on the gasification of Loy Yang coal in CO_2 and O_2 also indicated that this band was mainly attributed to the aromatic C=C stretching [14]. As discussed above, a fast growth in large aromatic rings in the three fuels was observed during the initial holding at high temperatures. With the aromatisation of nascent char, the size of ring systems increases and the aromatic C=C stretching can be restricted. Due to this, the IR band near 1600 cm^{-1} may have a significant drop during rapid ring condensation.

Figure 3-5 shows the changes in IR spectra of the nascent char of the two coals between 1800 and 1500 cm^{-1} during holding at high temperatures. The IR band of Loy Yang coal char at 1600 cm^{-1} showed a significant decrease at 800 °C within 1 s holding. With the temperature increase to 1000 °C in Fig. 3-5 (b), a significant decrease of this band occurred within 0.5 s, which was in accordance with the fast ring condensation at high temperature shown in Fig. 3-3 (b). Collie coal char exhibited a similar phenomenon to that of Loy Yang coal char. With the rapid changes in the ring systems at 900 and 1000 °C shown in Figs. 3-5 (c) and (d), Collie coal char showed a significant decrease in the intensity of IR spectrum at ~1600 cm^{-1} within 1 s at 900 °C and within even 0.1 s at 1000 °C. Therefore, the fast changes at ~1600 cm^{-1} in the IR spectrum of nascent chars confirmed the rapid and significant growth in large aromatic ring systems during fast pyrolysis, as discussed in the previous sections.

Mallee wood nascent char had strong bands at ~1400 cm^{-1} (shown in Fig. 3-6) that may be attributed to the very high concentration of oxygen or potassium in mallee wood [9, 26]. The band at ~1400 cm^{-1} largely overlaps the band at ~1600 cm^{-1} for mallee wood chars. Nevertheless, the changes in IR spectra of mallee wood char at ~1600 cm^{-1} are in broad agreement with those of coals.

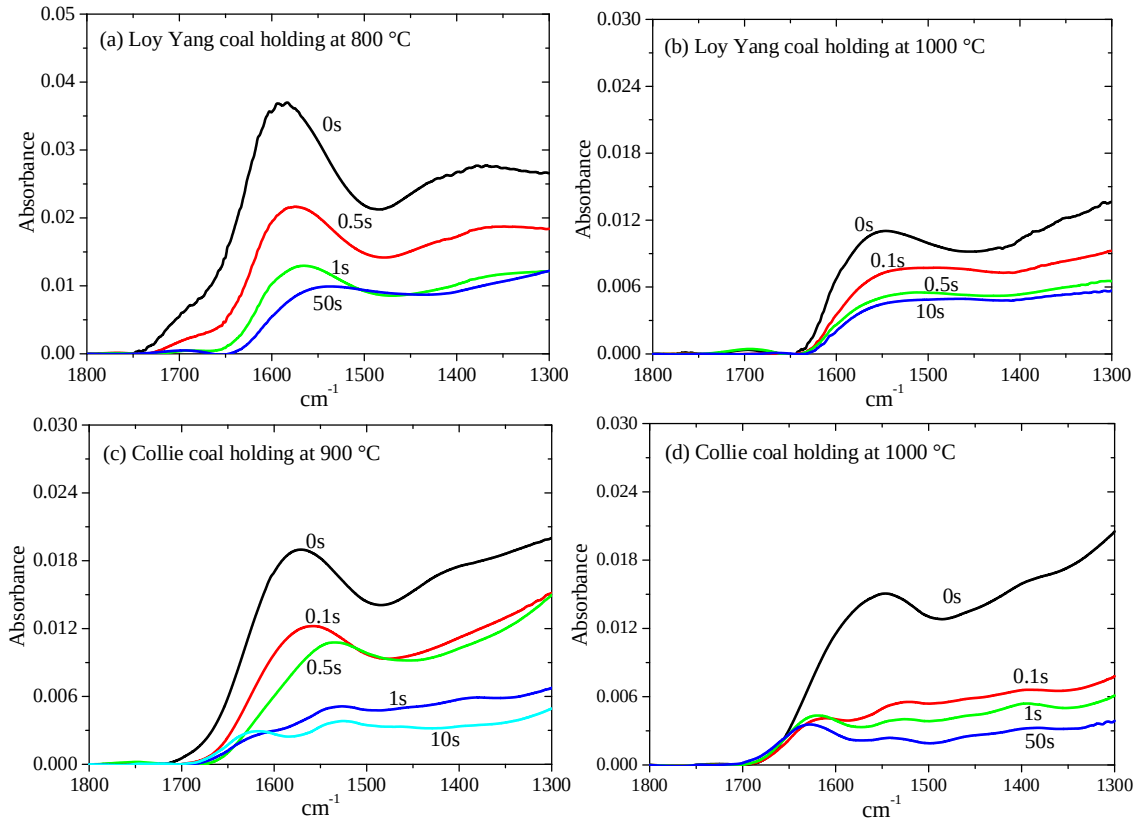

Figure 3-5 FT-IR spectra between 1800 and 1300 cm^{-1} of the coal chars.

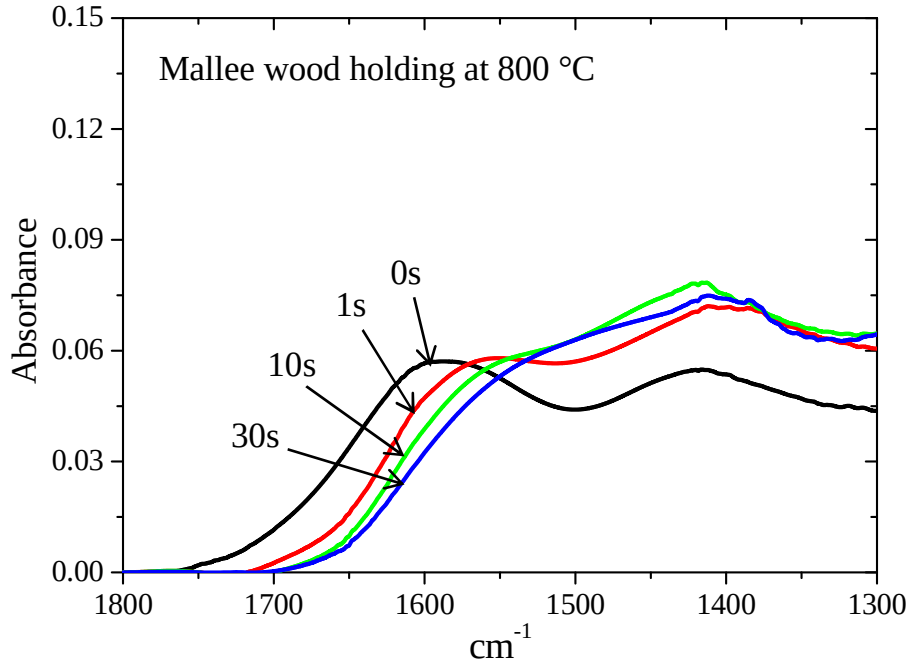

Figure 3-6 FT-IR spectra between 1800 and 1300 cm^{-1} of the mallee wood chars.

3.3.5 Changes in cross-linking structure during fast pyrolysis

Figure 3-7 shows the change in the ratio between the intensity of the S band (I_S) and the overall intensity ($I_{total\ Raman\ area}$) in the region of 800~1800 cm^{-1} as a function of holding time at different temperatures. The ratio of I_S to $I_{total\ Raman\ area}$ gives a brief indication of cross-linking structures in the char matrix [11]. It is clear that all three fuels show a significant increase in $I_S/I_{total\ Raman\ area}$ during holding at the temperature < 800 °C when there is significant thermal decomposition as shown in Fig. 3-1. This indicates that the thermal breakdown of some active groups (e.g. carboxyl and alkyl groups) created more free sites on char matrix that reconnect and form stable cross-linking structures. However, with the temperature increasing to ≥ 800 °C, all three fuels showed insignificant changes in the ratio of I_S to $I_{total\ Raman\ area}$. It suggests that many cross-linking structures that are formed at relatively low temperature are very stable even at 1200 °C during holding up to 5 s. Although some cross-linking structures might be broken at high temperature with reactions such as ring condensation, new cross-linking structures would form to preserve a stable carbon skeleton.

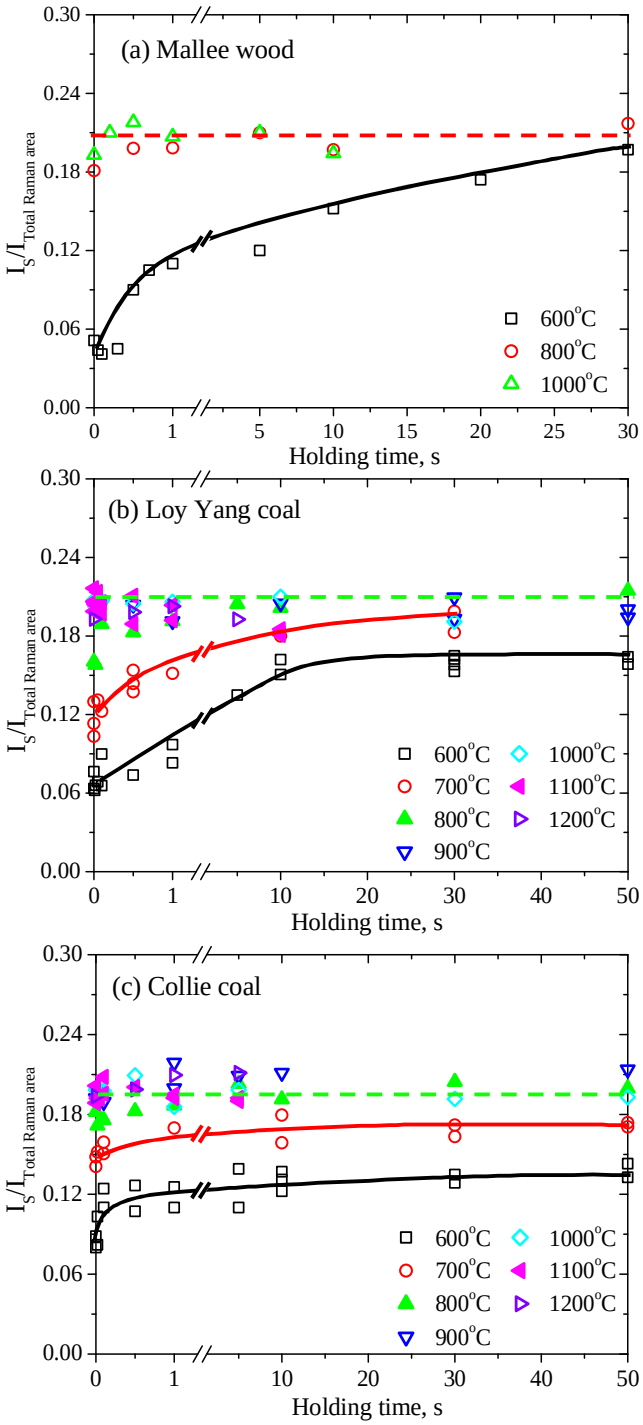

Figure 3-7 The relative S band intensities of three fuels as a function of holding time and temperature.

3.4 Conclusions

The changes in nascent char structure during the fast pyrolysis at temperatures from 600 °C to 1200 °C have been studied by combined features of a wire-mesh reactor with FT-Raman/IR spectroscopy.

1. There were insignificant changes in char yield at the temperatures > 600 °C for the mallee wood, > 800 °C for the Loy Yang brown coal and > 900 °C for the Collie sub-bituminous coal. However, significant decreases in the ratio of small to large rings occurred at these temperature ranges for the three fuels. The negligible change in char yield with a corresponding large decrease in the ratio of small to large rings is most likely attributed to ring condensation.

2. With increasing temperature, ring condensation would largely occur within very short holding times. For all three fuels, most of the ring condensation was observed within 0.1s holding at temperatures ≥ 1000 °C.

3. Although the distribution of the ring systems in the chars from these three fuels was largely different during the initial pyrolysis at 600 °C, their $I_{(Gr+Vl+Vr)}/I_D$ values were very close at temperatures ≥ 1000 °C.

4. The fast decrease in the FT-IR intensity of nascent char at ~1600 cm^{-1} corresponded to the rapid growth of large aromatic ring systems at the temperature ≥ 800 °C for Loy Yang coal and ≥ 900 °C for Collie coal. This supported the rapid enhancement of ring condensation at relatively high temperatures for two coals.

5. The formation of cross-linking structure was significant during holding at temperatures from 600 to 800 °C for all three fuels. The relative small changes in the cross-linking structure at high temperatures suggest that there may be some cross-linking structures broken at high temperatures with new cross-linking formed afterwards.

3.5 References

[1] Li C-Z. Special issue-gasification: a route to clean energy. Process Safety and Environmental Protection 2006;84: 407-8.

[2] Miura K, Hashimoto K, Silveston PL. Factors affecting the reactivity of coal char during gasification, and indices representing reactivity. Fuel 1989;68: 1461-75.

[3] Li C-Z. Some recent advances in the understanding of pyrolysis and gasification behaviour of Victorian brown coal. Fuel 2007;86:1664-83.

[4] Senneca O, Salatino P, Masi S. Microstructural changes and loss of gasification reactivity of chars upon heat treatment. Fuel 1998;77:1483-93.

[5] Wu H, Hayashi J-I, Chiba T, Takarada T, Li C-Z. Volatilisation and catalytic effects of alkali and alkaline earth metallic species during the pyrolysis and gasification of Victorian brown coal. Part V. Combined effects of Na concentration and char structure on char reactivity. Fuel 2004;83:23-30.

[6] Sheng C. Char structure characterised by Raman spectroscopy and its correlations with combustion reactivity. Fuel 2007;86:2316-24.

[7] Feng B, Bhatia SK, Barry JC. Structural ordering of coal char during heat treatment and its impact on reactivity. Carbon 2002;40:481-96.

[8] Sharma A, Kadooka H, Kyotani T, Tomita A. Effect of microstructural changes on gasification reactivity of coal chars during low temperature gasification. Energy & Fuels 2002;16:54-61.

[9] Asadullah M, Zhang S, Min Z, Yimsiri P, Li C-Z. Effects of biomass char structure on its gasification reactivity. Bioresource Technology 2010;101:7935-43.

[10] Keown DM, Hayashi J-I, Li C-Z. Drastic changes in biomass char structure and reactivity upon contact with steam. Fuel 2008;87:1127-32.

[11] Li X, Hayashi J-I, Li C-Z. FT-Raman spectroscopic study of the evolution of char structure during the pyrolysis of a Victorian brown coal. Fuel 2006;85:1700-7.

[12] Li X, Li C-Z. Volatilisation and catalytic effects of alkali and alkaline earth metallic species during the pyrolysis and gasification of Victorian brown coal.

Part VIII. Catalysis and changes in char structure during gasification in steam. Fuel 2006;85:1518-25.

[13] Li X, Hayashi J-I, Li C-Z. Volatilisation and catalytic effects of alkali and alkaline earth metallic species during the pyrolysis and gasification of Victorian brown coal. Part VII. Raman spectroscopic study on the changes in char structure during the catalytic gasification in air. Fuel 2006;85:1509-17.

[14] Tay H-L, Li C-Z. Changes in char reactivity and structure during the gasification of a Victorian brown coal: Comparison between gasification in O_2 and CO_2. Fuel Processing Technology 2010;91:800-4.

[15] Guo X, Tay H-L, Zhang S, Li C-Z. Changes in char structure during the gasification of a Victorian brown coal in steam and oxygen at 800 °C. Energy & Fuels 2008;22:4034-8.

[16] Tay H-L, Kajitani S, Zhang S, Li C-Z. Effects of gasifying agent on the evolution of char structure during the gasification of Victorian brown coal. Fuel 2013;103:22-8.

[17] Zhang S, Min Z, Tay H-L, Wang Y, Dong L, Li C-Z. Changes in char structure during the gasification of mallee wood: effects of particle size and steam supply. Energy & Fuels 2012;26:193-8.

[18] Zhang S, Min Z, Tay H-L, Asadullah M, Li C-Z. Effects of volatile-char interactions on the evolution of char structure during the gasification of Victorian brown coal in steam. Fuel 2011;90:1529-35.

[19] Li T, Zhang L, Dong L, Li C-Z. Effects of gasification atmosphere and temperature on char structural evolution during the gasification of Collie sub-bituminous coal. Fuel 2014;117:1190-5.

[20] Sathe C, Pang Y, Li C-Z. Effect of heating rate and ion-exchangeable cations on the pyrolysis yields from a Victorian brown coal. Energy & Fuels 1999;13:748-55.

[21] Jamil K, Hayashi J-I, Li C-Z. Pyrolysis of a Victorian brown coal and gasification of nascent char in CO_2 atmosphere in a wire-mesh reactor. Fuel 2004;83:833-43.

[22] Zhang L, Li T, Quyn D, Dong L, Qiu P, Li C-Z. Formation of nascent char structure during the fast pyrolysis of low-rank fuels. Fuel 2015;150:486-92.

[23] Gibbins JR, King RAV, Wood RJ, Kandiyoti R. Variable-heating-rate wire-mesh pyrolysis apparatus. Review of Scientific Instruments 1989;60:1129-39.

[24] Koch A, Krzton A, Finqueneisel G, Heintz O, Weber J-V, Zimny T. A study of carbonaceous char oxidation in air by semi-quantitative FTIR spectroscopy. Fuel 1998;77:563-9.

[25] Painter PC, Starsinic M, Squires E, Davis AA. Concerning the 1600 cm^{-1} region in the i.r. spectrum of coal. Fuel 1983;62:742-4.

[26] Yuh SJ, Wolf EE. FTIR studies of potassium catalyst-treated gasified coal chars and carbons. Fuel 1983;62:252-5.

Chapter 4

Changes in nascent char structure during the gasification of low-rank coals in CO_2

4.1 Introduction

Gasification is an important technology for the utilisation of low-rank coals due to their high gasification reactivity [1]. Through gasification, low-rank coals are converted to syngas (which mainly consists of CO and H_2) that can be used to produce hydrogen and to synthesise chemicals or liquid fuels. Apparently, unlike the pulverised-fuel combustion technology that emits CO_2, CO_2 is partially consumed as a gasification agent to produce CO in gasification technology. This is a more economical way of managing CO_2 than the conventional CO_2 capture technologies [2]. Therefore, it is essential to understand the reaction mechanism of coal/coal char-CO_2.

Recently, a central topic of discussion is the transformation of inorganic species and char structures during the gasification in CO_2 [3-5]. The quantitative analysis of catalysts is easy but the direct quantification of char structural features is a challenge. Raman spectroscopy has been used as a powerful technique to obtain the information about the carbon skeleton in char during the pyrolysis/gasification of low-rank coals [6-22] and biomass [23-27]. The reaction pathways between the gasification in O_2, CO_2 and H_2O are different at 800 °C [9, 18, 19]. When the temperature increases from 800 to 900 °C, the char-CO_2 or char-H_2O gasification pathways do not change [14]. Su and co-workers [12] studied the reaction pathway during the gasification of a Chinese bituminous coal in CO_2. With a fast heating rate, the evolution of char structure (distribution of ring systems and O-containing functional groups) mainly occurred during the initial stage of gasification in CO_2. However, previous research into the changes in char structure during gasification has mainly been carried out over a period of a few minutes. There is still a lack of experimental evidence about the structural evolution of nascent char regarding char-CO_2 gasification during the initial gasification (seconds). Therefore, it is necessary to find a proper method to study the initial (a few seconds or shorter) changes in the structure of nascent chars during gasification.

A wire-mesh reactor (WMR) that was frequently used in the investigation of primary pyrolysis [28-31] and gasification [32, 33] can provide a wide range of heating rate from 0.1 to 5000 K s^{-1} and high time resolution (increment of 10 ms). It is very suitable for the production of nascent char with even milliseconds holding at a pre-set peak temperature. In addition, a fast flow of carrier gas (at 0.1 m s^{-1}) continuously passes through the sample particles and immediately cools down the volatiles and takes them away from the coal/char particles. In other words, a WMR that can minimise volatile-char interaction is appropriate to be employed to investigate the initial char structure evolution only due to the gasification and thermal cracking.

Jamil and co-workers [32] studied the mechanism of the gasification of Loy Yang brown coal in CO_2 by the use of a WMR at 600 to 900 °C. They found that rapid weight losses due to the gasification of char happened during the heating process from 700 to 900 °C. The gasification rate strongly depended on the rate of thermal cracking in this temperature range. It also showed that there was increasingly significant effect of temperature on char gasification rate in CO_2 at > 800 °C, which might cause large changes in char structures. This needs to be studied by more experimental work.

In this study, a brown coal and a sub-bituminous coal were heated up rapidly to 1000 and 1200 °C with holding time up to 30 s. The brown coal was also prolysed (pure N_2) and gasified (5.3% CO_2 balanced with N_2) in a drop tube furnace (DTF) at 1200 °C with a holding time from 2.3 to 3.9 s. All chars were then analysed by FT-Raman spectroscopy and FTIR spectroscopy to gain insight into the evolution of the char structure during initial holding in CO_2 at relatively high temperatures.

4.2 Experimental

4.2.1 Samples preparation

For the experiments in WMR, two low-rank coals (Collie sub-bituminous coal from Western Australia and Loy Yang brown coal from Victoria) were applied. The sample preparation of two coals can be found elsewhere [14, 30]. Briefly, "as mined" coal was dried at low temperature (< 35 °C). The air-dried coal bulks was ground and screened to the size of 106-150 μm. The properties of the two coals were shown in Chapter 2.

For experiments in DTF, the air-dried Loy Yang coal was crashed in a blender (Hamilton Beach, Magnum Blender MB-911) to the size < 125 μm. The sample was further dried in a vacuum oven at 60 °C. The remaining moisture in coal to be used in DTF was from 0.78 to 1.1%.

4.2.2 Pyrolysis and gasification

The details of operation procedure for WMR can be found elsewhere [30]. Briefly, ~10 mg sample particles were sandwiched between two layers of stainless steel mesh. Two electrodes clamp two ends of mesh and supply an alternating current to heat the samples. A high flow of ultra-high purity helium/CO_2 passed through the sample particles at the rate of 0.1 m s^{-1} (measured under ambient conditions). Two different types of thermocouples were employed in two atmospheres. The K type thermocouples were used in He but the S type thermocouples were used for the experiments in CO_2.

As for DTF [34] (as was shown in Fig. 1-3), the Loy Yang coal sample was continuously fed into the 1200 °C hot furnace through a water-cooled feeding tube. After being carried by 5.3 vol% CO_2 balanced with N_2 in a few seconds, solid products were collected though a water-cooled probe. Large char particles straight

dropped in a filter with no gas flow passing through, while the fine char/soot particles were taken away with carrier gas through a bypass. The large char particles in the filter were collected for further analysis. The absolute pressure in DTF was 0.5 Mpa for gasification and ambient pressure for pyrolysis.

4.2.3 FT-Raman/IR spectroscopy for char characterisation

A Perkin-Elmer Spectrum GX FT-Raman/IR spectrometer was used to acquire the FT-Raman/IR spectra of chars. All the char samples were mixed and ground with spectroscopic grade potassium bromide (KBr). The concentration of char in char-KBr mixture was chosen to be 0.25% [35]. A 10 band deconvolution method was used to analyse the Raman spectra between 800 and 1800 cm^{-1} [15]. The total Raman area, Raman band ratios and FTIR intensity (600 to 1800 cm^{-1}) were applied to characterise the char structural features in this study.

4.3 Results and discussion

4.3.1 Char yields of Loy Yang coal during fast pyrolysis and gasification

The changes in char yield as a function of holding time during the pyrolysis/gasification of Loy Yang brown coal in WMR at 1000 °C and 1200 °C are illustrated in Fig. 4-1. The "0 s" holding means the char that only underwent the heating process with no holding at peak temperatures. At 1000 °C, compared with pyrolysis in He at 1000 °C, the char yield had an additional 3-4% weight loss during the initial 1.5 s gasification in CO_2. With further time at 1000 °C, a large decrease in char yield was observed from ~33 to ~7% from 1.5 to 10 s. At 1200 °C, significant additional weight loss (~2.5%) occurred at 0 s during fast heating (in 0.2 s) in CO_2 from 1000 to 1200 °C. The rate of the weight loss is 12.5 wt%-db s^{-1} (equals to 12.64 wt%-daf s^{-1}). It is worth emphasising that only ~1.2% weight loss was observed during heating from 1000 to 1200 °C in He. It means the rate of weight loss due to thermal cracking is 6 wt%-db s^{-1} (6.07 wt%-daf s^{-1}). Therefore, the gasification rate

was 6.57 wt%-daf s^{-1} that is similar to the thermal cracking rate 6.07 wt%-daf s^{-1}. This indicates that the initially high gasification rate of char is highly related to the thermal cracking, it is consistent to the work done by Jamil and co-workers who carried out gasification experiments in CO_2 at 700 to 900 °C [32]. During holding at 1200 °C, a very significant decrease in char yield took place within 1.7 s from ~32 to ~7%. The gasification reaction between nascent char and CO_2 at high temperatures was significant, which might result in the corresponding changes in char structure, as will be discussed in the following section.

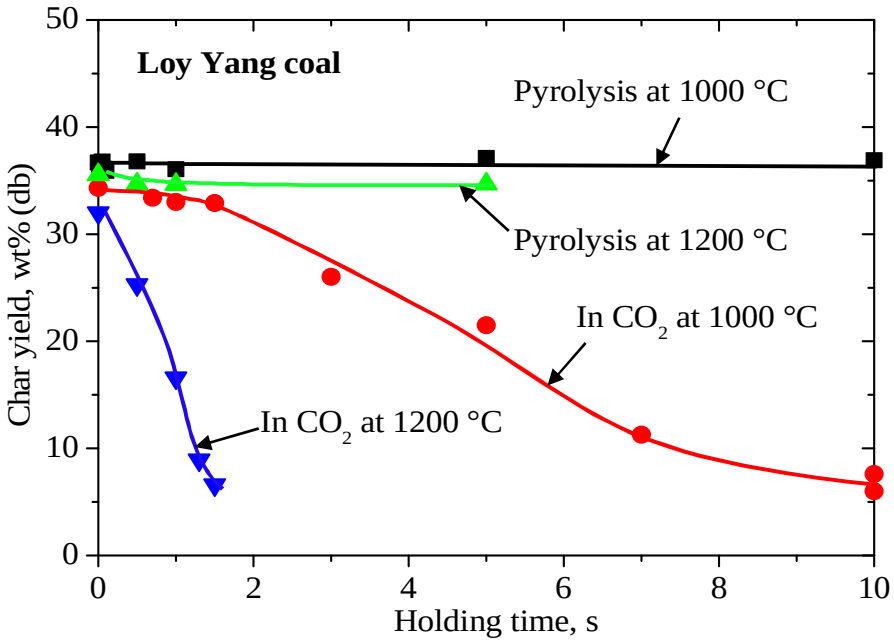

Figure 4-1 Changes in char yield as a function of holding time at 1000 and 1200 °C during the pyrolysis in He or the gasificaction in CO_2 in wire-mesh reactor for Loy Yang coal.

4.3.2 Structural changes in Loy Yang coal char during gasification in CO_2

Figures 4-2 and 4-3 show the changes in the total Raman area from 800 to 1800 cm^{-1} and the band area ratio of $I_{(Gr+Vl+Vr)}$ to I_D as a function of holding time in He/CO_2. The total Raman area is mainly determined by two factors: the O-containing functional groups that would enhance the total Raman intensity [15] and the aromatic ring systems that would increase the light absorptivity and reduce the total Raman intensity. The ratio of $I_{(Gr+Vl+Vr)}$ to I_D mainly reflects the ratio of small aromatic rings (3-5 fused benzene rings) to large ones ($\geq$ 6 rings) [15].

As is shown in Fig. 4-2, the total Raman area of Loy Yang coal char during the gasification in CO_2 was overall higher than that during pyrolysis in He at 1000 °C. The increase in total Raman area after reaction with CO_2 appears to be mainly due to the formation of O-containing functional groups and/or the consumption of ring systems. In Fig. 4-3, it is clear that the ratio between small and large aromatic rings during gasification is overall lower than that during pyrolysis at 1000 °C, which indicates that the ring systems are more condensed during the gasification in CO_2 than during pyrolysis. The more condensed ring systems would have caused the lower total Raman area, which was opposite to the observed higher total Raman area in CO_2 than in He. Because of that, the higher total Raman area (Fig. 4-2) in CO_2 can be mainly due to the formation of O-containing functional groups in CO_2 rather than the changes in aromatic ring systems.

A minimum in the total Raman intensity was observed at 1 s holding at 1000 °C. As for the pyrolysis at 1000 °C, the total Raman area significantly decreased within 1 s holding, which can be mainly attributed to the thermal annealing (aromatic ring condensation and loss of O-containing functional groups). Therefore, the minimum in the total Raman area at 1 s can be mainly attributed to the counteraction of two opposite effects: oxygenation and thermal annealing. As the thermal annealing during pyrolysis almost completed within 1 s, the total Raman area gradually increased from 1 to 3 s in CO_2 with the continuous formation of O-containing functional groups at 1000 °C. Very slow increases in total Raman area were

observed with the further holding from 3 to 10 s in CO_2. The nearly constant total Raman area from 3 to 10 s holding in CO_2 is due to the dynamic balance between the thermal cracking and the formation of O-containing functional groups.

When the temperature was increased to 1200 °C, the total Raman area of nascent char during holding in CO_2 was overall higher than that of nascent char during holding in He. The total Raman area rapidly increased within 0.5 s in CO_2 and then became roughly constant during holding from 0.5 to 1.7 s. It is clear that the formation of O-containing functional groups at 1200 °C is much quicker to reach the plateau than at 1000 °C, which might be related to the higher gasification rate [20] at 1200 °C as shown in Fig. 4-1.

The total Raman areas of the Loy Yang coal chars produced from DTF at 1200 °C are illustrated in Fig. 4-3 by the symbols of ✳ (pyrolysis) and × (gasification). Like the chars produced from WMR, the chars from the gasification in CO_2 gave much higher total Raman peak areas than those from the pyrolysis in He, confirming the rapid formation of O complex in CO_2 at 1200 °C. The total Raman areas of the pyrolysed chars from DTF were nearly the same as those from WMR, while the total Raman area of the chars gasified in DTF were lower than those of the chars gasified in WMR. As the concentration of CO_2 was 100 vol% in WMR but 5.3 vol% balanced with N_2 in DTF, the lower total Raman area might be mainly due to the slower gasification rate in lower CO_2 concentration atmosphere, which caused less formation of O complex in DTF than in WMR with the similar reaction time.

In Fig. 4-3, the distribution of ring systems also changed significantly during the holding in CO_2. During pyrolysis in He at 1000 °C, the ratio of small to large rings showed a rapid decrease within 0.5 s, with insignificant changes in char yield shown in Fig. 4-1. This is mainly due to the aromatic ring condensation. This fast enhancement of ring condensation also resulted in a rapid decrease in the ratio during the initial gasification of Loy Yang coal in CO_2 at 1000 °C. With further holding at 1000 °C, $I_{(Gr+Vl+Vr)}/I_D$ gradually decreased in CO_2 despite the little reduction in the $I_{(Gr+Vl+Vr)}/I_D$ during pyrolysis. This indicates significant changes in

char structure due to the reaction between char and CO_2. As a continuous decrease in char yield was also observed during holding at 1000 °C in CO_2 (Fig. 4-1), the decrease in the ratio of small to large aromatic rings in CO_2 should be mainly due to the selective consumption of the active small aromatic rings. With the temperature increase to 1200 °C in CO_2, the ratio of small to large rings rapidly decreased within 1 s, while the distribution of ring systems had insignificant change after the further holding from 1 to 1.5 s. As there was large decrease in char yield (from ~16 to ~7%) during this period of holding in CO_2 at 1200 °C shown in Fig. 4-1, this indicates that the reaction pathway changed from the selective consumption of small rings to the unselective consumption of small and large rings with the increasingly stable char structure.

The chars from DTF also showed significant decreases in the ratio of small to large rings during gasification in CO_2 compared with those during pyrolysis. This confirmed the selective consumption of small ring systems during initial gasification in CO_2. Insignificant changes in the $I_{(Gr+Vl+Vr)}/I_D$ of DTF char during holding from 2.3 to 3.2 s also confirmed that the changes in ring systems mainly happened during initial holding (at least < 2.3 s in DTF).

4.3.3 Changes in char yield during the pyrolysis/gasification of Collie coal

Fig. 4-4 shows the changes in char yield during the pyrolysis/gasification of Collie coal at 800, 1000 and 1200 °C in WMR. It is clear that, similar to Loy Yang brown coal [33], insignificant difference in the char yield between gasification in CO_2 and pyrolysis in He were observed during holding at 800 °C. When the temperature was increased to 1000 °C, contrary to the insignificant changes in char yield during pyrolysis, there were large decreases in char yield from ~57 to ~33% within 20 s holding in CO_2. At 1200 °C, it showed rapid decrease in char yield from ~53 to ~15% within 5 s in CO_2. Comparing with the decrease in char yield in Fig. 4-1, it is clear that the gasification rate of Collie sub-bituminous coal is lower than that of Loy Yang brown coal. This was expected from the difference in coal rank between the brown coal and the sub-bituminous coal.

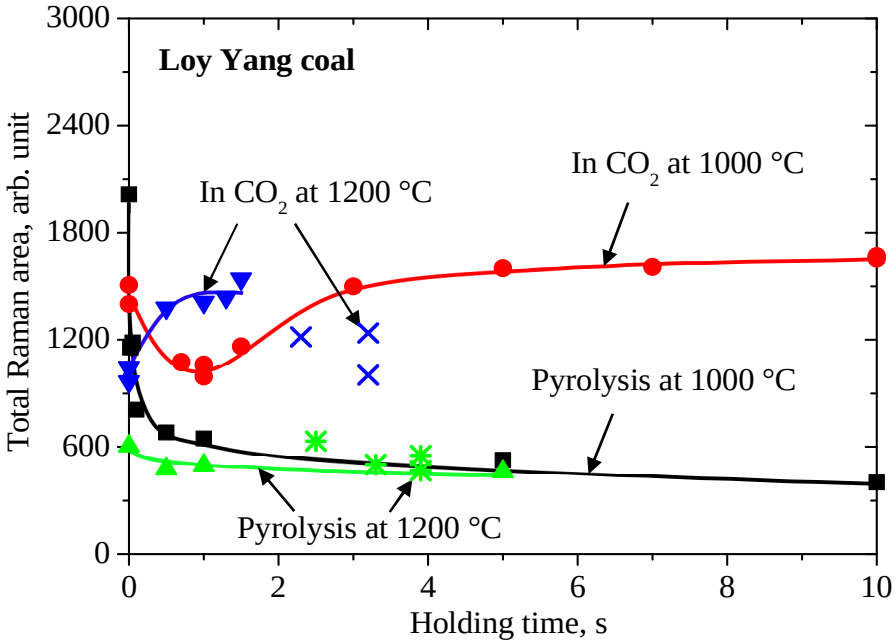

Figure 4-2 Changes in total Raman area as a function of holding time at 1000 and 1200 °C during the pyrolysis in He or the gasificaction in CO_2 of Loy Yang coal. ✳ (pyrolysis) and × (gasification) represent the chars produced in the drop tube reactor. ■, ●, ▲ and ▼ represent the chars produced in the wire-mesh reactor.

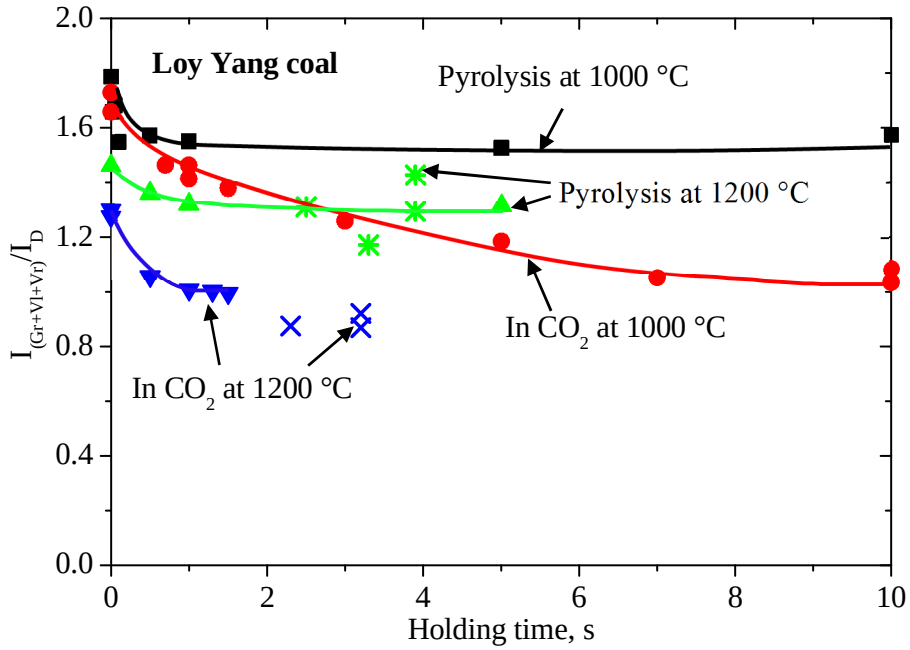

Figure 4-3 Changes in $I_{(Gr+Vl+Vr)}/I_D$ as a function of holding time at 1000 and 1200 °C during the pyrolysis in He or the gasificaction in CO_2 of Loy Yang coal. ✳ (pyrolysis) and × (gasification) represent the chars produced in the drop tube reactor. ■, ●, ▲ and ▼ represent the chars produced in the wire-mesh reactor.

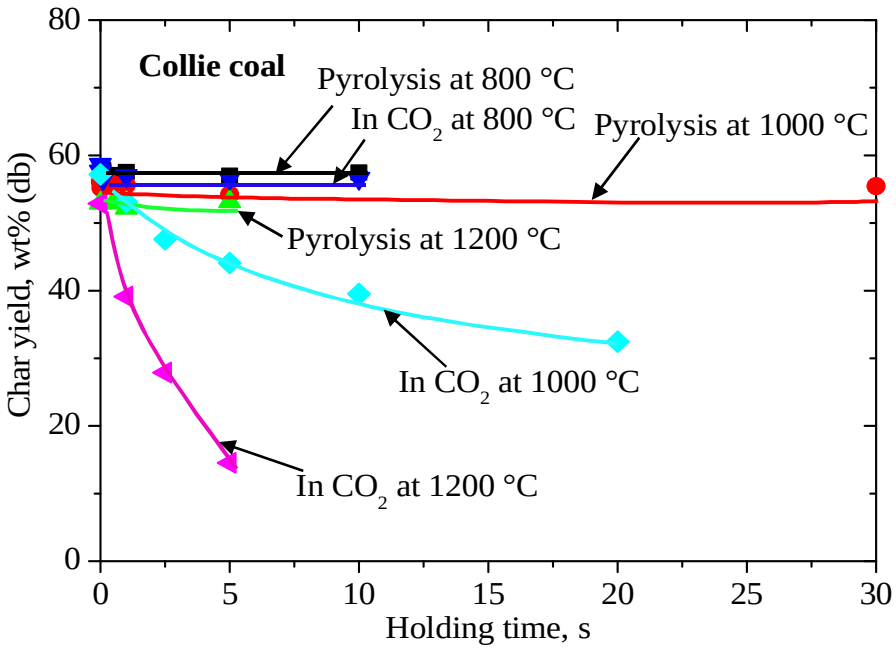

Figure 4-4 Changes in char yield as a function of holding time at 1000 and 1200 °C during the pyrolysis in He or the gasificaction in CO_2 for Collie coal. All chars were produced in the wire-mesh reactor.

4.3.4 Changes in char structure during the pyrolysis/gasification of Collie coal

Figures 4-5 and 4-6 show the changes in the total Raman areas between 800 and 1800 cm^{-1} and the band area ratio of $I_{(Gr+Vl+Vr)}$ to I_D as a function of holding time during the fast pyrolysis/gasification of Collie coal. In Fig. 4-5, similar to Loy Yang coal, Collie coal also showed a gradually higher total Raman area during the gasification in CO_2 than the pyrolysis in He. This indicates the formation of O-containing functional groups during holding in CO_2 at 1000 and 1200 °C. However, at 1000 °C, the increase in total Raman area for Collie coal was from ~450 (in He) to ~900 (in CO_2), which was much less than that for Loy Yang coal from ~450 (in He) to ~1650 (in CO_2). The difference can be due to the relatively slow gasification rate at 1000 °C for Collie coal, which formed less O complex with the same holding time [20]. When the temperature was increased to 1200 °C in CO_2, the total Raman area increased very fast within 2.5 s and then levelled off during the further holding from 2.5 to 5 s. This suggests that the rapid formation of O-containing functional groups in CO_2 occurs at 1200 °C and reaches the dynamic balance with the breakage of O-containing functional groups during holding from 2.5 to 5 s.

In Fig. 4-6, it is clear that there were large decreases in the ratio during the gasification in CO_2 compared with the changes in the ratio during the pyrolysis in He at 1000 and 1200 °C, which is mainly due to the selective consumption of small aromatic rings. The decrease in the ratio of small to large rings mainly occurred < 5 s holding at 1000 °C. When the temperature was increased to 1200 °C, comparing the ratio in gasification and pyrolysis, the ratio dropped from ~1.7 to ~1.4 with 0 s holding in two atmospheres and, similarly, the ratio dropped from ~1.3 to ~1 with 5 s holding in two atmospheres. It suggests that the changes in ring systems due to the gasification mainly happened during heating from 1000 to 1200 °C.

In the discussion presented above, temperature has been shown as an important parameter to influence the char structure as shown by Raman spectroscopic data. Therefore, an ultimate question would be if the gasification pathway would also

drastically change from 1000 to 1200 °C. This is done by plotting the Raman spectroscopic data as a function of char yield (conversion). Figure 4-7 shows the changes in $I_{(Gr+Vl+Vr)}/I_D$ as a function of char yield during gasification in CO_2. With the increase in temperature from 1000 to 1200 °C, the ratio of small to large rings showed insignificant change. This suggests that temperature has little effect on the reaction pathway during gasification in CO_2 for the two coals.

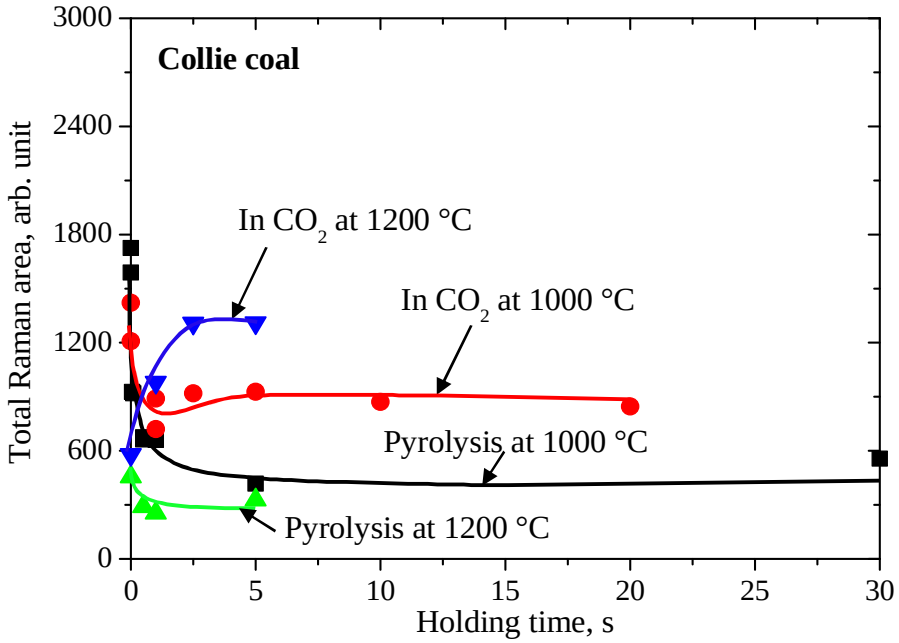

Figure 4-5 Changes in total Raman area as a function of holding time at 1000 and 1200 °C during the pyrolysis in He or the gasificaction in CO_2 for Collie coal. All chars were produced in the wire-mesh reactor.

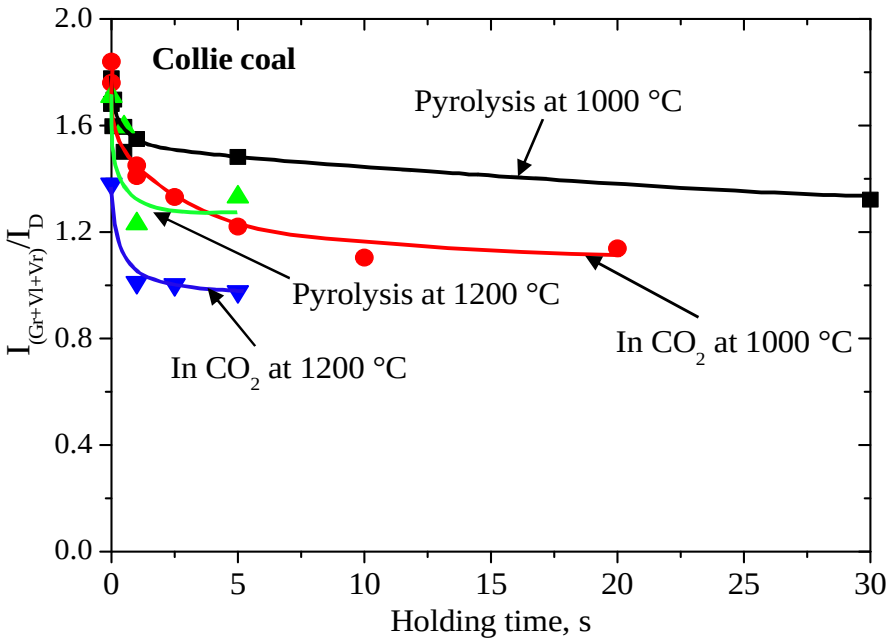

Figure 4-6 Changes in $I_{(Gr+Vl+Vr)}/I_D$ as a function of holding time at 1000 and 1200 °C during the pyrolysis in He or the gasificaction in CO_2 for Collie coal. All chars were produced in the wire-mesh reactor.

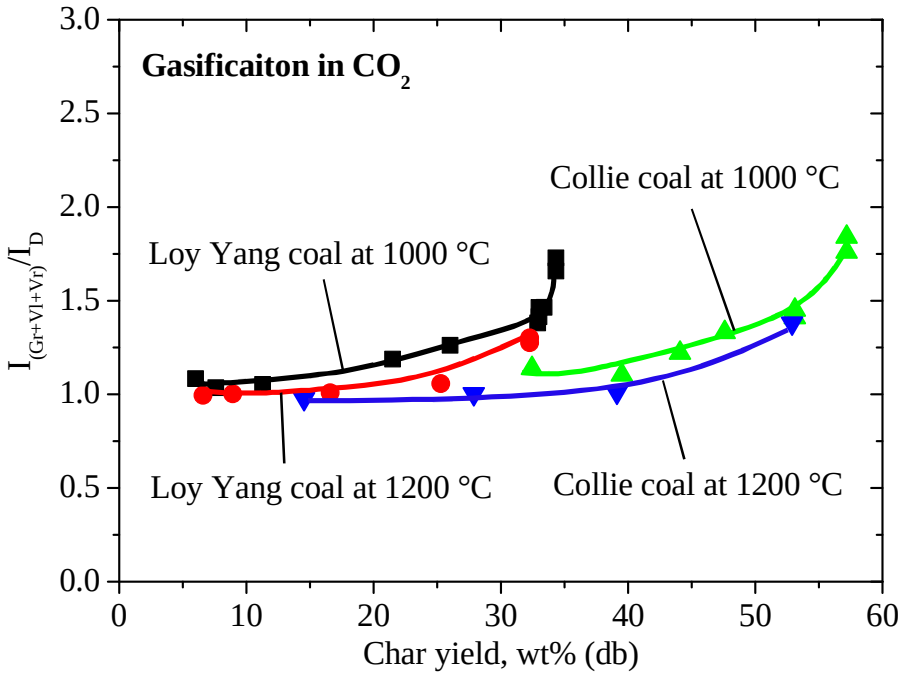

Figure 4-7 Changes in $I_{(Gr+Vl+Vr)}/I_D$ as a function of char yield at 1000 and 1200 °C during the gasificaction in CO_2 for the two coals. All chars were produced in the wire-mesh reactor.

4.3.5 Changes in char structure based on FTIR spectrum

The FTIR spectra (600 to 1800 cm^{-1}) of two coals during pyrolysis/gasification are shown in Figs. 4-8 and 4-9. The concentration of char in KBr was identical. The spectra had two strong peaks. One peak was located from ~1500 to ~ 1600 cm^{-1} that is mainly due to the aromatic ring (C=C) stretching vibrations and/or carbonyl functional groups [35]. Tay and co-workers [18] used 0.2 M H_2SO_4 to remove the AAEM species from the Loy Yang coal chars prepared in CO_2 at 800 °C. There was no bond shift from ~1600 (COO^-) to ~1700 cm^{-1} (COOH). This indicates that the strong peak at 1500 to 1600 cm^{-1} should be mainly attributed to the aromatic ring (C=C) stretching vibrations. Another strong peak was located at from ~900 to ~1300 cm^{-1}, which should mainly represent the C-O stretching [37].

In Fig. 4-8, it is clear that the chars from the pyrolysis of Loy Yang coal at 1000/1200 °C and Collie coal at 1000 °C showed gradual decrease in the IR intensity region from ~600 to ~1800 cm^{-1}, due to the thermal cracking of O-containing functional groups and enhancement of aromatic ring condensation. The chars from the Collie coal showed insignificant changes at 1200 °C, which indicates the very stable structure of Collie coal char at 1200 °C at even 0 s holding.

In Fig. 4-9 (a) and (b), the chars from two coals showed decreases in IR intensity (600 to 1800 cm^{-1}) during the initial 1 s holding and then increase during the further holding in CO_2 at 1000 °C. This initial reduction in IR intensity was the same as the changes in total Raman area (Figs. 4-2 and 4-5), which should be mainly due to the dominant effect of thermal annealing during the initial holding at 1000 °C. The increase in the intensity of C-O stretching (~900 to ~1300 cm^{-1}) might be partially responsible for the increase in total Raman area during holding at 1000 °C (> 1 s) and at 1200 °C (in Figs. 4-2 and 4-5). However, unlike the total Raman area that gradually level off during holding at 1000 °C and 1200 °C, the formation of O complex (C-O bond) continuously increased during holding according to the FTIR data. This suggests that there might be more than one type of O-containing functional groups formed during gasification in CO_2, while some are sensitive in the

Raman scattering but some are sensitive in FTIR absorption. Additionally, it was noted that the absorbance intensity at 1500-1600 cm^{-1} (C=C stretching in aromatic rings) increased corresponding to the intensity at 900 to 1300 cm^{-1} (C-O stretching) during gasification. This might be due to that the formation of O-containing functional groups attached on the aromatic rings, which consequently enhance the dipole moment of the aromatic rings vibration [37, 38].

During gasification in CO_2 at 1200 °C, Collie coal char showed a sharp peak at ~1100 cm^{-1} and a shoulder at ~1180 cm^{-1} while Loy Yang coal char only had a broad peak at ~1180 cm^{-1}. The peak at ~1180 cm^{-1} is mainly due to the formation of aromatic ether and/or phenol [36]. However, the sharp peak at ~1100 cm^{-1} might be due to the formation of O complex and/or due to another possibility: the higher mineral content in Collie coal than in Loy Yang coal (ash content in dry basis for Collie coal is 5.7 wt%; Loy Yang coal is 1.1 wt%, which shown in table 1). With the increase in char conversion during gasification, the intensity of minerals relatively increased with the continuous consumption of organic matter, causing the continuous increase in the intensity at ~1100 cm^{-1} [39, 40]. In order to clarify the contribution of minerals to the band at ~1100 cm^{-1}, a Collie char sample was ashed in TGA, following the procedure described by Li and co-workers [42]. The char sample was produced through gasifying Collie coal in CO_2 at 850 °C with 50 minutes holding in a fluidised-bed/fix-bed reactor [14], which can provide much more char sample than wire-mesh reactor. As shown in Fig. 4-10, the shape of the FTIR spectrum of the Collie coal char produced in fluidised-bed/fix-bed reactor is similar to the FTIR spectra of the Collie coal chars shown in this study (Fig. 4-9 (d)), which also has a strong peak at 1100 cm^{-1}. As for the FTIR spectrum of ash, it also showed a strong peak at 1100 cm^{-1}. It is clearly suggested that the high intensity of Collie coal char at 1100 cm^{-1} should be mainly due to the minerals.

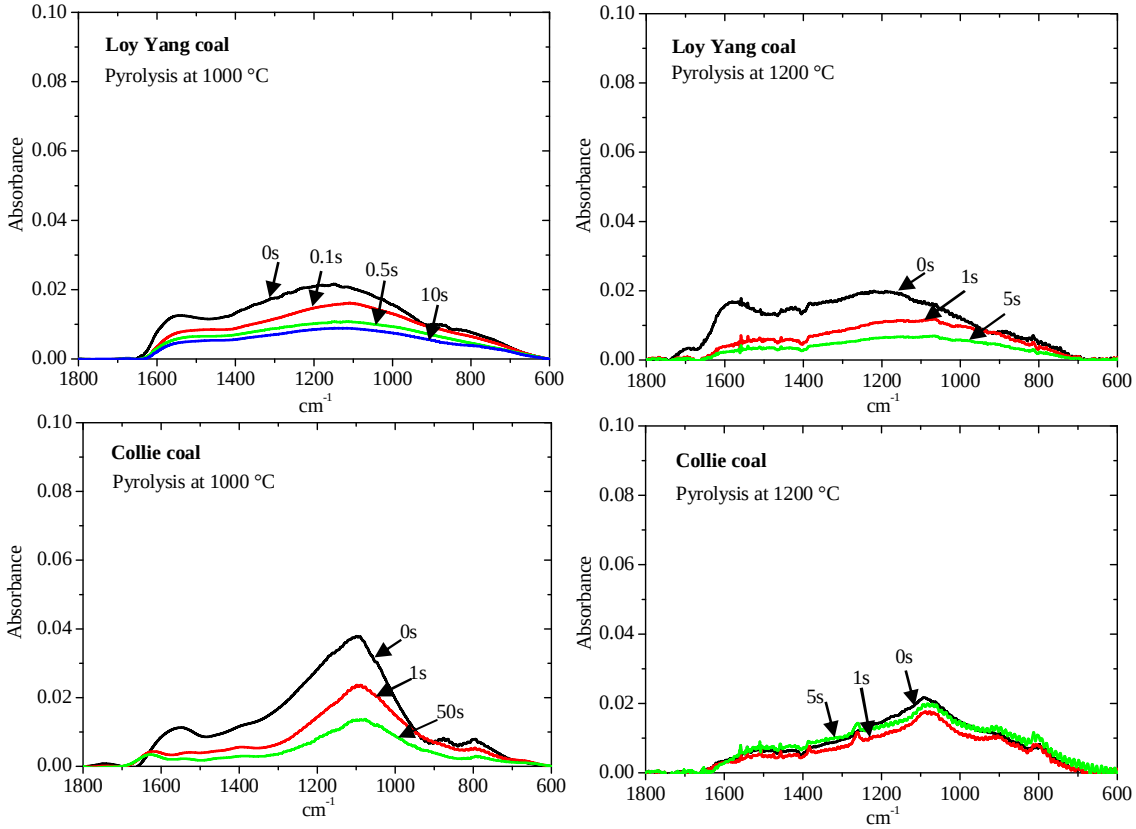

Figure 4-8 FTIR spectra from 600 to 1800 cm^{-1} as a function of holding time at 1000 and 1200 °C during the pyrolysis in He of two coals. All chars were produced in the wire-mesh reactor. The holding time at each peak temperature is shown. The concentration of char in KBr was identical.

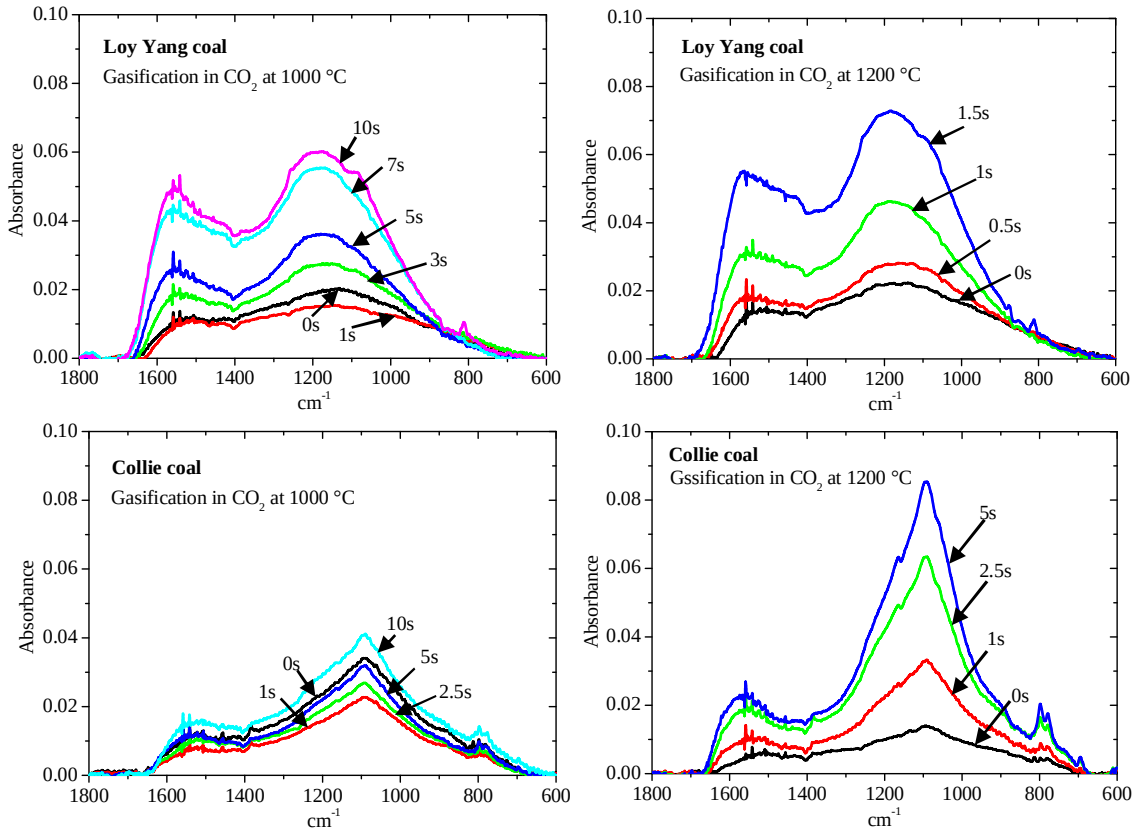

Figure 4-9 FTIR spectra at 600 to 1800 cm^{-1} as a function of holding time at 1000 and 1200 °C during the gasification in CO_2 of two coals. All chars were produced in the wire-mesh reactor. The holding time at each peak temperature is shown. The concentration of char in KBr was identical.

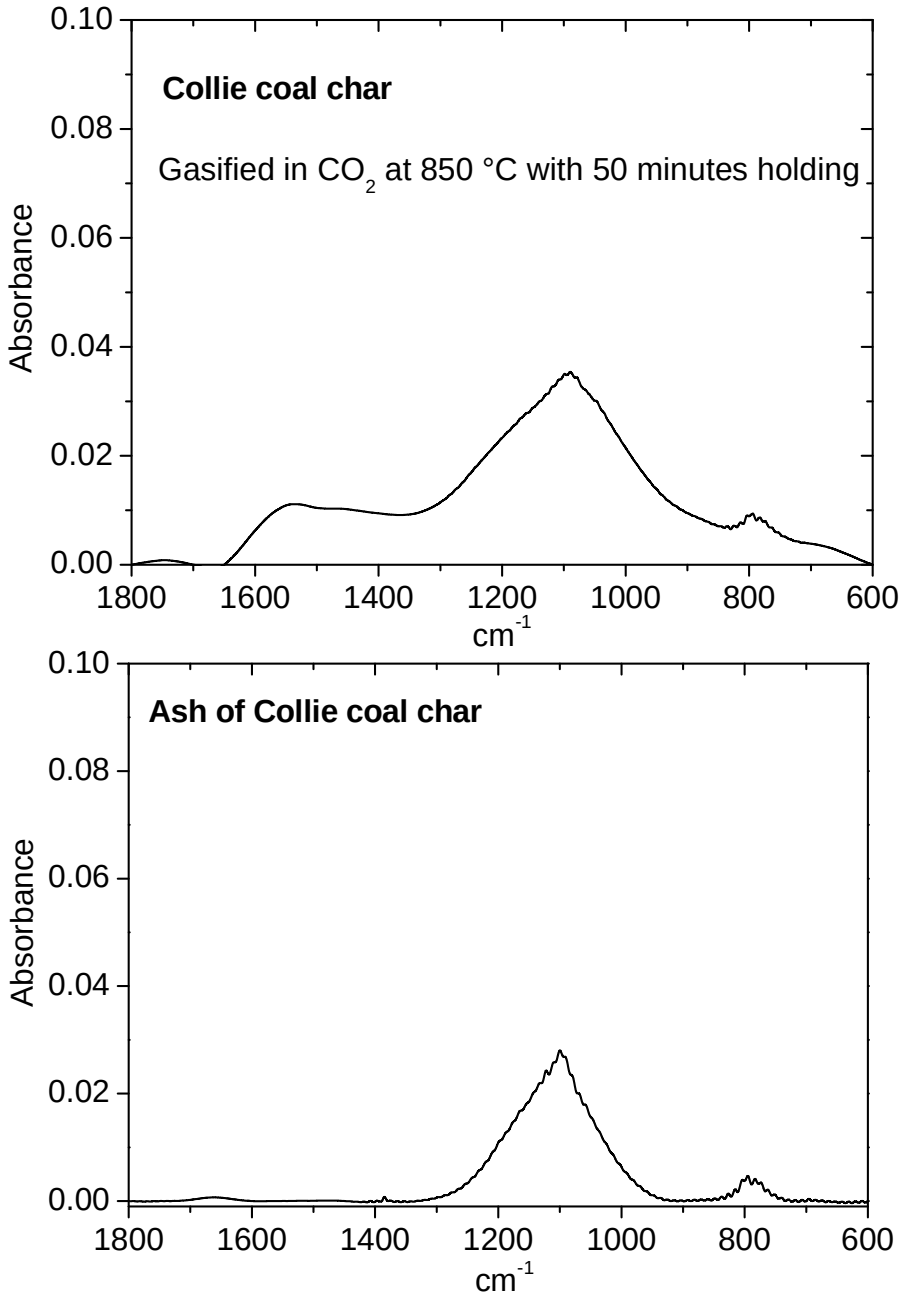

Figure 4-10 FTIR spectra of a Collie coal char and its ash from 600 to 1800 cm^{-1}. The char was produced through gasifying Collie coal in CO_2 at 850 °C with 50 minutes holding in a fluidised-bed/fix-bed reactor [14]. The concentration of ash in ash-KBr mixture equals the concentration of ash in char-KBr mixture.

4.4 Conclusions

The structural changes in nascent char were investigated during the fast gasification in CO_2/ pyrolysis in He for two coals at 1000 and 1200 °C. The results in this study show that:

1. A minimum in the total Raman area was observed for 1 s holding time at 1000 °C for two coals in CO_2. This indicates the counteracting effects of thermal annealing and oxygenation during the initial holding at 1000 °C.

2. With holding at 1000 °C (> 1 s) and 1200 °C in CO_2, the formation of O-containing functional groups and the change in ring systems rapidly took place and then gradually became steady with a few seconds residence at 1000 or 1200 °C.

3. For each coal, although the temperature affected the gasification rate significantly, the reaction pathway changed little between gasification at 1000 and 1200 °C.

4. There appear to be more than one type of O-containing functional groups formed during gasification in CO_2. Some are sensitive in the Raman scattering but some are sensitive in FTIR absorption.

5. The sites where the O complexes (in terms of FTIR spectroscopy) formed in chars are likely associated with aromatic rings and increase the intensity of C=C stretching vibration in aromatic rings accordingly.

6. The strong peak at 1100 cm^{-1} (FTIR spectrum) for Collie coal char mainly due to the minerals in char.

4.5 References

[1] Li C-Z. Special issue-gasification: a route to clean energy. Process Safety and Environmental Protection 2006;84:407-8.

[2] Skodras G, Nenes G, Zafeirou N. Low rank coal-CO_2 gasification: Experimental study, analysis of the kinetic parameters by Weibull distribution and compensation effect. Applied Thermal Engineering 2015;74:111-8.

[3] Wu H, Hayashi J-I, Chiba T, Takayuki T, Li C-Z. Volatilisation and catalytic effects of alkali and alkaline earth metallic species during the pyrolysis and gasification of Victorian brown coal. Part V. Combined effects of Na concentration and char structure on char reactivity. Fuel 2004;83:23-30.

[4] Li C-Z. Some recent advances in the understanding of pyrolysis and gasification behaviour of Victorian brown coal. Fuel 2007;86:1664-83.

[5] Li C-Z. Importance of volatile-char interactions during the pyrolysis and gasification of low-rank fuels-A review. Fuel 2013;112:609-23.

[6] Chabalala VP, Wagner N, Potgieter-Vermaak S. Investigation into the evolution of char structure using Raman spectroscopy in conjunction with coal petrography; Part 1. Fuel Processing Technology 2011;92:750-56.

[7] Jiménez F, Mondragón F, López D. Structure changes in coal chars after pressurized pyrolysis. Journal of Analytical and Applied Pyrolysis 2012;95:164-70.

[8] Zhu X, Sheng C. Influences of carbon structure on the reactivities of lignite char reacting with CO_2 and NO. Fuel Processing Technology 2010;91:837-42.

[9] Guo X, Tay H-L, Zhang S, Li C-Z. Changes in char structure during the gasification of a Victorian brown coal in steam and oxygen at 800 °C. Energy & Fuels 2008;22:4034-8.

[10] Sheng C. Char structure characterised by Raman spectroscopy and its correlations with combustion reactivity. Fuel 2007;86:2316-24.

[11] Wang M, Roberts DG, Kochanek MA, Harris DJ, Chang LP, Li C-Z. Raman spectroscopic investigations into links between intrinsic reactivity and char chemical structure. Energy & Fuels 2014;28:285-90.

[12] Su S, Song Y, Wang Y, Li TT, Hu S, Xiang J, Li C-Z. Effects of CO_2 and heating rate on the characteristics of chars prepared in CO_2 and N_2 atmospheres. Fuel 2015;142:243-9.

[13] Zhang S, Min ZH, Tay H-L, Asadullah M, Li C-Z. Effects of volatile-char interactions on the evolution of char structure during the gasification of Victorian brown coal in steam. Fuel 2011;90:1529-35.

[14] Li T, Zhang L, Dong L, Li C-Z. Effects of gasification atmosphere and temperature on char structural evolution during the gasification of Collie sub-bituminous coal. Fuel 2014;117:1190-5.

[15] Li X, Hayashi J-I, Li C-Z. FT-Raman spectroscopic study of the evolution of char structure during the pyrolysis of a Victorian brown coal. Fuel 2006;85:1700-7.

[16] Li X, Li C-Z. Volatilisation and catalytic effects of alkali and alkaline earth metallic species during the pyrolysis and gasification of Victorian brown coal. Part VIII. Catalysis and changes in char structure during gasification in steam. Fuel 2006;85:1518-25.

[17] Li X, Hayashi J-I, Li C-Z. Volatilisation and catalytic effects of alkali and alkaline earth metallic species during the pyrolysis and gasification of Victorian brown coal. Part VII. Raman spectroscopic study on the changes in char structure during the catalytic gasification in air. Fuel 2006;85:1509-17.

[18] Tay H-L, Li C-Z. Changes in char reactivity and structure during the gasification of a Victorian brown coal: Comparison between gasification in O_2 and CO_2. Fuel Processing Technology 2010;91:800-4.

[19] Tay H-L, Kajitani S, Zhang S, Li C-Z. Effects of gasifying agent on the evolution of char structure during the gasification of Victorian brown coal. Fuel 2013;103:22-8.

[20] Tay H-L, Kajitani S, Wang S, Li C-Z. A preliminary Raman spectroscopic perspective for the roles of catalysts during char gasification. Fuel 2014;121:165-72.

[21] Tay H-L, Kajitani S, Zhang S, Li C-Z. Inhibiting and other effects of hydrogen during gasification: Further insights from FT-Raman spectroscopy. Fuel 2014;116:1-6.

[22] Wang B, Sun L, Su S, Xiang J, Hu S, Fei H. Char structural evolution during pyrolysis and its influence on combustion reactivity in air and oxy-fuel conditions. Energy & Fuels 2012;26:1565-74.

[23] Zhang S, Min Z, Tay H-L, Wang Y, Dong L, Li C-Z. Changes in char structure during the gasification of mallee wood: effects of particle size and steam supply. Energy & Fuels 2012;26:193-8.

[24] Asadullah M, Zhang S, Min Z, Yimsiri P, Li C-Z. Effects of biomass char structure on its gasification reactivity. Bioresource Technology 2010;101:7935-43.

[25] Asadullah M, Zhang S, Li C-Z. Evaluation of structural features of chars from pyrolysis of biomass of different particle sizes. Fuel Processing Technology 2010; 91:877-81.

[26] Keown DM, Hayashi J-I, Li C-Z. Drastic changes in biomass char structure and reactivity upon contact with steam. Fuel 2008;87:1127-32.

[27] Keown DM, Li X, Hayashi J-I, Li C-Z. Characterization of the structural features of char from the pyrolysis of cane trash using fourier transform-Raman spectroscopy. Energy & Fuels 2007;21:1816-21.

[28] Sathe C, Hayashi J-I, Li C-Z. Release of volatiles from the pyrolysis of a Victorian lignite at elevated pressures. Fuel 2002;81:1171-8.

[29] Gibbins J.R., King R.A.V., Wood R.J., Kandiyoti R.. Variable-heating-rate wire-mesh pyrolysis apparatus. Review of Scientific Instruments 1989;60:1129-39.

[30] Sathe C, Pang Y, Li C-Z. Effect of heating rate and ion-exchangeable cations on the pyrolysis yields from a Victorian brown coal. Energy & Fuels 1999;13:748-55.

[31] Sathe C. Fates and roles of alkali and alkaline earth metallic species during the pyrolysis of low-rank coals. PhD Thesis, Monash University, 2001.

[32] Jamil K, Hayashi J-I, Li C-Z. Pyrolysis of a Victorian brown coal and gasification of nascent char in CO_2 atmosphere in a wire-mesh reactor. Fuel 2004;83:833-43.

[33] Jamil K. Pyrolysis and gasification of Victorian brown coal in inert and reactive gas atmospheres. PHD Thesis. Monash University, 2005.

[34] Kajitani S, Suzuki N, Ashizawa M, Hara S. CO_2 gasification rate analysis of coal char in entrained flow coal gasifier. Fuel 2006;85:163-9.

[35] Zhang L, Li T, Quyn D, Dong L, Qiu P, Li C-Z. Formation of nascent char structure during the fast pyrolysis of mallee wood and low-rank coals. Fuel 2015;150:486-92.

[36] Supaluknari S, Larkins FP. An FTIR study of Australian coals: characterization of oxygen functional groups. Fuel Processing Technology 1988;19:123-40.

[37] Lin-Vien D, Colthup Norman B, Fateley William G, Grasselli Jeanette G. The handbook of infrared and Raman characteristic frequencies of organic molecules. San Diego, CA, USA: Academic press; 1991 p. 476-90.

[38] Painter PC, Snyder RW, Starsinic M, Coleman MM, Kuehn DW, Davis A. Concerning the application of FT-IR to the study of coal : a critical assessment of band assignments and the application of spectral analysis programs. Applied Spectroscopy 1981;35:475-85.

[39] Solomon PR. Relation between coal structure and thermal decomposition products. Adv. Chem. Ser.1981;192:95-112.

[40] Painter PC, Coleman MM, Jenkins RG, Walker PL Jr. Fourier transform infrared study of acid-demineralized coal. Fuel 1978; 57:125-6.

[41] Painter PC, Coleman MM, Jenkins RG, Whang PW, Walker PL Jr. Fourier transform infrared study of mineral matter in coal. A novel method for quantitative mineralogical analysis. Fuel 1978;57:337-44.

[42] Li C-Z, Sathe C, Kershaw JR, Pang Y. Fates and roles of alkali and alkaline earth metals during the pyrolysis of a Victorian brown coal. Fuel 2000;79:427-38.

Chapter 5

Changes in char structure during the thermal treatment of nascent chars in N_2 and the in-situ gasification in O_2

5.1 Introduction

Gasification is an increasingly evolving clean energy technology that has been widely applied in industry. One of the advantages is that it is particularly suitable for the utilisation of low rank fuels to produce synthesis gas due to their high gasification reactivity [1]. During gasification, there are four main factors influencing the char reactivity [2]: the chemical form of catalyst, the concentration of catalyst, the distribution of catalyst on char (pore) surface and the physico-chemical structure of char. Among these factors, the changes in char structure would directly affect the reactivity itself and also affect the distribution of AAEM species or the holding capacity of AAEM species of char. The latter would in turn influence the char reactivity [3-4].

Due to the significant roles of char structure in gasification, many techniques have been developed to characterise structural features of char, such as X-ray diffraction (XRD), high-resolution transmission electron microscopy (HRTEM), FT-IR spectroscopy, Raman spectroscopy, etc. Particularly, Raman spectroscopy has been widely used to understand the highly disordered carbonaceous matters in low-rank fuels during pyrolysis and gasification [5-23]. The Raman spectrum in the area between 800 and 1800 cm^{-1} was deconvoluted into 10 bands that can provide the detailed information about the structural features such as the O-containing functional groups (total Raman area), the aromatic ring systems (D band and Gr+Vl+Vr band), the crosslinking structures (S band) and aliphatic structures (R band) [5].

The reaction of coal char with O_2 is inevitable in a gasifier, hence many mechanism studies in this field have been performed extensively. Some highly ordered carbon materials such as graphite and pitch coke were used to investigate the gasification mechanism [24-26]. These findings cannot be directly applied to the study of gasification of low-rank fuels, which consist of highly disordered carbon. Widely, the gasification of low-rank fuels in O_2 has been investigated by employing Raman spectroscopy. Li and co-workers [7] compared the catalytic with the non-catalytic gasification (in air) mechanism. It is believed that the catalyst causes the gasification

reaction to unselectively take place at the sites associated with the catalysts. Keown and co-workers [12] studied on the biomass char structure evolution during gasification in O_2. This showed the preferential consumption of small aromatic rings and aliphatic structures that caused the char structure to became more condensed. However, there was little study focusing on the structural changes during the gasification of "nascent" char in O_2. As was investigated in my previous work [23, 27], nascent char structure changed significantly during initial holding at temperatures from 600 to 1200 °C, which indicated large differences between the char structure of nascent char and aged char. Additionally, nascent char structure, which keeps some reactive structures such as O-containing functional groups, may play a different role in the gasification reactions in O_2 compared to aged char.

In this study, two nascent chars were produced from the fast pyrolysis of Loy Yang coal and Collie coal in a wire-mesh reactor which was capable of minimising the volatile-char interactions. After the acquisition of two nascent chars, they firstly underwent further pyrolysis by TGA from room temperature to 600 °C. The changes in the chemical structural features of nascent chars during the further pyrolysis in N_2 were characterised by the use of FT-Raman spectroscopy in order to understand the very active structures in nascent char. The reaction between nascent char and O_2 was carried out at 370 °C to avoid ignition and to guarantee gasification occurred in the chemical-reaction-controlled regime. The changes in char reactivity and structure during the gasification of two different coals or in two different O_2 concentrations were thus discussed.

5.2 Experimental

5.2.1 Nascent char samples preparation

Two nascent chars were produced from the pyrolysis of two coals (Loy Yang brown coal and Collie sub-bituminous coal) in a wire-mesh reactor [23]. Briefly, around 10 mg raw coal was loaded into the wire-mesh reactor, heating up to 600 °C at

1000 K s^{-1} with 0 s holding. Since the amount of char from one experiment was limited (~5mg for Loy Yang coal and ~7 mg for Collie coal), the experiment was repeated 10 times for each coal and then the chars were well mixed and stored in the fridge preparing for the further experiments in thermogravimetric analyser (TGA).

5.2.2 Pyrolysis of the nascent chars again in TGA

The nascent char was put into the crucible of a Perkin-Elmer Pyris 1 TGA and was heated to different peak temperatures up to 600 °C in N_2 at a heating rate of 20 K s^{-1}. After it reached the target temperature, the TGA would stop heating and the char would be cooled down by sweeping of N_2 at 0.1 L min^{-1} without contact with air. After the sample temperature dropped down to room temperature, the sample was taken out and finely ground with KBr for subsequent Raman spectroscopic analysis.

5.2.3 Further in-situ gasification of nascent char in O_2 and the specific reactivity analysis

Two O_2 concentrations were used in this study: 5% and 21%. 370 °C was chosen as the gasification peak temperature. After the nascent char was pyrolysed to 370 °C in N_2, the gas was directly switched to 5% or 21% O_2 balanced with N_2 and the temperature was holding at 370 °C. After the acquisition of the weight loss curve as a function of holding time, the specific reactivity (R) was calculated according to the equation

$$R = -\frac{1}{W}\frac{dW}{dt} \qquad (1)$$

where W represents the weight (daf basis) of the char at any given time t. During the gasification in O_2, the chars at different char conversion levels were collected and mixed with KBr for Raman analysis.

5.2.4 FT-Raman spectroscopy for char characterization

A Perkin-Elmer GX FT-Raman spectrometer was used for the characterisation of the

char structure. The char sample was firstly mixed and ground with the spectroscopic grade potassium bromide (KBr). The weight percentage of char in mixture was chosen at 0.25% according to the previous study [23]. The Raman spectra in the wavenumber range between 800 and 1800 cm^{-1} were curve-fitted with 10 Gaussian bands by GRAMS/32 AI software (version 6.0). The total Raman area, (G_r+V_l+V_r) bands, D band, S band and R band were used to characterise the structural features of chars [5].

5.3 Results and discussion

5.3.1 Changes in the char structure during the thermal treatment of nascent chars in TGA

5.3.1.1 Further weight loss during the pyrolysis of nascent chars again in TGA

Figure 5-1 shows the changes in char conversion as a function of peak temperature. It is clear that reheating the nascent char would lead to further weight loss with temperature rising from room temperature to 600 °C. Significant weight loss was observed after the temperature arriving at higher than 400 °C. The weight loss of Loy Yang coal nascent char was greater than that of Collie coal nascent char during the pyrolysis, indicating the lower stability of Loy Yang coal nascent char than the Collie char.

5.3.1.2 Changes in char structures during the further pyrolysis of nascent chars

The total Raman area peak from 800 to 1800 cm^{-1} and the different band area ratios obtained for the further pyrolysed nascent chars are shown in Fig. 5-2. Firstly, the changes in the total Raman area as a function of temperature are illustrated in Fig. 5-2 (a). The total Raman area is mainly influenced by two factors. The first one is the existence of O-containing functional groups which could enhance the total Raman area by the direct contribution of Raman peak intensity itself and, more

significantly, by having a resonance effect with the attached aromatics that will subsequently enhance the Raman intensity of the aromatics [16-17, 28]. The second factor is that the big aromatic ring systems have higher light absorptivity [5], thereby weakening the total Raman intensity.

In Fig. 5-2 (a), the total Raman area of Collie coal char clearly decreased at the temperature from 270 to 420 °C. This is mainly due to the loss of O-containing functional groups at low temperature range. As for the Loy Yang coal char, the total Raman area showed a slight decrease at the temperature from 270 to 370 °C and then increased during heating from 370 to 600 °C. It is indicated that, besides the release of the O-containing functional groups, there may be some other reactions happening during the pyrolysis of Loy Yang coal nascent char at temperature > 370 °C. First possible reaction is the thermal cracking of aromatic rings which may reduce the light absorptivity of nascent char and then relatively enhance the total Raman intensity. However, this is relatively unlikely because the temperature was not sufficiently high to cause significant cracking of aromatic structures. Secondly, since not all types of O-containing functional groups can contribute to the enhancement of Raman intensity [16], there might be some transformations of the chemical forms of the O-containing functional groups from lower Raman intensity groups (which have weak resonance with aromatic rings) to relatively higher ones (which have better resonance effects), thus causing non-monotonous change in total Raman area.

Figure 5-2 (b) shows the changes in $I_{(Gr+Vl+Vr)}/I_D$ during the nascent char conversion. The bands of (Gr+Vl+Vr) and D mainly represent the small aromatic ring systems (with 3-5 rings) and the large aromatic ring systems (with > 6 rings), respectively. The ratio of $I_{(Gr+Vl+Vr)}$ to I_D can be used as a useful parameter to reflect the distribution of aromatic ring systems in char matrix.

In Fig. 5-2 (b), $I_{(Gr+Vl+Vr)}/I_D$ of Loy Yang coal nascent char showed a gradual decrease at the temperature from 270 °C. This might be due to the selective release of small aromatic rings and/or the conversion of small to large rings. At low temperature ranging from 270 to 370 °C, there was less than 3% decrease in char

yield. It reveals the little possibility of the selective release of small rings. Moreover, as discussed above, there should be some release or transformation of O-containing functional groups within this temperature range. It is suggested that the relative growth of large rings might be attributed to the bond breaking of some active O-containing functional groups on the heteroaromatics and the formation of new aromatic rings subsequently. With the temperature rising to higher than ~370 °C, the further gradual reduction in $I_{(Gr+Vl+Vr)}/I_D$ should be also due to the selective release of some active small rings, which combine with the transformation of O-containing structure to result in ~12% weight loss (in Fig. 5-1) and the increase in total Raman area [in Fig. 5-2 (a)]. For Collie coal nascent char, there was much less change in the distribution of ring systems than Loy Yang coal nascent char. It is confirmed that the stability of Collie coal nascent char is higher, possibly due to more condensed aromatic ring systems [$I_{(Gr+Vl+Vr)}/I_D$ of ~2.1 in Fig. 5-2 (b)], than that of Loy Yang coal nascent char [$I_{(Gr+Vl+Vr)}/I_D$ of ~3.2 in Fig. 5-2 (b)].

Figure 5-2 (c) shows the changes in the ratio of I_S to total Raman area as a function of pyrolysis temperature. S band can be considered as an approximate measurement of the cross-linking structures [14]. For Loy Yang coal nascent char, $I_S/I_{\text{Total Raman area}}$ considerably increased during heating from 270 to 600 °C. This might be due to the formation of new alkyl-aryl or other cross-linking structures during the reactions taken place at low temperature. Collie coal nascent char showed less increase in $I_S/I_{\text{Total Raman area}}$ than Loy Yang coal nascent char, showing the higher stability of Collie coal char structure.

The ratio of I_R to $I_{\text{Total Raman area}}$ that represents the structures like alkanes and cyclic alkanes or the C-H band on aromatic rings is illustrated in Fig. 5-2 (d). R band which only accounted for ~8 and ~5% of total Raman area for Loy Yang nascent char and Collie coal nascent char respectively showed slight decreases in the band ratio during heating up to 600 °C. It might be due to the reactions of dealkylation and dehydrogenation during the reheating of nascent chars.

Taking together all the Raman data of further changes in nascent char structure

during pyrolysis, it is clear that the nascent char structure was very active, especially some O-containing functional groups that were broken even at ~300 °C. However, the process of deoxygenation affected more on the changes in nascent char structure of Loy Yang coal than that of the higher ranked Collie coal, owing to the more condensed and more cross-linked structures in Collie coal nascent char. The effects of these different char properties on the following gasification in O_2 will be discussed in the sections below.

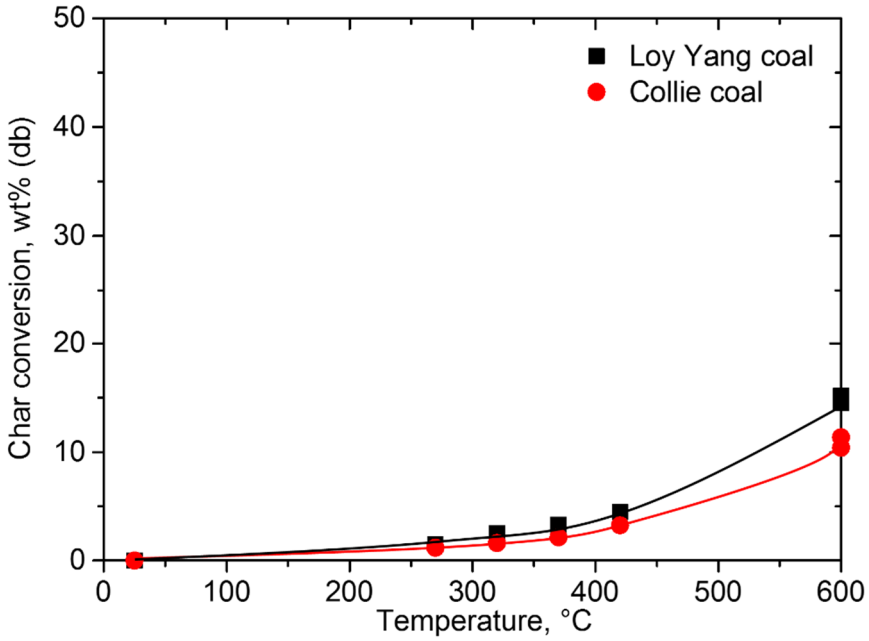

Figure 5-1 The further char conversion of the nascent char as a function of pyrolysis temperature in TGA. The Loy Yang coal nascent char and Collie coal nascent char were produced in the wire-mesh reactor at 1000 K s^{-1} heating to 600 °C with 0 s holding time.

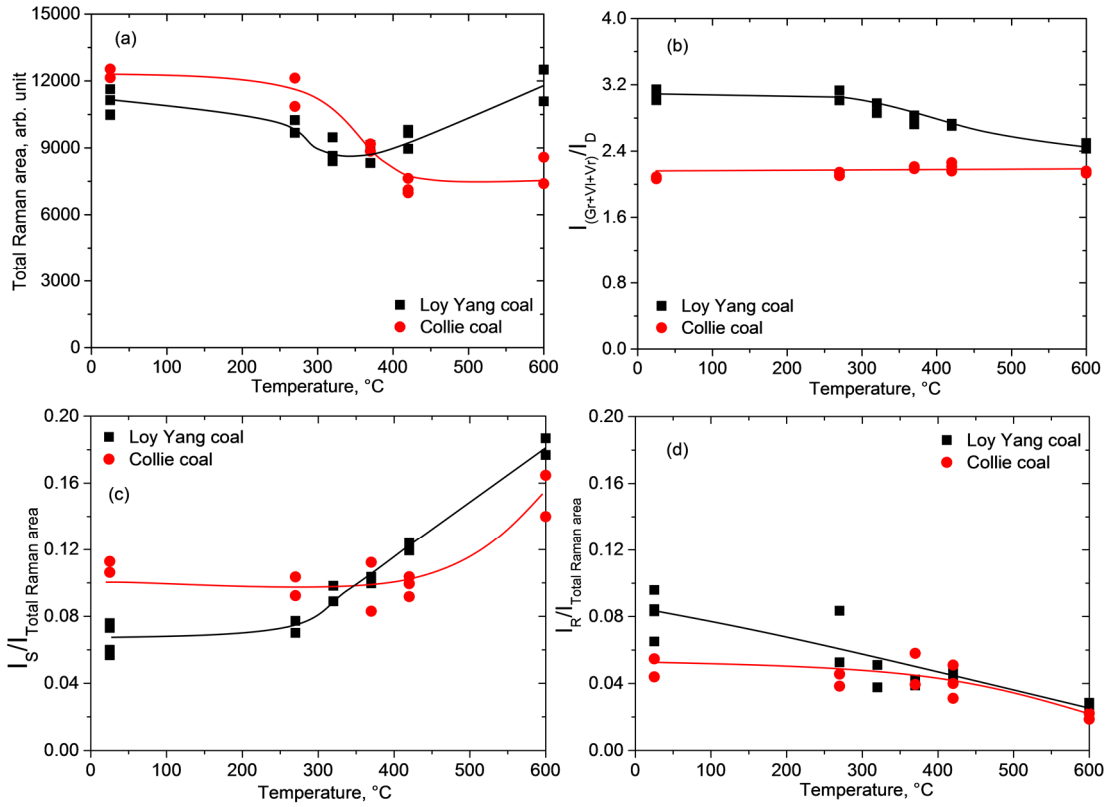

Figure 5-2 The further changes in char structure of the nascent char as a function of pyrolysis temperature in TGA. The Loy Yang coal nascent char and Collie coal nascent char were produced in the wire-mesh reactor at 1000 K s^{-1} heating to 600 °C with 0 s holding time.

5.3.2 Loy Yang coal nascent char reactivity during gasification in two different O_2 concentration atmospheres

Figure 5-3 shows the nascent char reactivity as a function of char conversion in two different O_2 concentration atmospheres: 21% O_2 balanced with N_2 and 5% O_2 balanced with N_2. The gasification was carried out at low temperature (370 °C) in TGA.

In Fig. 5-3, as expected, the reactivity of nascent char gasified in 21% O_2 was much higher than that gasified in 5% O_2, whereas the shapes of two reactivity curves were very similar. Specifically, two peaks were shown in the reactivity curves. The first one appeared at the initial char conversion of ~5% followed by a gradual decrease at the char conversion < 40%. This initial rapid gasification rate seemed unlikely to be due to the catalytic effect of AAEM species in nascent char. The AAEM species concentration in char would continuously increase with the char conversion (removal of carbonaceous matter) as there would be little release of AAEM species during the oxidation of char at 370 °C [29]. As a result, with the accumulation of AAEM species in the char, the reactivity should monotonously increase during the initial char conversion [3-4]. However, the reactivity in Fig. 5-3 showed a monotonous decrease with the char conversion from ~5 to ~40%. Therefore, it is assumed that the changes of char reactivity peak at ~5% conversion were most likely due to the presence of some active char structures that were rapidly gasified during the initial gasification in O_2.

The second peak was observed at the char conversion of ~90% after the monotonous increase in the reactivity from the conversion of ~40 to ~90%. It should be mainly due to the accumulation of AAEM species on the char (pore) surface [2]. This accumulation may have two origins. Firstly, the removal of carbonaceous structures by gasification would increase the overall concentration of AAEM species. Secondly and more importantly, this may be due to the migration of AAEM species in char. The changes in char reactivity as a function of AAEM concentration was illustrated in Fig. 5-4. If the initial AAEM concentration in nascent char was assumed at 1%, it

is clear that the reactivity is not linear as a function of the AAEM concentration at the char conversion from ~40 to ~90% in O_2. This implies the significant effect of the migration of AAEM species on char reactivity, which may be largely related to the structural changes in char during the gasification in O_2. The following section will discuss about the changes in char structure during the gasification of nascent char in O_2.

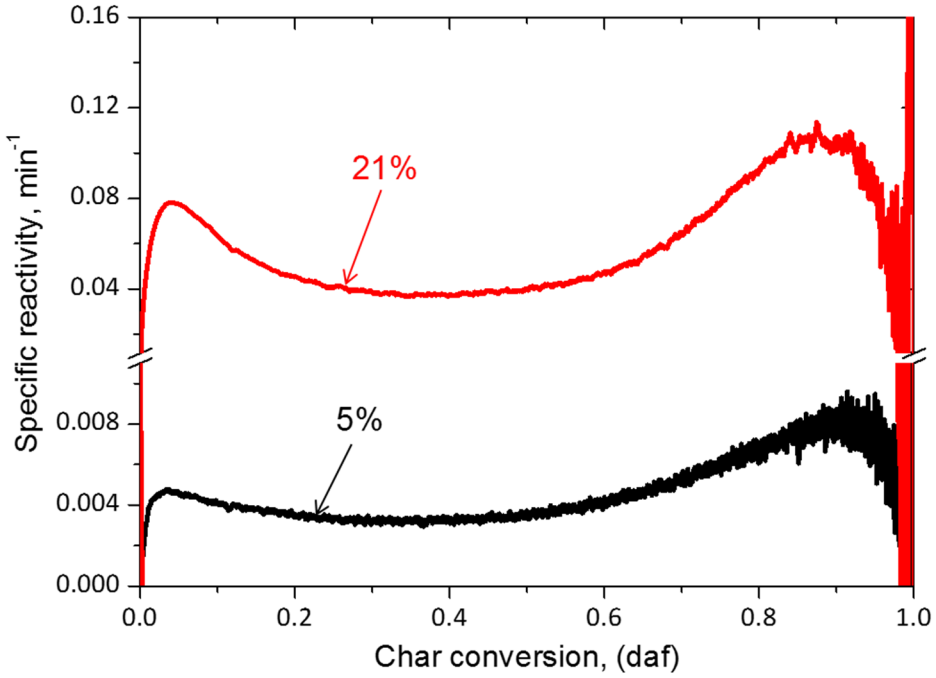

Figure 5-3 Specific reactivity of Loy Yang coal nascent char analysed at 370 °C in two atmospheres: 21% O_2 balance with N_2; 5% O_2 balance with N_2. The nascent char was produced in the wire-mesh reactor at 600 °C with 1000 K s^{-1} heating rate and 0 s holding time.

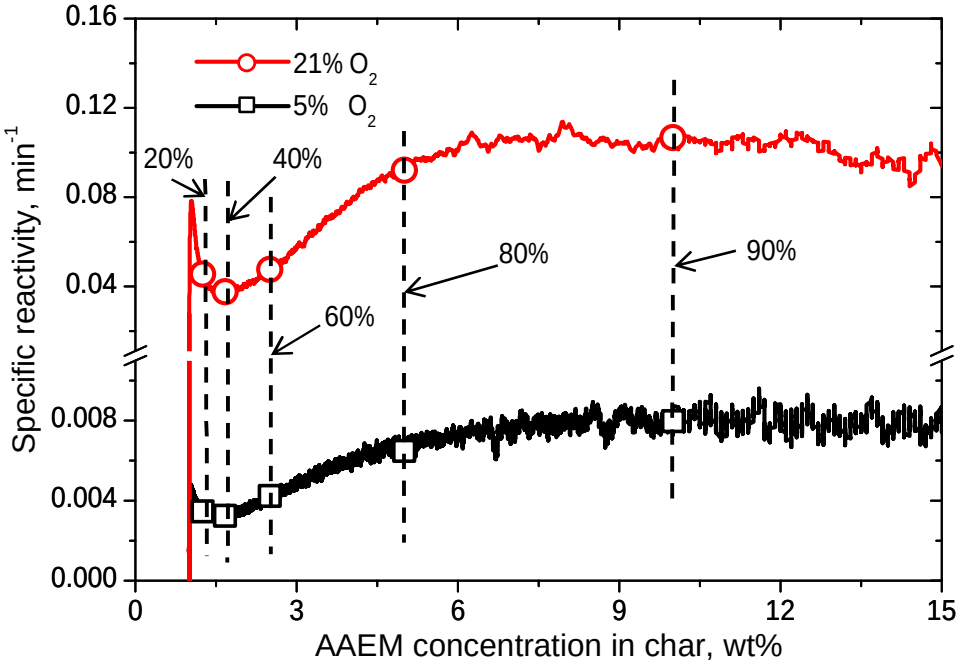

Figure 5-4 Specific reactivity of Loy Yang coal nascent char as a function of AAEM concentration. Reactivity analysed at 370 °C in two atmospheres: 21% O_2 balance with N_2; 5% O_2 balance with N_2. The nascent char was produced by wire-mesh reactor at 600 °C with 1000 K s^{-1} heating rate and 0s holding time. The percentages in the figure means the char conversion.

5.3.3 Structural changes in Loy Yang coal nascent char during gasification in O_2

5.3.3.1 Changes in total Raman area during gasification in O_2

Figure 5-5 (a) shows the changes in the total Raman area between 800 and 1800 cm^{-1} during the slow pyrolysis (20 K s^{-1}) of nascent char in TGA to 370 °C and in-situ gasification in 5%/21% O_2 balanced with N_2 at 370 °C.

As is shown in Fig. 5-5 (a), the total Raman area shows a large decrease during the initial pyrolysis of nascent char from room temperature to 370 °C. As was discussed in Section 5.3.1.2, this might be due to the loss of some active O-containing functional groups. In the following step, after the char contacted with O_2, the total Raman area showed a gradual increase with the char conversion growing to ~80%. It might be owing to the newly formed O-containing functional groups (high Raman intensity) during the gasification and/or the consumption of aromatic ring systems. After the char conversion increase to > ~80%, the total Raman area showed a large decrease, which was similar to the significant decrease in reactivity shown in Fig. 5-3. This can be attributed to the increasing concentration of highly condensed carbonaceous matter (larger aromatic rings) in char at high char conversion. The dispersion of Na would be deteriorated with the enrichment of larger aromatic ring systems in char and would subsequently decrease the char gasification reactivity [15]. Moreover, at high conversion levels, the minerals should constitute a large proportion of char and might affect the shape of Raman spectrum. However, no significant peaks were observed at the wavenumber < 1500 cm^{-1} [30], suggesting the little effect of mineral matter on the Raman intensity of carbonaceous structure in this study. Comparing the gasification in two different O_2 concentration atmospheres, only showed a slightly higher total Raman area in 5% O_2 than that in 21% O_2, while the nascent char in 21% O_2 had significantly higher reactivity than that in 5% O_2 (shown in Fig. 5-3). As was mentioned above, the increasing total Raman area might be affected by the additional O-containing functional groups and/or the consumption of aromatic ring systems. During the gasification in the lower O_2 concentration

atmosphere, the gasification rate is slower (Fig. 5-3), allowing more chance for the O-containing structures to survive in the char or on the char surface.

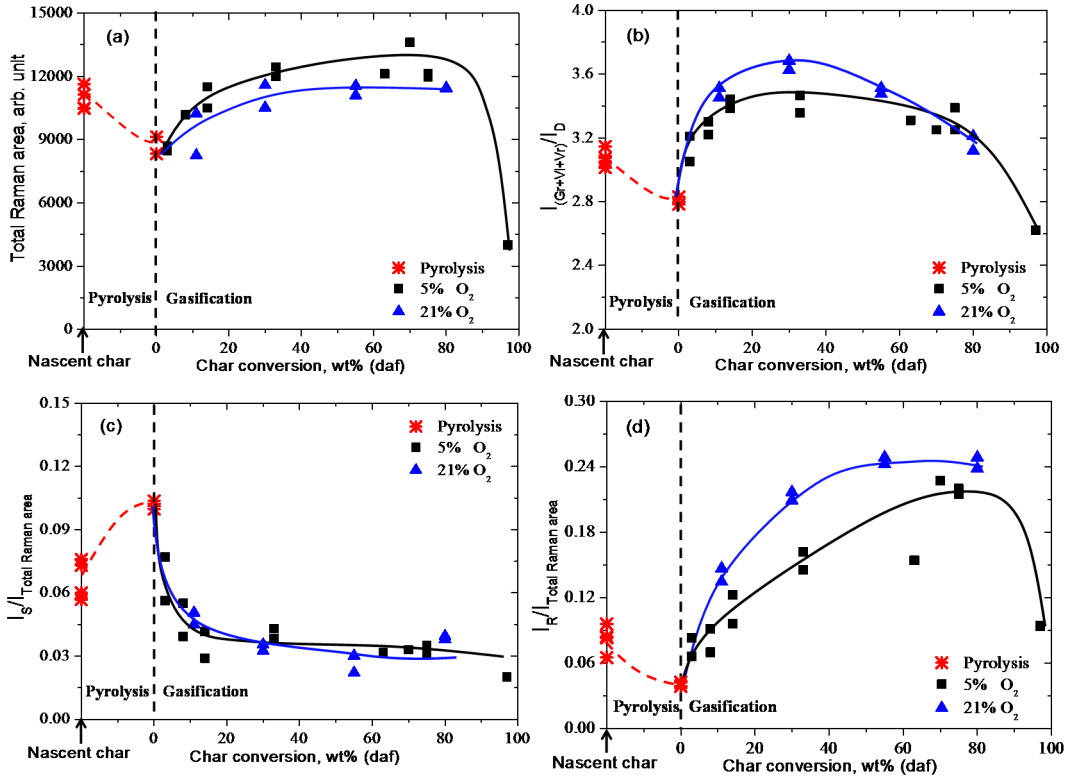

Figure 5-5 The structural changes in Loy Yang nascent char during the reheating to 370 °C in N_2 and the in-situ gasification at 370 °C in two atmospheres: 21% O_2 balanced with N_2; 5% O_2 balanced with N_2.

5.3.3.2 Changes in ring systems during gasification in O_2

Figure 5-5 (b) shows the changes in $I_{(Gr+Vl+Vr)}/I_D$ during the slow pyrolysis (20 K s^{-1}) of nascent char to 370 °C and the in-situ gasification in 5%/21% O_2 balanced with N_2 at 370 °C. The changes in $I_{(Gr+Vl+Vr)}/I_D$ also illustrates two distinct trends between pyrolysis and gasification of nascent char. During the initial pyrolysis of nascent char (from room temperature to 370 °C), the ratio of small to large aromatic rings decreased from ~3.1 to ~2.6. After the thermal treated char reacted with O_2, it had a significant increase in $I_{(Gr+Vl+Vr)}/I_D$ during the initial ~20% char conversion. It is believed that there is a significant conversion of large to small aromatic rings during the initial gasification in O_2. It seems that more active sites existed on large aromatic rings than that on small ones, where the O_2 would preferentially react with to form O-containing functional groups [Fig. 5-5 (a)]. Subsequently, the O-containing functional groups might further activate the associated aromatic rings and cause the cleavage of large rings. It is envisaged that these active sites on large aromatic rings might be generated from the partial deoxygenation during the initial pyrolysis process and/or originally existed in Loy Yang coal nascent char.

With the char conversion increasing from ~20 to ~60%, insignificant change in $I_{(Gr+Vl+Vr)}/I_D$ was observed during the gasification in O_2. This reveals that, a dynamic balance between the generation and consumption of O-containing structures was maintained during this period of gasification. This was confirmed by the relatively stable reactivity within this char conversion range shown in Fig. 5-3. The gasification started to unselectively occur on whole ring systems. With the increasing cleavage of aromatic rings, some sites associated with catalytic species, which were initially hindered by the aromatic ring systems, was exposed on the char (pore) surface and subsequently increased the reactivity during the conversion from 60% to 90%. Finally, the fast decrease in the ratio of small to large rings confirms the above discussion that the remaining highly condensed ring systems would cause the lower reactivity of the char at high conversion level.

The difference between the ratio [$I_{(Gr+Vl+Vr)}/I_D$] in 5% O_2 and 21% O_2 was slight. As

was discussed, during initial pyrolysis to 370 °C, some large aromatic rings were formed due to the deoxygenation. Although deoxygenation proceeded much slower than other gasification reactions, this reaction would also take place during the following gasification in O_2 and tend to affect the char structure more in the slower gasification rate atmosphere (5% O_2). As a result of that, $I_{(Gr+Vl+Vr)}/I_D$ was smaller during gasification in 5% O_2 than in 21% O_2.

5.3.3.3 Changes in the band ratio of I_S to $I_{Total\ Raman\ area}$ during gasification in O_2

Figure 5-5 (c) shows the changes in the ratio of I_S to $I_{Total\ Raman\ area}$ during the slow pyrolysis (20 K s^{-1}) of nascent char in TGA to 370 °C and the subsequent in-situ gasification in 5% or 21% O_2 balanced with N_2 at 370 °C. During initial pyrolysis, a large increase was observed in $I_S/I_{Total\ Raman\ area}$ from room temperature to 370 °C. It has been discussed that the newly formed C-C bond between alkyl-aryl should be mainly due to the loss of O-containing functional groups. However, when the nascent char reacted with O_2, $I_S/I_{Total\ Raman\ area}$ decreased considerably within 20% char conversion. It is indicated that, apart from the preferential gasification on the large aromatic rings during the initial char conversion shown in the last section, the gasification would also have priority to take place on sites like alkyl-aryl C-C structures. This agrees with our previous finding [7]. There was little difference in the trend of $I_S/I_{Total\ Raman\ area}$ between gasification in two atmospheres having different O_2 concentrations. This reveals that the reaction leading to the cleavage of cross-linking structures would be quick and little affected by the overall gasification rate. These cross-linking structures would be consumed rapidly and decrease to only around 4% of the total Raman area within 20% char conversion.

5.3.3.4 Formation of dangling structures during the gasification of nascent char in O_2

The R band mainly represents structures like alkanes and cyclic alkanes or the C-H bond on aromatic rings. These structures are very active and are fast broken off during the pyrolysis at 600 °C [14, 23]. As is shown in Figs. 5-2 (d) and 5-5 (d),

$I_R/I_{Total\ Raman\ area}$ showed a slight decrease during the pyrolysis of nascent char in TGA at 370 °C. As discussed in Section 5.3.1.2, this was within expectation because there were still some aliphatic or cyclic aliphatic structures existing in the nascent char, which released during the reheat of nascent char in TGA. The structural features of the char changed drastically (in terms of R band) when the char contacted with O_2. The significant growth of the percentage of R band in total Raman intensity was observed during the gasification of the char up to about 80% char conversion. This reveals the formation of some aliphatic or sp^3-rich structures during gasification. These newly formed structures would be mainly due to the partial breakage of aromatic rings, which converted to the dangling structures hanging on the rest of aromatic rings. Since these dangling structures may also undergo the gasification/thermal cracking during the gasification at 370 °C, the fact that less dangling structure formed in 5% O_2 than that in 21% O_2 might be attributed to the slow gasification rate in 5% O_2.

5.3.4 Comparison of the reactivity of the Collie coal nascent char with the Loy Yang nascent char

Figure 5-6 shows the reactivity of the two nascent chars during the gasification in O_2 at 370 °C. It can be clearly seen that, one broad plateau was presented in the reactivity of Collie coal char at the conversion $\leq$ 20% followed by monotonous decrease in the remaining conversion process while two peaks were shown in the reactivity of Loy Yang coal char plotted as a function of char conversion. This continuous reduction of reactivity with the accumulation of AAEM species indicated that the reactivity of Collie coal nascent char was mainly determined by the changes in char structures. In other words, the inorganics in the Collie coal had much lower catalytic effects during gasification than those in the Loy Yang coal.

5.3.5 Different reaction pathway of two nascent chars during the gasification in O_2

Figure 5-7 shows the transformation of total Raman area and band ratios during the

slow pyrolysis (20 K s^{-1}) of nascent chars in TGA to 370 °C and further in-situ gasification in 5% O_2 balanced with N_2 at 370 °C.

During the initial pyrolysis, the significant decrease in total Raman area of Collie coal char was mainly due to the loss of O-containing functional groups. As was discussed in Section 5.3.1.2, it might be due to the higher stability of char structures in Collie coal nascent char than that of Loy Yang coal nascent char.

During the gasification in 5% O_2, a slight increase in the total Raman area of Collie coal char was noticed in Fig. 5-7 (a). It is suspected that less O-containing functional groups (less oxidisation) were formed during the gasification of Collie coal than that of Loy Yang coal. Tay and co-workers [31] found that the oxygenation taking place during char gasification would increase the gasification rate at 800 °C. Therefore, the overall lower gasification reactivity of Collie coal char in O_2 might be partially due to the lower oxygenation extent of Collie coal char than Loy Yang coal char.

As for the changes in ring systems during gasification shown in Fig. 5-7 (b), the ratio of small to large rings of Collie coal char increased much less than that of Loy Yang coal char during the initial gasification (< 20%) and then gradually decreased during the further char conversion. Correlating to the little formation of O-containing functional groups and dangling structures shown in Fig. 5-7 (a) and (d) in Collie coal char, it is believed that the gasification pathway of Collie coal char is different from that of Loy Yang coal char at 370 °C. As for the more condensed char structure of Collie coal than Loy Yang coal, O_2 was very difficult to change the Collie coal nascent char structure, especially the ring systems. The only significant change in Collie coal char structure was the large decrease in the cross-linking structures during the initial~20% char conversion shown in Fig. 5-7 (c), partly responsible for a broad plateau in char reactivity during the initial ~20% char conversion shown in Fig. 5-6.

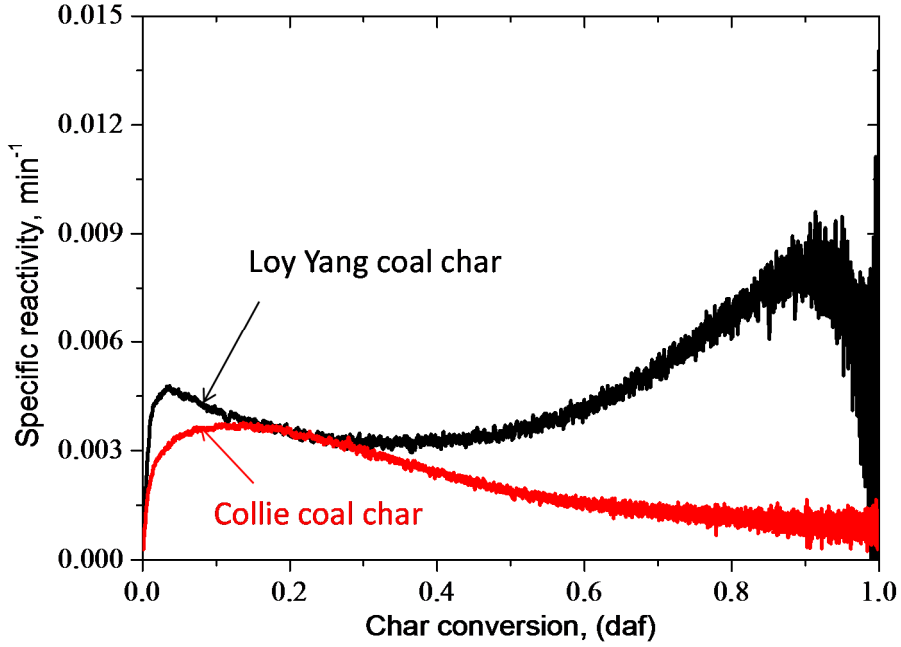

Figure 5-6 Specific reactivity of two nascent chars (Loy Yang coal char and Collie coal char) analysed at 370 °C in 5% O_2 balanced with N_2. The nascent chars were produced in the wire-mesh reactor at 600 °C with 1000 K s^{-1} heating rate and 0 s holding time.

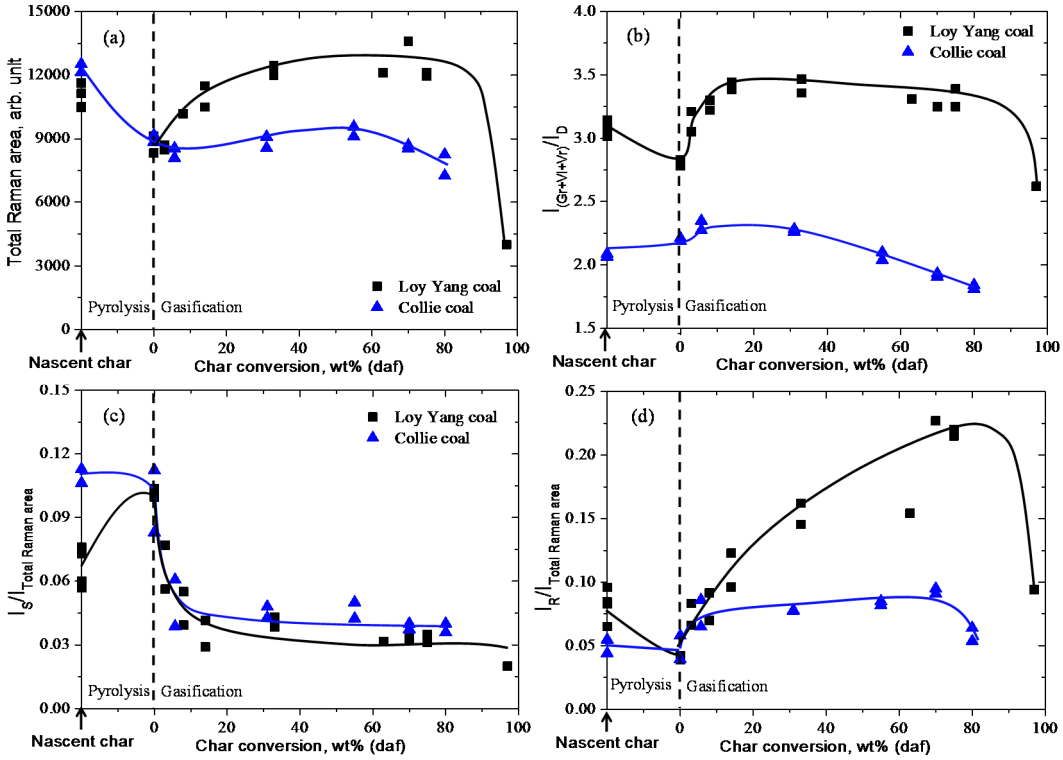

Figure 5-7 The structural changes in the two nascent chars (Loy Yang coal char and Collie coal char) during reheating to 370 °C in N_2 and the in-situ gasification at 370 °C in 5% O_2 balance with N_2.

5.4 Conclusions

This study investigated the structural changes in nascent chars during the thermal treatment to 600 °C and in-situ gasification in O_2 at 370 °C.

1. Some very active structures especially O-containing functional groups, which appear to break off during reheat of nascent char at low temperature (> 270°C) were found in nascent chars. The deoxygenation caused more structural changes in Loy Yang brown coal char than in Collie sub-bituminous coal char.

2. There are two peaks in the reactivity of Loy Yang brown coal nascent char. The initial one appears to be mainly due to the active char structure and the second one may be caused by both the effect of AAEM concentration and char structure. One peak at the initial char conversion was observed in the reactivity of Collie sub-bituminous coal nascent char, which is mainly related to the structural features rather than catalytic species.

3. As well as the great changes in char structure during the thermal treatment, significant changes in Loy Yang brown coal nascent char structure were observed during the gasification in O_2. Firstly, a lot of dangling structures were formed from the cleavage of aromatic rings (especially the large ones). Secondly, the preferential open up of cross-linking structures would also enhance the gasification reactivity.

4. The structural changes were more difficult to take place during gasification in O_2 in Collie sub-bituminous coal nascent char than in Loy Yang brown coal nascent char. The rapid open-up of cross-linking structures may be responsible for the initial high gasification reactivity of Collie coal nascent char.

5.5 References

[1] Li C-Z. Editorial: special issue-gasification: a route to clean energy. Process Safety and Environmental Protection, 2006; 84: 407-408.

[2] Li C-Z. Some recent advances in the understanding of the pyrolysis and gasification behaviour of Victorian brow coal. Fuel 2007;86:1664-83.

[3] Quyn DM, Wu H, Hayashi J-I, Li C-Z. Volatilisation and catalytic effects of alkali and alkaline earth metallic species during the pyrolysis and gasification of Victorian brown coal. Part IV. Catalytic effects of NaCl and ion-exchangeable Na in coal on char reactivity. Fuel 2003;82:587-93.

[4] Wu H, Hayashi J-I, Chiba T, Takarada T, Li C-Z. Volatilisation and catalytic effects of alkali and alkaline earth metallic species during the pyrolysis and gasification of Victorian brown coal. Part V. Combined effects of Na concentration and char structure on char reactivity. Fuel 2004;83:23-30.

[5] Li X, Hayashi J-i, Li C-Z. FT-Raman spectroscopic study of the evolution of char structure during the pyrolysis of a Victorian brown coal. Fuel 2006;85:1700-7.

[6] Li X, Li C-Z. Volatilisation and catalytic effects of alkali and alkaline earth metallic species during the pyrolysis and gasification of Victorian brown coal. Part VIII. Catalysis and changes in char structure during gasification in steam. Fuel 2006;85:1518-25.

[7] Li X, Hayashi J-I, Li C-Z. Volatilisation and catalytic effects of alkali and alkaline earth metallic species during the pyrolysis and gasification of Victorian brown coal. Part VII. Raman spectroscopic study on the changes in char structure during the catalytic gasification in air. Fuel 2006;85:1509-17.

[8] Zhu X, Sheng C. Influence of carbon structure on the reactivity of lignite char reacting with CO_2 and NO. Fuel Processing Technology 2010;91:837-42.

[9] Li Y, Yang H, Hu J, Wang X, Chen H. Effect of catalyst on the reactivity and structure evolution of char in petroleum coke steam gasification. Fuel 2014;117:1174-80.

[10] Asadullah M, Zhang S, Min Z, Yimsiri P, Li C-Z. Effects of biomass char structure on its gasification reactivity. Bioresource Technology

2010;101:7935-43.

[11] Keown DM, Hayashi J-I, Li C-Z. Drastic changes in biomass char structure and reactivity upon contact with steam. Fuel 2008;87:1127-32.

[12] Keown DM, Li X, Hayashi J, Li C-Z. Evolution of biomass char structure during oxidation in O_2 as revealed with FT-Raman spectroscopy. Fuel Processing Technology 2008;89:1429-35.

[13] Dong S, Alvarez P, Paterson N, Dugwell DR, Kandiyoti R. Study on the effect of heat treatment and gasification on carbon structure of coal char and metallurgical cokes using Fourier transform Raman spectroscopy. 2009;23:1651-61.

[14] Sheng C. Char structure characterised by Raman spectroscopy and its correlations with combustion reactivity. Fuel 2007;86:2316-2324.

[15] Chabalala VP, Wagner N, Potgieter-Vermaak S. Investigation into the evolution of char structure using Raman spectroscopy in conjunction with coal petrography; Part 1. Fuel Processing Technology 2011;92:750-6.

[16] Qi X, Guo X, Xue L, Zheng C. Effect of iron on Shenfu coal char structure and its influence on gasification reactivity. Journal of Analytical and Applied Pyrolysis 2014;110:401-7.

[17] Tay H-L, Li C-Z. Changes in char reactivity and structure during the gasification of a Victorian brown coal: Comparison between gasification in O_2 and CO_2. Fuel Processing Technology 2010;91:800-4.

[18] Guo X, Tay H-L, Zhang S, Li C-Z. Changes in char structure during the gasification of a Victorian brown coal in steam and Oxygen at 800 °C. Energy & Fuels 2008;22:4034-8.

[19] Tay H-L, Kajitani S, Zhang S, Li C-Z. Effects of gasifying agent on the evolution of char structure during the gasification of Victorian brown coal. Fuel 2013;103:22-8.

[20] Zhang S, Min Z, Tay H-L, Wang Y, Dong L, Li C-Z. Changes in char structure during the gasification of mallee wood: effects of particle size and steam supply. Energy & Fuels 2012;26:193-8.

[21] Zhang S, Min Z, Tay H-L, Asadullah M, Li C-Z. Effects of volatile-char interactions on the evolution of char structure during the gasification of

Victorian brown coal in steam. Fuel 2011;90:1529-1535.

[22] Li T, Zhang L, Dong L, Li C-Z. Effects of gasification atmosphere and temperature on char structural evolution during the gasification of Collie sub-bituminous coal. Fuel 2014;117:1190-1195.

[23] Zhang L, Li T, Quyn D, Dong L, Qiu P, Li C-Z. Formation of nascent char structure during the fast pyrolysis of low-rank fuels. Fuel 2015;150:486-92..

[24] Moulijn JA, Kapteijn F. Towards a unified theory of reactions of carbon with oxygen-containing molecules. Carbon 1995;33:1155-65.

[25] Livneh T, Bar-Ziv E, Senneca O, Salatino P. Evolution of reactivity of highly porous chars from Raman microscopy. Combustion Science and Technology 2000;153:65-82.

[26] Bar-Ziv E, Kantorovich II. Mutual effects of porosity and reactivity in char oxidation. Progress in Energy and Combustion Science 2001;27:667-97.

[27] Zhang L, Li T, Quyn D, Dong L, Qiu P, Li C-Z. Structural transformation of nascent char during the fast pyrolysis of low-rank fuels. Fuel and Processing Technology 2015;138:390-6.

[28] Leites LA, Bukalov SS. Raman intensity and conjugation with participation of ordinary sigma-bonds. Journal of Raman Spectroscopy 2001;32:413-24.

[29] Li C-Z, Sathe C, Kershaw JR, Pang Y. Fates and roles of alkali and alkaline earth metals during the pyrolysis of a Victorian brown coal. Fuel 2000;79:427-38.

[30] Nakamoto K. Infrared and Raman spectra of inorganic and coordination compounds. 6th ed. New York: Wiley; 2008.

[31] Tay H-L, Kajitani S, Wang S, Li C-Z. A preliminary Raman spectroscopic perspective for the roles of catalysts during char gasification. Fuel 2014;121:165-72.

Chapter 6

Effects of alkali and alkaline earth metallic species and char structure on the nascent char reactivity

6.1 Introduction

The behaviour of alkali and alkaline earth metallic (AAEM) species is one of the central topics about the utilisation of biomass [1-3] and coals [4-6] during gasification and combustion. On one hand, AAEM species can behave as a good catalyst, which enhances the gasification/combustion reactivity of char. On the other hand, AAEM species are notorious for causing ash-related problems such as fouling and slagging in the pulverised-fuel combustion systems and erosion/corrosion of turbine blades. Therefore, it is essential to investigate the volatilisation of AAEM species and their catalytic effect on gasification reactivity.

The gasification of coal is a complicated process. When coal particles are fed into a gasifier, it initially undergoes dewatering and pyrolysis. In the step of pyrolysis, primary volatiles are immediately formed and explosively released, leaving the remaining solid residue as nascent char. The nascent char still keeps high reactivity [7] and determines the overall gasification reactivity. However, the following reactions, such as the interaction with volatiles (especially with H radicals [8]) and selective consumption of small aromatic rings by gasification agents [9, 10], would bring about the rapid deactivation of char and slow down the gasification rate. It is well known that the rate-limiting step of gasification is char gasification (especially "aged" char) [11]. Previous studies have mainly focused on the factors influencing the reactivity of the "aged/stable" char that underwent volatile-char interaction and extended (several minutes) gasification [5, 12-15], in which the factors influencing the "nascent" char reactivity were neglected.

The evolution of nascent char reactivity during the gasification of two coals in O_2 (increasing char conversion) at low temperature was investigated in Chapter 5. The reasons, responsible for the high reactivity of nascent char during gasification in O_2, were discussed by assuming an AAEM concentration in the nascent char (prepared at 600 °C with 0 s holding). The findings suggested there were cooperating effects between AAEM species and char structure on char reactivity during the gasification of a single nascent char in O_2. However, it is still unclear about the effects of AAEM

species and char structure on the reactivity of different chars (with different holding time/temperature). Additionally, for Collie coal, AAEM species showed negligible effect on the nascent char reactivity for the char prepared at 600 °C holding 0 s. Nevertheless, with the fast changes in char structure during the initial holding at different temperatures (shown in Chapter 2 and 3), the role of AAEM species and char structure on char reactivity may alter with further holding or heating to higher temperature. It is clear that there is insufficient knowledge about the combined effects of char structure and AAEM catalysts on the reactivity of nascent char. This is at least partly due to the differences in procedure for preparing a nascent char experimentally.

The wire-mesh reactor (WMR) is well-known in that it can achieve very short holding time (increments of 10 ms), fast heating rate ($\geq$ 1000 °C s^{-1}) and minimised volatile-char interaction, which are very suitable for nascent char preparation [16-21]. In this study, the two low-rank coals were fast pyrolysed in a wire-mesh reactor at temperatures from 600 to 1200 °C. The reaction conditions were the same as that in Chapters 2 and 3. The exact concentrations of AAEM species in nascent char and the specific reactivity of nascent char were measured. The effects of AAEM species concentrations and char structural changes on the nascent char reactivity during the initial holding at different temperatures will be discussed below.

6.2 Experimental

6.2.1 Coal samples and pyrolysis experiments

Western Australia Collie sub-bituminous coal and Victorian Loy Yang brown coal were used in this study. The preparation and the properties of coal samples have been described in the second chapter. The nascent chars that prepared for the measurement of AAEM concentrations and the analysis of char reactivity were produced under the same experimental conditions as those in Chapter 2 and 3. Briefly, the heating rate was chosen as 1000 K s^{-1} to achieve the flash pyrolysis. The

holding time at peak temperature was from 0 to 5 s. All the experiments were carried out under atmospheric pressure.

6.2.2 Quantification of AAEM species in coal/char samples

The quantification of AAEM species mainly followed the previous method [22]. The procedure consisted of three steps: ashing, digestion and quantification. All chars produced from one experiment, ~4 mg for Loy yang coal char and ~6 mg for Collie coal char, were put in a platinum crucible. The char samples were ashed in a muffle furnace in air and the heating rate was very slow to minimise ignition. The heating program was set as follows: Firstly, coal/char sample was heated from room temperature to 300 °C at the heating rate of 5 °C min^{-1}. Secondly, the coal/char sample was further heated from 300 to 375 °C at 1 °C min^{-1} followed by 10 minutes holding at 375 °C, in which temperature range a high possibility of nascent char ignition existed. Thirdly, temperature was increased to 415 at 5 °C min^{-1} with 10 mins holding at 415 °C. Finally, the sample was heated to 600 °C at 5 °C min^{-1} with 30 mins holding at 600 °C. Subsequently, the ash was naturally cooled down to room temperature.

The platinum crucible together with the ash was placed in a Teflon beaker and dissolved with a solution of HF and HNO_3 (1:1 vol%). 6 ml of acid mixture was used to guarantee that the crucible was fully submerged in the acid. The covered Teflon beaker was then placed on a hot plate at ~ 80 °C for 16 h. After that, the lid on the beaker was removed for the evaporation of liquid. The residue was washed by 2% HNO_3 to a 10 ml vial. The AAEM concentration in the solution was then quantified by a Perkin-Elmer Optima 7300 DV inductively coupled plasma optical emission spectrometer (ICP-OES).

As WMR only accepts small amount of samples (typically no more than 10 mg), the homogeneity of the AAEM concentration in raw coal determines the feasibility of the small-scale experiment. Therefore, the repeatability of the AAEM concentration in the two raw coals was tested and shown in Table 6-1 and 6-2. This suggests that

the concentration of K in Loy Yang coal is too low to be quantified accurately in this study.

6.2.3 Characterisation of char reactivity

Char reactivity was measured in air by a Perkin-Elmer Pyris 1 thermogravimetric analyser (TGA). The peak temperature was chosen at 370 ℃ in TGA for the char pyrolysed at 600/800 ℃ and 400 ℃ in TGA for the char pyrolysed at 1000/1200 ℃. The method for the calculation of reactivity has been described in Chapter 5. Since nascent char is very reactive and the char would be exposed to air for a period, the oxidation of char in air may affect the nascent char reactivity. Therefore, the repeatability of nascent char reactivity during different residence time in ambient air was investigated and shown in Fig. 6-1. The results indicate there is little effect of the oxidation on nascent char reactivity in ambient air.

Table 6-1 Repeated tests for the concentrations of AAEM species in Collie coal (All data are on dry basis)

	Na %	**K %**	**Mg %**	**Ca %**
	0.0186	0.0125	0.0551	0.0772
	0.0180	0.0124	0.0554	0.0757
	0.0178	0.0129	0.0547	0.0740
	0.0181	0.0119	0.0545	0.0761
	0.0176	0.0119	0.0543	0.0752
	0.0176	0.0119	0.0545	0.0760
	0.0178	0.0127	0.0551	0.0755
	0.0179	0.0123	0.0558	0.0770
	0.0183	0.0128	0.0562	0.0766
	0.0183	0.0126	0.0560	0.0797
Average	0.0180	0.0124	0.0552	0.0763
Max relative error*	3.22%	4.37%	1.80%	4.49%

*Max relative error =Max ($\left| \frac{AAEM\% - \overline{AAEM\%}}{\overline{AAEM\%}} \right|$)

Table 6-2 Repeated tests for the concentrations of AAEM species in Loy Yang coal (All data are on dry basis)

	Na %	**K%**	**Mg %**	**Ca%**
	0.0991	0.0025	0.0669	0.0869
	0.0992	0.0019	0.0673	0.0865
	0.0988	0.0024	0.0684	0.0852
	0.0961	0.0021	0.0652	0.0813
	0.0964	0.0024	0.0660	0.0817
	0.0963	0.0023	0.0655	0.0811
	0.0945	0.0022	0.0654	0.0853
	0.0979	0.0020	0.0655	0.0855
	0.0961	0.0030	0.0659	0.0809
	0.1014	0.0025	0.0678	0.0855
	0.0963	0.0025	0.0677	0.0801
	0.0977	0.0032	0.0683	0.0899
	0.0982	0.0019	0.0673	0.0829
	0.1017	0.0024	0.0689	0.0861
	0.0992	0.0020	0.0681	0.0840
	0.1016	0.0024	0.0694	0.0856
Average	0.0982	0.0024	0.0671	0.0843
Max relative error*	3.78%	33.00%	3.37%	6.66%

*Max relative error =Max ($\left| \frac{\mathrm{AAEM\%} - \overline{\mathrm{AAEM\%}}}{\overline{\mathrm{AAEM\%}}} \right|$)

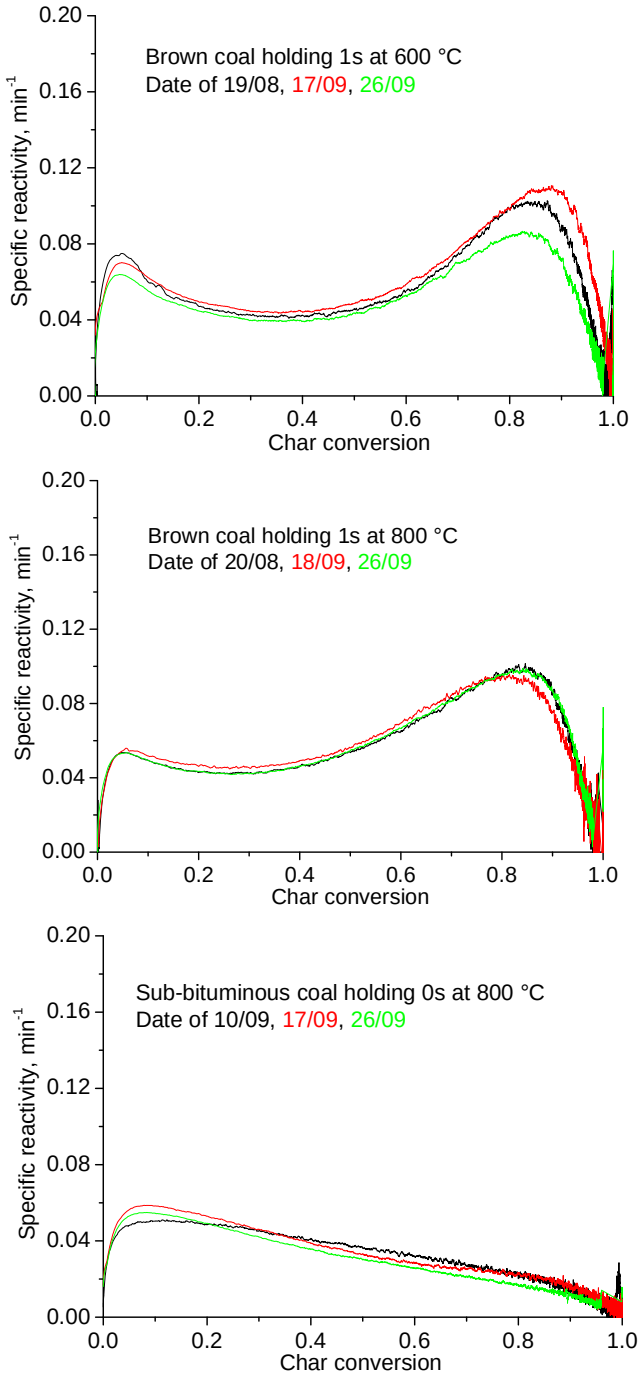

Figure 6-1 The effect of residence time in ambient air on the nascent char reactivity. (The char was produced at the first date)

6.3 Results and discussion

6.3.1 Volatilisation of AAEM species as a function of temperature and holding time for two coals

The retention of AAEM species for Loy Yang coal and Collie coal as a function of temperature (600 to 1200 °C) and holding time (0 to 5 s) is illustrated in Figs. 6-2 and 6-3, respectively. As was mentioned above, the K concentration in Loy Yang coal is too low to be considered in this study. Therefore, only the retention of Na, Mg and Ca will be discussed for Loy Yang coal, while Na, K, Mg and Ca for Collie coal.

For Loy Yang coal (shown in Fig. 6-2), ~10 to 15% volatilisation of each element was observed with 0 s holding at 600 °C (heating from room temperature to 600 °C). This significant release of AAEM species was consistent with previous studies [22], which might be due to the easy decomposition of AAEM carboxylates at low temperature. In addition, the unique feature of WMR that it continuously provides a stream of high flow rate gas passing through char would minimise volatile-char interaction and enhance the release of AAEM species (reduction of recombination). With the temperature increasing from 600 to 1000 °C, only a slight decrease in the retention of AAEM species was observed within 5 s holding at peak temperature. This was mainly due to the more stable bonds formed between AAEM species and char matrix (CM) after repeated bond-breaking and bond-forming. Further heating Loy Yang coal to 1200 °C, significant volatilisation of Na (retention dropped from ~76 to ~59%) and Mg (retention dropped from ~74 to ~65%) were observed with 5 s holding, while the retention of Ca changed very little. Comparing the releasing difficulty among each element, it is clear that Na is the easiest one to break off and Mg is easier to release than Ca. In other words, the stability of chemical forms for the three elements in Loy Yang coal char is Na < Mg < Ca. The volatilisation of AAEM species in Collie coal is shown in Fig. 6-3, except K that had ~10% volatilisation during pyrolysis (10% is close to the system error shown in Table 6-2), insignificant loss of Na, Ca and Mg was observed even at 1200 °C with 5 s holding.

It indicates that the chemical forms of AAEM species in Collie coal are much more stable than those in Loy Yang coal.

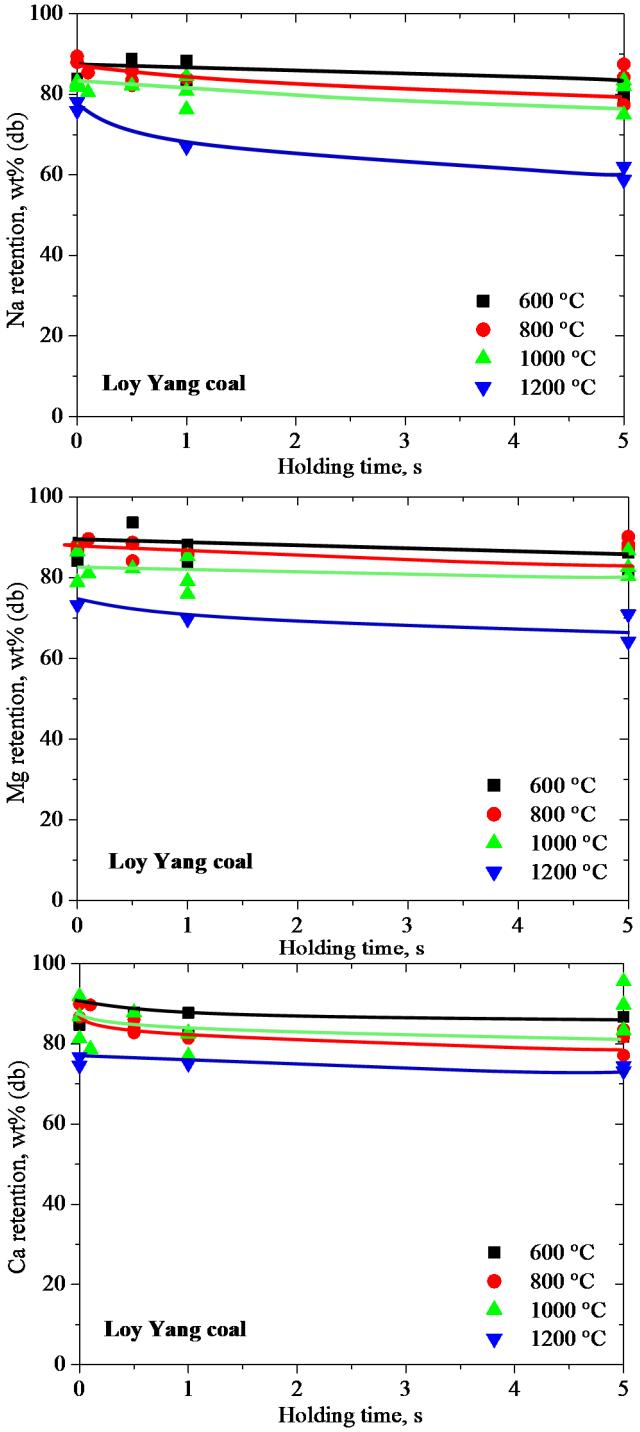

Figure 6-2 Retention of Na, Mg and Ca as a function of holding time during the fast pyrolysis of Loy Yang coal from 600 to 1200 °C.

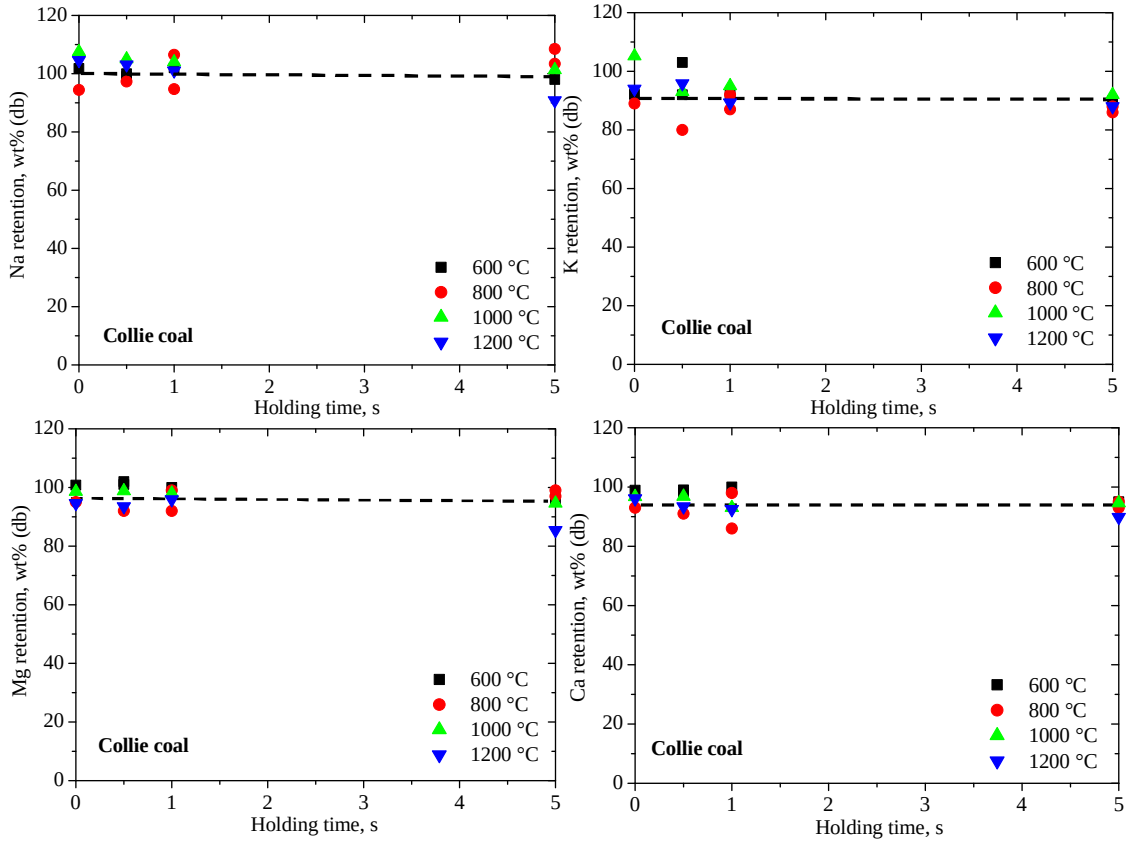

Figure 6-3 Retention of Na, K, Mg and Ca as a function of holding time during the fast pyrolysis of Collie coal from 600 to 1200 °C.

6.3.2 Effects of AAEM concentration and char structure on nascent char reactivity

6.3.2.1 Reactivity of Loy Yang coal char

According to previous studies [22], minimal amounts of AAEM species would volatilise during the slow oxidation of coal/char in O_2 at temperature ≤ 600 °C. Therefore, in the process of char reactivity measurement, where the temperature is only at ≤ 400 °C in this study, no volatilisation of AAME species would take place. As a result of that, the specific reactivity as a function of char conversion can be directly converted to the reactivity as a function of AAEM concentration in char. The total AAEM concentration for Loy Yang coal is calculated as the concentration of Na (monovalent) added to double concentrations of Ca and Mg (divalent). The total AAEM concentration for Collie coal is calculated as the total amount of the concentrations of Na/K and double concentration of Mg/Ca. It is worth emphasising that the specific reactivity was plotted as a function of the concentration of Na, double concentration of Mg/Ca or their combination as well, yet the shape of reactivity changed little. Therefore, only the total amount of AAEM concentration has been used as the abscissa is in this study in Fig. 6-4. Additionally, in order to have a clear comparison between the changes in char structure and reactivity, the Raman data used in Fig. 6-5 were redrawn based on the data shown in Chapter 2 and 3.

As is shown in Fig. 6-4 (a), reactivity changed little within 5 s holding at 600 °C, while a large evolution of aromatic ring systems was observed during the initial 5 s holding at 600 °C ($I_{(Gr+Vl+Vr)}/I_D$ decreased from ~3.1 to ~2.6) in Fig. 6-5. This implies that the reactive sites for thermal cracking at 600 °C may not be necessarily the preferential reaction sites during the gasification in O_2 at low temperatures. Moreover, as was discussed in Chapter 5, the O-containing functional groups are very reactive, which may release or transform during the slow heating of nascent char at low temperature and subsequently affect the reaction pathway during the gasification in O_2 (especially during the initial char conversion). As is shown in

Fig. 6-4, little changes in O-containing functional groups (in terms of total Raman area) were observed within 5 s holding at 600 °C. This is consistent with little change in reactivity. The insignificant changes in char reactivity also reveals that the short residence time at 600 °C did not significantly change the dispersion of AAEM species and the chemical nature of AAEM-char matrix.

In Fig. 6-4 (b), at 800 °C, a large decrease in char reactivity occurred during the initial 1 s holding at the same AAEM concentration. It reveals the significant effect of char structure on reactivity. As was discussed in Chapter 3 (shown in Fig. 6-5), Loy Yang coal started to have significant aromatic ring condensation and great loss of O-containing functional groups at 800 °C within 1 s, which seems largely affecting the char reactivity. The increase in char reactivity at the char conversion from 40% to 80% is almost linear with the AAEM concentration, indicating that the gasification rate is associated with the AAEM species at this conversion range. However, the decrease in the reactivity at the same AAEM concentration during holding suggests the significant role of char structure. With the increasing stability of char matrix, the bond between AAEM-char matrix turned to be more stable and correspondingly decreased the gasification rate.

Figure 6-4 (c) shows the changes in char reactivity during holding at 1000 °C. As was mentioned in Experimental, the temperature for the reactivity measurement in TGA was chosen at 370 °C for the nascent char produced at 600 and 800 °C, which would ignite at 400 °C. Since no ignition of chars produced at 1000 °C was observed during the reactivity measurement in TGA at 400 °C, the char reactivity must be lower than that of the chars produced at 800 °C. The significant loss of O-containing functional groups and condensation of ring systems during heating from 800 °C to 1000 °C (shown in Fig. 6-5) would be the main reasons responsible for this large deactivation. During holding at 1000 °C, the reactivity changed little within the initial 60% char conversion. Compared with 600 and 800 °C char, the initial high reactivity at < 40% conversion became very weak at 1000 °C. This indicates that the original reactive portion of nascent char had been broken off or converted into more stable structures. The reactivity was linear with AAEM concentration at low char

conversion < 60%, which shows the dominant role of AAEM concentration in this conversion range. However, the reactivity became gradually different from chars produced at different holding times at later char conversion levels. At lower char conversion levels, the AAEM species dominated the char reactivity. However, at higher conversion levels, both char structure and AAEM species dominated the reactivity.

For the chars pyrolysed at 1200 °C, as is shown in Fig. 6-4 (d), the reactivity significantly decreased within 1 s holding during the pyrolysis to produce chars. It might be partly due to the rapid enhancement of ring condensation within 1 s holding. Nevertheless, the change in char structure is very slight and the char structure is already very stable with 0 s holding at 1200 °C. As is shown in Fig. 6-5, holding for 1 s during pyrolysis at 1200 °C resulted in little further char structural changes. Therefore, the decrease in reactivity [Fig. 6-4 (d)] with holding time during pyrolysis at 1200 °C should be related to the behaviour of AAEM species. As was shown in Fig. 6-2, there was a fast volatilisation of Na and Mg during pyrolysis with holding time at 1200 °C.

In summary, the data in Figs. 6-4 and 6-5 show some complicated relationships between the char reactivity with O_2 at 370/400 °C and the char properties as are represented by Raman –derived char structural parameter as well as by the AAEM concentrations. For the pyrolysis temperature of 600 °C, the active char structure was typified by the high Raman intensity and high $I_{(Gr+Vl+Vr)}/I_D$ ratios. Following the consumption of some very reactive structure, AAEM concentration was the dominant factor in determining the char-O_2 reactivity at 370 °C with at > 80% char conversion when only relative inert char structures were left. At high pyrolysis temperatures e.g. 1200 °C, the char structure was relatively inert even at 0 s holding time during pyrolysis. The volatilisation of AAEM species during pyrolysis became the dominant reason for the observed decreases in char-O_2 reactivity at 400 °C. Even so, the char structure became important at char conversion > 80% because only inert char components were left.

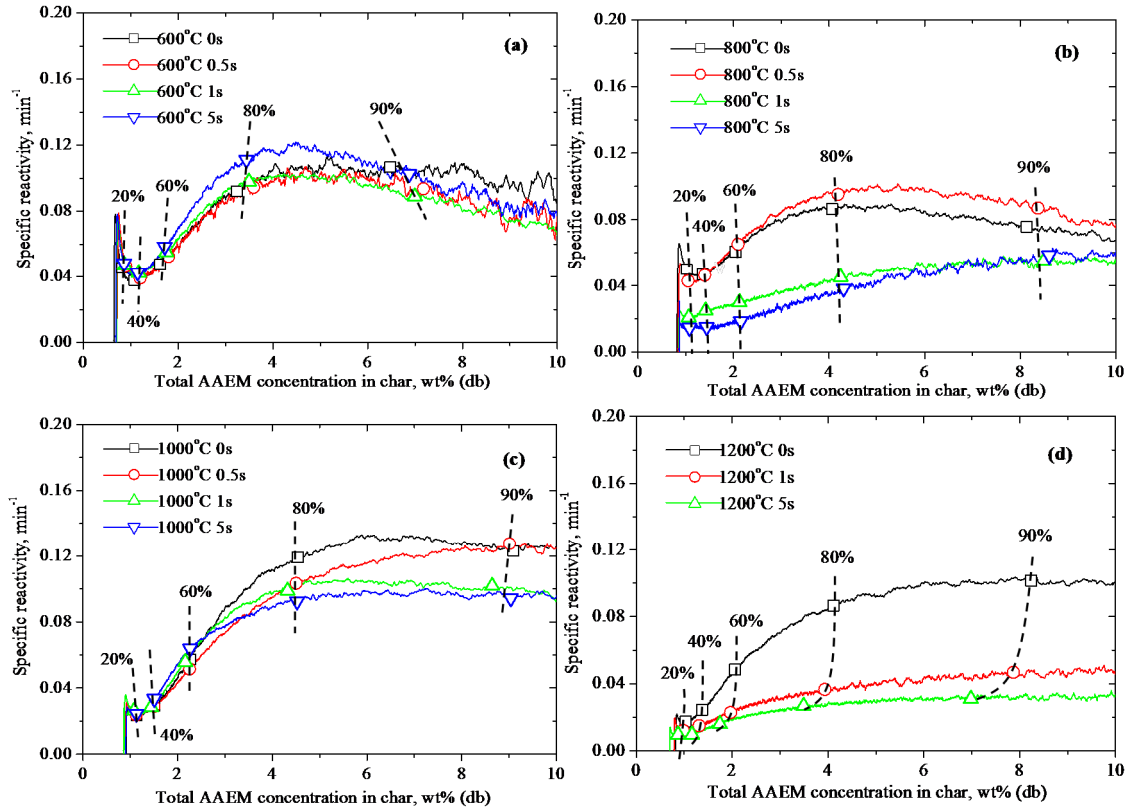

Figure 6-4 Specific reactivity in air of Loy Yang coal chars as a function of AAEM concentration. The percentages in the graph mean the different char conversion. The reactivity of the chars in (a) and (b) was measured at 370 °C in TGA. The reactivity of the chars in (c) and (d) was measured at 400 °C in TGA.

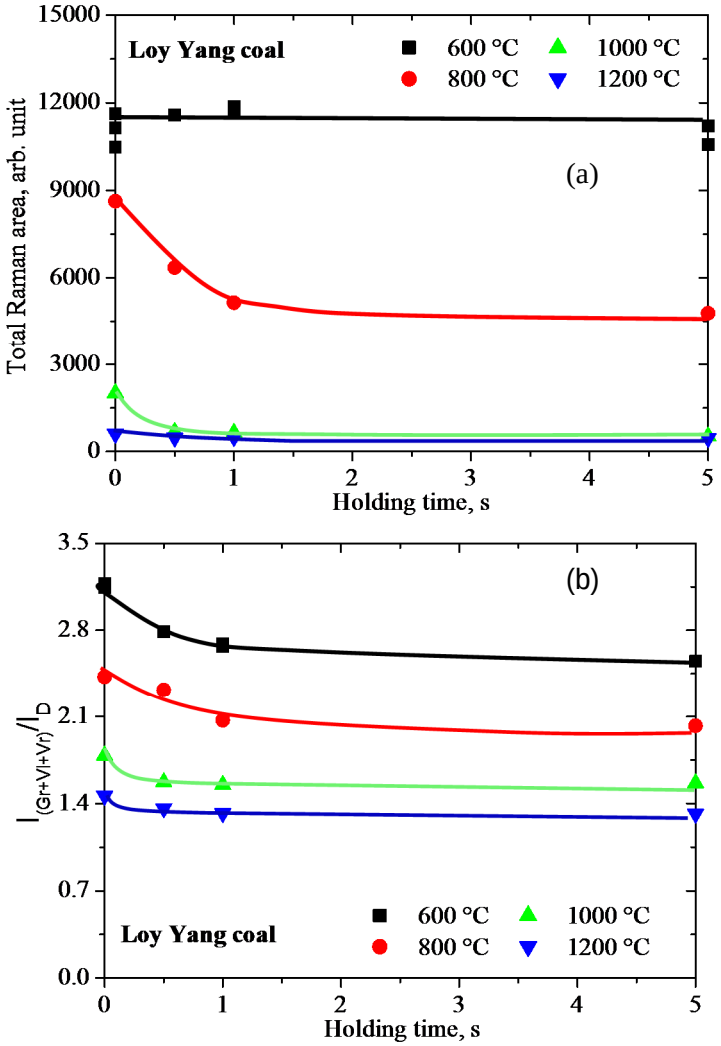

Figure 6-5 Changes in char structure during fast pyrolysis of Loy Yang coal. (Based on the data in Chapter 2 and 3)

6.3.2.2 Char-O_2 reactivity of Collie coal char

Figure 6-6 shows the evolution of char reactivity as a function of AAEM concentration in char from the pyrolysis of Collie coal at temperatures from 600 to 1200 °C and holding time from 0 to 5 s. Figure 6-7 shows the corresponding changes in char structures. In Fig. 6-6, the Collie coal char reactivity as a function of AAEM concentration showed much different shapes from the Loy Yang coal char reactivity. As was discussed in Chapter 5, it is mainly due to much more stable chemical form of AAEM species in Collie coal than those in Loy Yang coal. This is supported by the little volatilisation of AAEM species even at 1200 °C (discussed in Section 6.3.1).

As is shown in Fig 6-6 (a) and (b), only a strong peak was observed for each char reactivity at the conversion < 20% due to the presence of some very reactive structures in the chars. Instead of increases in char-O_2 reactivity with increasing AAEM concentration, rapid decreases in char reactivity were observed for chars produced at 600 and 800 °C. Compared with the changes in char structure shown in Fig 6-7, the distribution of aromatic ring systems changed little during 5 s holding at 600 and 800 °C, while the release of O-containing functional groups (decreases in the total Raman area) was consistent with the decrease in reactivity. This implies the important role of O-containing functional groups on low temperature char (nascent char) reactivity. Recently, Tay and co-workers [23] also found that the O-containing structures were responsible for the enhancement of char gasification rate at 800 °C.

When increasing pyrolysis temperature to 1000 °C, the shape of the specific reactivity was different from those at low pyrolysis temperature. There was no initial peak within 40% char conversion. Only a linear trend of reactivity as a function of AAEM concentration was observed at < 60% conversion. It reveals that AAEM species do have some catalytic effects on the char-O_2 reactivity for Collie coal. It appears that the highly reactive char structures in the 600 and 800 °C chars have masked the possible catalytic effects of AAEM species. The specific char-O_2 reactiivty linearly increased as a function of AAEM concentration, although the chars produced with different holding times at 1000 °C differed in their levels of

char-O_2 reactivity. It confirms the cooperating effects of AAEM species and char structure on reactivity. As is shown in Fig. 6-7, there was a rapid enhancement of ring condensation during the pyrolysis with 1 s holding at 1000 °C, which should be responsible for the fast decrease in the char-O_2 reactivity during the pyrolysis with 1 s holding at 1000 °C. Further increasing temperature to 1200 °C (in Fig. 6-6), the pyrolysed char showed very low reactivity. It might be due to the further condensed char structure. For the chars produced from the pyrolysis at 1200 °C, a rapid decrease in char reactivity occurred within 0.5 s, which is the same as the rapid increase in ring condensation within 0.5 s holding shown in Fig. 6-7.

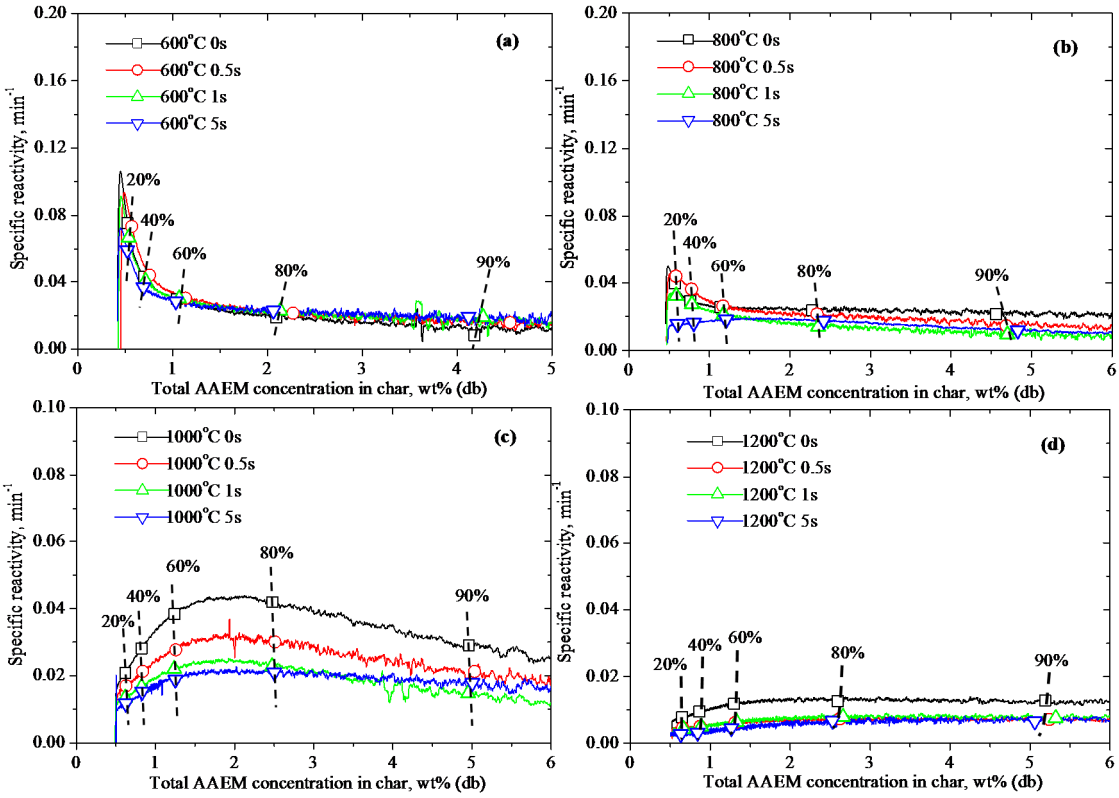

Figure 6-6 Specific reactivity of Collie coal chars as a function of AAEM concentration. The percentages in the graph mean the char conversion levels during the char-O_2 reaction in TGA. The reactivity of chars in (a) and (b) were measured at 370 °C in TGA. The reactivity of chars in (c) and (d) were measured at 400 °C in TGA.

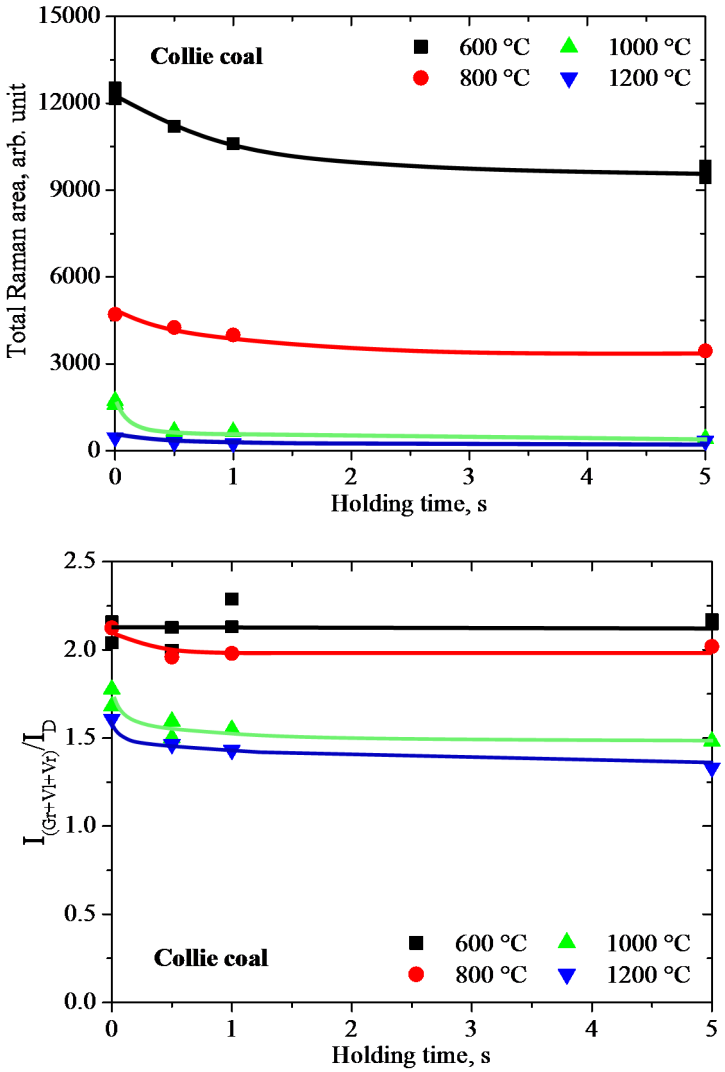

Figure 6-7 Changes in char structure during the fast pyrolysis of Collie coal. (Based on the data in Chapters 2 and 3)

6.4 Conclusions

This study investigated the effects of char structure and AAEM species on nascent char–O_2 gasification reactivity at low temperatures. It seems that both factors play important roles in the changes in char-O_2 reactivity.

1. The chemical forms of AAEM species in Collie coal chars are much more stable than those in Loy Yang coal chars. The catalytic effects of AAEM species largely depend on its chemical form in coal/char.

2. Nascent char has some very reactive structures, which cause high reactivity during the initial ~ 20% char conversion during the char-O_2 reactions. These active structures seem at least partly related to the O-containing functional groups. This type of structure would diminish during holding at 800 °C or heating to ≥ 1000 °C during pyrolysis.

3. The catalytic effects of AAEM species are largely affected by the changes in nascent char structure, especially the increasing condensation of aromatic ring systems and the loss of O-containing functional groups. On one hand, with the increasingly stable char structure, the catalytic effects of AAEM are relatively prominent on the char reactivity such as the dominant role of AAEM species on the reactivity for 1000 °C chars of two coals. On the other hand, the catalytic effects of AAEM species on the char-O_2 reactions are inhibited by the increasing stability of the char structure.

6.5 References

[1] David S, Brain K, Julian RHR. Review of literature on catalysts for biomass gasification. Fuel Processing Technology 2001;73:155-73.

[2] Jale Y, Steve E, Andrea K, Mehmet S, Mithat Y. Biomass gasification in supercritical water: II. Effect of catalyst. International Journal of Hydrogen Energy 2008;33:4520-6.

[3] Zhu WK, Song WL, Lin WG. Catalytic gasification of char from co-pyrolysis of coal and biomass. Fuel Processing Technology 2008;89:890-6.

[4] Molina A, Mondragon F. Reactivity of coal gasification with steam and CO_2. Fuel 1998;77:1831-39.

[5] Li C-Z. Some recent advances in the understanding of the pyrolysis and gasification behaviour of Victorian brown coal. Fuel 2007;86:1664-83.

[6] Quyn DM, Wu HW, Hayashi J, Li C-Z. Volatilisation and catalytic effects of alkali and alkaline earth metallic species during the pyrolysis and gasification of Victorian brown coal. Part IV. Catalytic effects of NaCl and ion-exchangeable Na in coal on char reactivity. Fuel 2003;82:587-93.

[7] Jamil K, Hayashi J-I, Li C-Z, Pyrolysis of a Victorian brown coal and gasification of nascent char in CO_2 atmosphere in a wire-mesh reactor. Fuel 2004;83:833-43.

[8] Li C-Z. Importance of volatile-char interactions during the pyrolysis and gasification of low-rank fuels-A review. Fuel 2013;112:609-23.

[9] Li X, Hayashi J-I, Li C-Z. Volatilisation and catalytic effects of alkali and alkaline earth metallic species during the pyrolysis and gasification of Victorian brown coal. Part VII. Raman spectroscopic study on the changes in char structure during the catalytic gasification in air. Fuel 2006;85:1509-17.

[10] Keown DM, Li X, Hayashi J-I, Li C-Z. Evolution of biomass char structure during oxidation in O_2 as revealed with FT-Raman spectroscopy. Fuel Processing Technology 2008;89:1429-35.

[11] Tomita A, Ohtsuka Y. Gasification and combustion of brown coal. In: Li C-Z, editor. Advances in the science of Victorian brown coal. Oxford: Elsevier; 2004. P. 223-85 [chapter 5].

[12] K. Miura, K. Hashimoto, P.L. Silveston, Factors affecting the reactivity of coal char during gasification, and indices representing reactivity, Fuel 68 (1989) 1461-1475.

[13] O. Senneca, P. Salatino, S. Masi, Microstructural changes and loss of gasification reactivity of chars upon heat treatment, Fuel 77 (1998) 1483-1493.

[14] H. Wu, J.-I. Hayashi, T. Chiba, T. Takarada, C.-Z. Li, Volatilisation and catalytic effects of alkali and alkaline earth metallic species during the pyrolysis and gasification of Victorian brown coal. Part V. Combined effects of Na concentration and char structure on char reactivity, Fuel 83 (2004) 23-30.

[15] Asadullah M, Zhang S, Min Z, Yimsiri P, Li C-Z. Effects of biomass char structure on its gasification reactivity. Bioresource Technology 2010;101:7935-43.

[16] Sathe C, Hayashi J-I, Li C-Z. Release of volatiles from the pyrolysis of a Victorian lignite at elevated pressures. Fuel 2002;81:1171-8.

[17] Gibbins J.R., King R.A.V., Wood R.J., Kandiyoti R.. Variable-heating-rate wire-mesh pyrolysis apparatus. Review of Scientific Instruments 1989;60:1129-39.

[18] Sathe C, Pang Y, Li C-Z. Effect of heating rate and ion-exchangeable cations on the pyrolysis yields from a Victorian brown coal. Energy & Fuels 1999;13:748-55.

[19] Sathe C. Fates and roles of alkali and alkaline earth metallic species during the pyrolysis of low-rank coals. PhD Thesis, Monash University, 2001.

[20] Jamil K, Hayashi J-I, Li C-Z. Pyrolysis of a Victorian brown coal and gasification of nascent char in CO_2 atmosphere in a wire-mesh reactor. Fuel 2004;83:833-43.

[21] Jamil K. Pyrolysis and gasification of Victorian brown coal in inert and reactive gas atmospheres. PHD Thesis. Monash University, 2005.

[22] Li C-Z, Sathe C, Kershaw JR, Pang Y. Fates and roles of alkali and alkaline earth metals during the pyrolysis of a Victorian brown coal. Fuel 2000;79:427-38.

[23] Tay H-L, Kajitani S, Wang S, Li C-Z. A preliminary Raman spectroscopic perspective for the roles of catalysts during char gasification. Fuel 2014;121:165-72.

Chapter 7

Conclusions and Recommendations for Future Work

7.1 Introduction

The purpose of this study was to gain knowledge of the structural evolution of nascent char during the pyrolysis in He and the gasification in CO_2/O_2. Moreover, the effect of the transformation of nascent char structure and AAEM species on char-air reactivity was also investigated. The results will be useful for the development of low-emission gasification-based technologies for the utilisation of biomass and low-rank coal. The main conclusion of each part will be summarised in the following sections.

7.2 Conclusions

7.2.1 Formation of nascent char structure during the fast pyrolysis of mallee wood and low-rank coals

1. The combined use of wire-mesh reactor and Raman spectroscopy was an effective method to quantify the structural transformation from raw fuels to nascent chars.

2. The chemical structures of mallee wood were much different from two low-rank coals in terms of Raman spectroscopy. However, after the explosive release of primary volatiles (fast heating to 600 °C), the chemical structure of mallee wood char approached that of coal char.

3. Different from mallee wood, Loy Yang coal and Collie coal changed slightly in ring systems and crosslinks during the initial release of primary volatiles (during the fast heating from room temperature to 600 °C). As most tar was released with primary volatiles, the insignificant change in the aromatic ring systems of the two coals revealed that the newly formed aromatic rings mainly released with volatiles with little influence on the original ring systems in coal.

4. During holding at 600 °C, three fuels showed different changes in aromatic ring systems. It seemed that the feedstock that was richer in small aromatic rings more easily underwent breakage or condensation of ring systems. Moreover, only mallee wood showed significant ring condensation during holding at 600 °C.

7.2.2 Structural transformation of nascent char during the fast pyrolysis of mallee wood and two low-rank coals

1. The three fuels displayed insignificant decreases in char yield after reaching different pyrolysis temperatures (mallee wood at ≥ 600 °C, Loy yang coal at ≥ 800 °C and Collie coal at ≥ 900 °C). Nevertheless, the ratio of small to large aromatic rings (reflected by $I_{(Gr+Vl+Vr)}/I_D$) largely decreased at these temperature ranges for three fuels. The insignificant changes in char yield with the significant decreases in the ratio of small to large aromatic rings indicated that there was aromatic ring condensation occurring with the release of only light gas: probably H_2. Furthermore, the ring condensation took place very rapidly at high temperatures. For example, within 0.1 s holding, most of ring condensation has already completed at 1000 °C for three fuels.

2. FT-IR intensity at 1600 cm^{-1}, which was assigned to the C=C stretching in aromatic rings, was used to verify the rapid increase in ring condensation at high temperatures. With the growth in large aromatic rings, the vibration of C=C stretching was restricted and subsequently weakened the intensity at 1600 cm^{-1}. Therefore, the observed decrease in the intensity at 1600 cm^{-1} supported the rapid enhancement of ring condensation at relatively high temperatures for two coals.

3. Cross-links were mainly formed during initial holding at ≤ 800 °C. With further increasing temperature, the formation and breakage of cross-links were in dynamic balance with little change in the total amount of cross-links.

7.2.3 Changes in nascent char structure during the gasification of low-rank coals in CO_2

1. During the heating from 1000 to 1200 °C in CO_2, the gasification rate was 6.57 wt%-daf s^{-1}, similar to the thermal cracking rate 6.07 wt%-daf s^{-1}. This indicated that the initial high gasification rate of char was highly related to the thermal cracking at relatively high temperatures.

2. During the holding at 1000 °C in CO_2, the changes in the char structure of two coals were determined by the opposite effects of thermal annealing and oxygenation during the initial holding. This caused a minimum in the total Raman area with 1 s holding at 1000 °C for two coals in CO_2.

3. Temperature has been shown to be a significant parameter to influence the char structure in terms of Raman spectroscopic data. However, the reaction pathways during gasification at 1000 and 1200 °C are similar.

4. There should be more than one type of O-containing functional groups formed during gasification in CO_2 at 1000 and 1200 °C. Some O complexes are sensitive in the Raman scattering but some are sensitive in FTIR absorption.

5. Collie coal char had a very sharp peak at 1100 cm^{-1} in FTIR spectrum, which appears to be mainly due to the minerals in char.

7.2.4 Changes in char structure during the thermal treatment of nascent char in N_2 and the in-situ gasification in O_2

1. Reheating nascent char in TGA in N_2 from 270 to 600 °C, a minimum total Raman area was observed at 370 °C. It indicated that there might be some transformations of the O-containing functional groups from lower Raman intensity groups (which have weak resonance with aromatic rings) to higher ones (which have better resonance effects) at $\geq$ 370 °C.

2. Nascent char contained some reactive O-containing functional groups, which broke off during the reheating of nascent chars at low temperature > 270 °C for two coals. During the deoxygenation, Loy Yang coal nascent char showed more changes in char structures than Collie coal nascent char, which might be due to the more condensed and cross-linked structures in Collie coal nascent char than in Loy Yang coal char.

3. During the gasification in O_2, the changes in the reactivity with char conversion had two peaks for Loy Yang brown coal nascent char. The initial one should be mainly due to the active char structure and the second one should be due to both the effects of AAEM concentration and char structure. Only one peak at the initial char conversion was presented in the reactivity of Collie sub-bituminous coal nascent char, which is mainly related to the char structure rather than catalytic species.

4. Significant changes in Loy Yang coal nascent char structure were observed during the gasification in O_2. Firstly, large amount of O-containing functional groups were formed. Secondly, dangling structures were formed from the breakage of aromatic rings (especially large ones). Thirdly, the preferential breakage of cross-linking structures would also open-up the char structure and enhance the gasification reactivity. However, the Collie sub-bituminous coal nascent char showed much less change in char structure than that in the Loy Yang brown coal nascent char, except that, the significant cleavage of cross-links might be responsible for the initial high reactivity of Collie coal nascent char.

7.2.5 Effects of alkali and alkaline earth metallic species and char structure on the nascent char reactivity

1. Collie coal showed much less effects of AAEM species on its nascent char reactivity than Loy Yang coal, which appears to be mainly due to the less reactive chemical form of AAEM species in Collie coal/chars than in Loy Yang coal/char.

2. The nascent char reactivity was affected by both AAEM species and char structures. The catalytic effects of AAEM species are greatly related to the changes in nascent char structure. On one hand, with the increasing stabilisation of char structure, the catalytic effects of AAEM species are relatively prominent on the char reactivity such as the dominant role of AAEM species on the reactivity for 1000 °C chars (with char conversion < 80% for Loy Yang coal char and < 70% for Collie coal char). On the other hand, the catalytic effects of AAEM species on the char-O_2 reactions are inhibited by the high stability of the char structure.

In general, the initial different chemical structures (especially the different structures between biomass and coals) of three feedstocks affected significantly their reaction pathways for the formation of nascent char structure. For example, the feedstock that was richer in small aromatic rings underwent breakage or condensation of ring systems more easily. However, the char structure of three different feedstocks approached each other with increasing holding time and temperature. Temperature was another significant parameter influencing the formation and transformation of char structure during fast pyrolysis. With increasing temperature, char structure became more stable and the rate of the evolution of char structure became increasingly fast. At relatively high temperature (e.g. 1000 °C), the changes in char structure took place even within 1 s. The structural changes in nascent char during gasification in CO_2 was also largely affected by temperature, while the reaction pathway of nascent char gasification changed little during heating from 1000 to 1200 °C in CO_2. The char-O_2 reactivity, which was investigated from the aspects of nascent char structure and AAEM retention in char, was found to be largely affected by the changes in char structure. For the nascent chars, especially for low-temperature chars, the reaction of very reactive char structure dominated the char-O_2 reactivity at the initial stage of char conversion. While the char structure became more stable and the concentration of AAEM species in char increased, the AAEM species had more effect on the char-O_2 reactivity. Meanwhile, the catalytic effect of AAEM species became less profound by the increasing stable char structure.

7.3 Future work

1. This study investigated the transformation of nascent char structure and the volatilisation of AAEM species during pyrolysis at the temperature range from 600 to 1200 °C. In the commercial gasification-based technologies, such as entrained flow gasifier, the system can be operated at even high temperature, e.g. 1500 °C or higher. Therefore, it is recommended to adjust the setting and configuration of wire-mesh reactor to be suitable for the high temperature experiments to verify/extend the findings over a wider range of temperature.

2. It is worth using other reactors, especially a drop tube reactor that can provide time scales similar to the wire-mesh reactor, to make comparison of the results obtained from different reactors, thereby acquiring more experimental evidences about the effect of volatile-char interaction on the pyrolysis/ gasification of nascent char. Moreover, this study only used CO_2 and O_2 as the gasification agents. It is recommended to investigate the effect of steam or gas mixtures (steam, CO_2 and/or O_2) on the nascent char structure, the volatilisation and transformation of AAEM species or the changes in nascent char reactivity.

3. The wire-mesh reactor is suitable for the in-situ optical measurement due to its transparent shell and small-scale heating zone. The online temperature measurement by infrared thermometer is a practical example. Therefore, it is recommended to combined use of wire-mesh reactor with optical instrument such as Raman/IR spectroscopy to online study the transformation of char structure.

Appendix I

Permission of Reproduction from the Copyright Owner

Title: FT-Raman spectroscopic study of the evolution of char structure during the pyrolysis of a Victorian brown coal

Author: Xiaojiang Li,Jun-ichiro Hayashi,Chun-Zhu Li

Publication: Fuel

Publisher: Elsevier

Date: September 2006

Order Completed

Thank you very much for your order.

This is a License Agreement between Lei Zhang ("You") and Elsevier ("Elsevier"). The license consists of your order details, the terms and conditions provided by Elsevier, and the payment terms and conditions.

Get the printable license.

License Number	3817620132485
License date	Feb 28, 2016
Licensed content publisher	Elsevier
Licensed content publication	Fuel
Licensed content title	FT-Raman spectroscopic study of the evolution of char structure during the pyrolysis of a Victorian brown coal
Licensed content author	Xiaojiang Li,Jun-ichiro Hayashi,Chun-Zhu Li
Licensed content date	September 2006
Licensed content volume number	85
Licensed content issue number	12-13
Number of pages	8
Type of Use	reuse in a thesis/dissertation
Portion	figures/tables/illustrations
Number of figures/tables /illustrations	2
Format	both print and electronic
Are you the author of this Elsevier article?	No
Will you be translating?	No
Original figure numbers	figure 4 and table 1
Title of your thesis/dissertation	Transformation of Char Structure and Alkali and Alkali Earth Metallic Species during Pyrolysis and Gasification
Expected completion date	Feb 2016
Estimated size (number of pages)	150
Elsevier VAT number	GB 494 6272 12
Permissions price	0.00 USD
VAT/Local Sales Tax	0.00 USD / 0.00 GBP
Total	0.00 USD

ORDER MORE... CLOSE WINDOW

Title:	CO2 gasification rate analysis of coal char in entrained flow coal gasifier
Author:	Shiro Kajitani,Nobuyuki Suzuki,Masami Ashizawa,Saburo Hara
Publication:	Fuel
Publisher:	Elsevier
Date:	January 2006

Order Completed

Thank you very much for your order.

This is a License Agreement between Lei Zhang ("You") and Elsevier ("Elsevier"). The license consists of your order details, the terms and conditions provided by Elsevier, and the payment terms and conditions.

Get the printable license.

License Number	3812250219032
License date	Feb 18, 2016
Licensed content publisher	Elsevier
Licensed content publication	Fuel
Licensed content title	CO2 gasification rate analysis of coal char in entrained flow coal gasifier
Licensed content author	Shiro Kajitani,Nobuyuki Suzuki,Masami Ashizawa,Saburo Hara
Licensed content date	January 2006
Licensed content volume number	85
Licensed content issue number	2
Number of pages	7
Type of Use	reuse in a thesis/dissertation
Portion	figures/tables/illustrations
Number of figures/tables /illustrations	1
Format	both print and electronic
Are you the author of this Elsevier article?	No
Will you be translating?	No
Title of your thesis/dissertation	Transformation of Char Structure and Alkali and Alkali Earth Metallic Species during Pyrolysis and Gasification
Expected completion date	Feb 2016
Estimated size (number of pages)	150
Elsevier VAT number	GB 494 6272 12
Permissions price	0.00 USD
VAT/Local Sales Tax	0.00 USD / 0.00 GBP
Total	0.00 USD

ORDER MORE... CLOSE WINDOW

Copyright Clearance Center RightsLink® Home Account Info Help Live Chat

Title: Formation of nascent char structure during the fast pyrolysis of mallee wood and low-rank coals

Author: Lei Zhang,Tingting Li,Dimple Quyn,Li Dong,Penghua Qiu,Chun-Zhu Li

Publication: Fuel

Publisher: Elsevier

Date: 15 June 2015

Logged in as:
Lei Zhang
LOGOUT

Order Completed

Thank you very much for your order.

This is a License Agreement between Lei Zhang ("You") and Elsevier ("Elsevier"). The license consists of your order details, the terms and conditions provided by Elsevier, and the payment terms and conditions.

Get the printable license.

License Number	3810111365616
License date	Feb 15, 2016
Licensed content publisher	Elsevier
Licensed content publication	Fuel
Licensed content title	Formation of nascent char structure during the fast pyrolysis of mallee wood and low-rank coals
Licensed content author	Lei Zhang,Tingting Li,Dimple Quyn,Li Dong,Penghua Qiu,Chun-Zhu Li
Licensed content date	15 June 2015
Licensed content volume number	150
Licensed content issue number	n/a
Number of pages	7
Type of Use	reuse in a thesis/dissertation
Portion	full article
Format	both print and electronic
Are you the author of this Elsevier article?	Yes
Will you be translating?	No
Title of your thesis/dissertation	Transformation of Char Structure and Alkali and Alkali Earth Metallic Species during Pyrolysis and Gasification
Expected completion date	Feb 2016
Estimated size (number of pages)	150
Elsevier VAT number	GB 494 6272 12
Permissions price	0.00 USD
VAT/Local Sales Tax	0.00 USD / 0.00 GBP
Total	0.00 USD

ORDER MORE... CLOSE WINDOW

Title: Structural transformation of nascent char during the fast pyrolysis of mallee wood and low-rank coals

Author: Lei Zhang,Tingting Li,Dimple Quyn,Li Dong,Penghua Qiu,Chun-Zhu Li

Publication: Fuel Processing Technology

Publisher: Elsevier

Date: October 2015

Order Completed

Thank you very much for your order.

This is a License Agreement between Lei Zhang ("You") and Elsevier ("Elsevier"). The license consists of your order details, the terms and conditions provided by Elsevier, and the payment terms and conditions.

Get the printable license.

License Number	3810111499484
License date	Feb 15, 2016
Licensed content publisher	Elsevier
Licensed content publication	Fuel Processing Technology
Licensed content title	Structural transformation of nascent char during the fast pyrolysis of mallee wood and low-rank coals
Licensed content author	Lei Zhang,Tingting Li,Dimple Quyn,Li Dong,Penghua Qiu,Chun-Zhu Li
Licensed content date	October 2015
Licensed content volume number	138
Licensed content issue number	n/a
Number of pages	7
Type of Use	reuse in a thesis/dissertation
Portion	full article
Format	both print and electronic
Are you the author of this Elsevier article?	Yes
Will you be translating?	No
Title of your thesis/dissertation	Transformation of Char Structure and Alkali and Alkali Earth Metallic Species during Pyrolysis and Gasification
Expected completion date	Feb 2016
Estimated size (number of pages)	150
Elsevier VAT number	GB 494 6272 12
Permissions price	0.00 USD
VAT/Local Sales Tax	0.00 USD / 0.00 GBP
Total	0.00 USD

Copyright Clearance Center RightsLink® Home Account Info Help Live Chat

Title: Changes in nascent char structure during the gasification of low-rank coals in CO2

Author: Lei Zhang,Shiro Kajitani,Satoshi Umemoto,Shuai Wang,Dimple Quyn,Yao Song,Tingting Li,Shu Zhang,Li Dong,Chun-Zhu Li

Publication: Fuel

Publisher: Elsevier

Date: 15 October 2015

Logged in as:
Lei Zhang
LOGOUT

Order Completed

Thank you very much for your order.

This is a License Agreement between Lei Zhang ("You") and Elsevier ("Elsevier"). The license consists of your order details, the terms and conditions provided by Elsevier, and the payment terms and conditions.

Get the printable license.

License Number	3810111234899
License date	Feb 15, 2016
Licensed content publisher	Elsevier
Licensed content publication	Fuel
Licensed content title	Changes in nascent char structure during the gasification of low-rank coals in CO2
Licensed content author	Lei Zhang,Shiro Kajitani,Satoshi Umemoto,Shuai Wang,Dimple Quyn,Yao Song,Tingting Li,Shu Zhang,Li Dong,Chun-Zhu Li
Licensed content date	15 October 2015
Licensed content volume number	158
Licensed content issue number	n/a
Number of pages	8
Type of Use	reuse in a thesis/dissertation
Portion	full article
Format	both print and electronic
Are you the author of this Elsevier article?	Yes
Will you be translating?	No
Title of your thesis/dissertation	Transformation of Char Structure and Alkali and Alkali Earth Metallic Species during Pyrolysis and Gasification
Expected completion date	Feb 2016
Estimated size (number of pages)	150
Elsevier VAT number	GB 494 6272 12
Permissions price	0.00 USD
VAT/Local Sales Tax	0.00 USD / 0.00 GBP
Total	0.00 USD

ORDER MORE... CLOSE WINDOW